3. OXIDATION BEHAVIOR AND EMBRITTLEMENT THRESHOLD OF STANDARD E110 CLADDING: PROGRAM, TEST PROCEDURES, DISCUSSION OF TEST RESULTS

3.1. The program concept and technical requirements to experimental works

Previous investigations of the mechanical behavior of oxidized claddings under the LOCA conditions revealed a series of practical problems. Two of those are related directly to the present investigation:

- a definite separation of such conceptions as the "cladding fragmentation threshold" and "cladding embrittlement threshold" is lacking on analyzing the study results;
- the results of works performed by different researchers are discussed and compared without the analysis of test conditions and regard for peculiar features of procedures employed to determine the output parameters.

As for the first of the problems, the following approach was proposed to specify two criterion conditions of the cladding:

1. The cladding fragmentation threshold characterizes the actual loss of the cladding structural integrity under the impact of a complex combination of loading factors. This threshold can be determined for each of the typical sections of the accident scenario and for each of the post-accident actions only with the help of well-planned integral experiments with fuel rods and simulators of fuel rods.
2. The embrittlement threshold characterizes the conditions under which the cladding ductility is close to zero. In this case, it is of importance that the appropriate threshold value be determined by relatively simple parametric experiments including those using uniaxial mechanical tests.

It is evident that, from the theoretical point of view, the cladding fragmentation threshold should be the major subject of investigation within the context of this program. However, in spite of the fact that almost 30 years after the time when the first licensing criterion for safety was developed, the following basic conclusion about the basis of the criterion has not changed up to now: "There is some lack of certainty as to just what nature of stresses would be encountered during the LOCA" [1]. In turn, the insufficiency of such knowledge leads to the difficulty of justifying requirements on the basis of integral experiments. Therefore, with due respect to the importance of such experiments as a thermal shock, it should be acknowledged that the experimental determination of the embrittlement threshold for claddings -- with the subsequent introduction of coefficients regulating the necessary minimum margin for the residual ductility in oxidized claddings -- was and remains the basic method for the practical safety studies.

Therefore, the further analysis of possible variants for the experiments was restricted to the following list of mechanical tests for oxidized claddings:

- impact tests;
- three-point bending tests;
- tensile tests;
- ring compression tests.

The consideration of these variants showed that:

- impact tests do not allow one to obtain a stress-strain curve in the explicit form and, besides, these tests are not standardized so that one could not directly compare the results obtained for different claddings in different countries;
- three-point bending tests present a very promising type of study; however, the procedure requirements are not quite developed and the comparative data base for these test is practically lacking;

- tensile tests present the most valuable type of mechanical tests; however, tensile tests of claddings with a high level of oxidation require to improve of test techniques and, besides, a comparative data base obtained from these tests is extremely limited;
- ring compression tests present the simplest and accessible type of tests allowing to obtain good statistical data within a limited time. Therefore, this type of tests has a representative data base containing the results of previous investigations of alloys E110, Zry-4, M5, Zirlo.

Taking into account all stated above, the final choice of the method to determine the embrittlement threshold for the E110 cladding was made in favor of ring compression tests. Nevertheless, it should be noted that this type of tests has a series of disadvantages the basic ones of which are as follows:

- the lack of standard requirements imposed on geometrical sizes of tested specimens (specimen length);
- the lack of physically justified rules for the interpretation of test results.

Therefore, special scoping tests were stipulated in the program of these studies. The aim of these tests was to obtain a data base necessary to specify the requirements to the test conditions and to justify the processing procedures for obtained results. It should be noted that the list of procedural issues revealed at the stage of this program development included several problems associated with the oxidation conditions.

The first of these problems may be characterized by the following propositions:

- from the formal point of view, the E110 alloy embrittlement threshold must be determined and compared with the license embrittlement criterion;
- the license embrittlement criterion for the E110 alloy (18%) is based on the employment of the VNIINM conservative correlation for the E110 oxidation kinetic description [2];
- just the same approach is used for Zircaloy-4 alloy (15% in France and 17% in U.S.) but in this case the Baker-Just conservative correlation is often employed [3];
- both conservative correlations were developed according to individual (as applied to each alloy) rules, and the conservatism degree was not necessarily the same. Therefore, a direct comparison of the mechanical behavior of these two alloys (and others such as M5 and Zirlo) with one of the conservative correlations is not meaningful from the physics point of view;
- it is evident that the practical solution of this problem may be provided on moving from the conservative correlations to best-estimated correlations with a simultaneous transformation of the license criteria into the same system of coordinates (i.e., as-measured);
- in this case, the proposed approach allows to solve one more important problem, namely, to obtain a data base characterizing the behavior of claddings fabricated from different alloys in the system of coordinates (ECR vs. time), as it is evident that both these factors are competitively significant in the consideration of accident processes.

However, earlier work demonstrated that different researchers developed a number of different correlations for the E110 alloy oxidation kinetics [4, 5, 6, 7, 8, 9, 10]. Therefore, it was decided to obtain additional data that would allow us to pick the best estimated correlation from those. The initial program stage would thus include the following:

- provide a sufficient quantity of oxidation tests in the research Program necessary to obtain additional data on the E-110 alloy oxidation kinetics;
- perform oxidation within the range of 5-20% ECR.

The final stage of the scoping tests was dedicated to determination of requirements to be imposed on the types of claddings to be tested, on the oxidation conditions and on the parameters of mechanical tests with regard to such potentially significant factors as:

- oxidation type (single-sided or double-sided);
- oxidation temperature;
- heating and cooling rates;

- cladding material (as-received E110, E110K, E635 tubes, as-received E110 cladding (E110A), irradiated commercial E110 cladding);
- temperature of mechanical tests.

To optimize the quantity of tests, it was decided to divide the Program into three relatively independent stages:

1. Scoping tests.
2. Reference tests.
3. Sensitivity studies.

The goals, tasks and results of scoping tests will be discussed in the section 3.2 of the report. Table 3.1 presents the logical principles laid into the basis of the development of reference tests and sensitivity studies as well as the parameters of these tests.

Table 3.1. The list of tasks and technical requirements

Program stage	Major tasks	Technical requirements	Motivation
1. Reference tests	To determine the zero ductility threshold of E110 cladding as a function of the following oxidation parameters: • cladding heating rate • cladding cooling rate • ECR To find the optimal test mode for the sensitivity studies	1.1. Varied parameters: • heating rate: – 0.5 C/s – 25 C/s • cooling rate: – 0.5 C/s – 25 C/s – 200(170–270) C/s – ECR: 1.2. Fixed parameters: • cladding type: as-received E110 cladding tube • coolant (oxidation medium): water steam (0.1 MPa) • oxidation type: double-sided • hold temperature: 1100 C • combination of oxidation modes: – F/F (fast heating (25 C/s) and fast cooling (25 C/s)) – F/Q (fast heating (25 C/s) and quench cooling (200 C/s)) – S/S (slow heating (0.5 C/s) and slow cooling (0.5 C/s)) – F/S (fast heating (25 C/s) and slow cooling (0.5 C/s)) – S/F (slow heating (0.5 C/s) and fast cooling (25 C/s)) • parameters of mechanical tests: – 20 C – 1 mm/min	• Different heating rates allow to determine the sensitivity of embrittlement phenomena to the initial stage of cladding oxidation history (oxidation in the $\alpha-\beta$ temperature range) • Different cooling rates allow to determine the sensitivity of embrittlement phenomena to: – $\beta \rightarrow \alpha'$ phase transient conditions – thermal stresses under cooling conditions • Five combinations of heating and cooling rates (F/F, F/Q, S/S, F/S, S/F) allow to reveal definitely the impact of appropriate parameters on mechanical properties of claddings

Program stage	Major tasks	Technical requirements	Motivation
2. Sensitivity studies 2.1. Tests with Zry-4 cladding	To perform several oxidation and mechanical tests with the Zry-4 cladding and to compare the obtained results with the published Zry-4 data	2.1.1. Varied parameters: • combination of heating and cooling rates: – S/S – F/F • ECR: 11–12 % 2.1.2. Fixed parameters: • cladding type: as-received Zry-4 • coolant: water steam • oxidation type: double-sided • hold temperature: 1100 C • parameters of mechanical tests: – 20 C – 1 mm/min	• Comparison of Zry-4 data obtained in the frame of this work with the Zry-4 data obtained previously allows to verify the whole set of experimental procedures • Comparison of the E110 and Zry-4 data allows to reveal general differences in the physical behavior of these alloys under oxidation conditions • Two combinations of heating and cooling rates allow to reveal the sensitivity of the Zry-4 cladding to oxidation conditions
2.2. Oxidation type	To perform a single-sided oxidation of E110 cladding and to compare single-sided and double-sided test results	2.2.1. Varied parameters: • ECR range: 7–12 % 2.2.2. Fixed parameters: • cladding type: as-received E110 tube • coolant: water steam • oxidation type: single-sided • hold temperature:1100 C • F/F combination of heating and cooling rates • parameters of mechanical tests: – 20 C – 1 mm/min	• A single-sided oxidation characterizes cladding behavior in the undeformed part of the rod (away from balloon) • French data base on the embrittlement threshold of the M5 alloy has been developed for a single-sided oxidation • Comparative data base (single-sided, double-sided oxidized claddings) allows to estimate the dependence of test results on the oxidation type
2.3. Oxidation temperature	To perform a double-sided oxidation of E110 cladding at different hold temperatures and to reveal the sensitivity of the cladding behavior to this parameter	2.3.1. Varied parameters: • hold temperature: – 800, 900, 950, 1000, 1100, 1200 C • ECR: 6–13 % 2.3.2. Fixed parameters: • cladding type: as-received E110 tube • coolant: water steam • oxidation type: double-sided • F/F combination of heating and cooling rates • parameters of mechanical tests: – 20 C – 1 mm/min	• The E110 embrittlement phenomena could be sensitive to the hold temperature in accordance with the previous test data base • Comparative data base obtained for different temperatures allows to estimate this effect

Program stage	Major tasks	Technical requirements	Motivation
2.4. Alloying composition	To perform a double-sided oxidation of as-received E110K, E635 cladding tubes and to determine the sensitivity of cladding behavior to alloying composition	2.4.1. Varied parameters: • cladding material type: – E110K – E635 • ECR: 7–14 % 2.4.2. Fixed parameters: • coolant: water steam • oxidation type: double-sided • F/F combination of heating and cooling rates • hold temperature: 1100 C • parameters of mechanical tests: – 20 C – 1 mm/min	• The E110K alloy has a high concentration of oxygen (approximately the same as the M5 alloy has). Oxygen is considered as an alloying component in case of concentrations like that • The E635 alloy has Fe and Sn as alloying components (similar to those in the Zirlo alloy) • The comparative data base with E110, E110K, E635 test results allows to understand the sensitivity of oxidation behavior of Zr-Nb alloys to the major chemical components of the cladding material
2.5. Temperature of mechanical tests	To perform ring compression tests at 135 C and several ring tensile tests at different temperatures and to determine the sensitivity of embrittlement phenomena to the temperature of mechanical tests	2.5.1. Varied parameters: • temperature of ring compression tests: 20, 135, 200, 300 C • temperature of ring tensile tests: 135, 200, 300 C 2.5.2. Fixed parameters: • E110 oxidized cladding tubes after a double-sided oxidation at 1100 C and F/F combination of heating and cooling rates	• The first safety embrittlement criterion (17 % ECR) was validated at 135 C (the saturation temperature during the reflood) • Possible earlier embrittlement of the E110 alloy may be associated with the generation of hydrides at low temperatures. But it is known that hydrogen solubility in zirconium alloys is a strict function of the temperature • The comparison of mechanical tests performed at different temperatures allows to reveal the sensitivity of the E110 embrittlement behavior to post-LOCA conditions

Program stage	Major tasks	Technical requirements	Motivation
2.6. Type of mechanical tests	To perform several ring tensile tests, several three-point bending tests and to develop the data base characterizing the representativity of the E110 embrittlement threshold determined due to ring compression tests	2.6.1. Varied parameters: • type of mechanical tests: – ring tensile tests; – three-point bending tests 2.6.2. Fixed parameters: • the E110 oxidized cladding after a double-sided oxidation at 1100 C and F/F combination of heating and cooling rates	• The comparative data obtained for three types of mechanical tests (compression, tensile, bending) allow to estimate the representativity of oxidation limits developed on the basis of ring compression tests.
2.7. Fuel burnup	To perform the scoping tests (oxidation and ring compression) with E110 commercial irradiated claddings refabricated from VVER fuel rods and to compare obtained results with the data base on as-received claddings	2.7.1. Varied parameters: • hold temperature: 1000, 1100, 1200 C • combination of heating and cooling rates: S/S, S/F, F/F • ECR: 6–16 % (as-measured) 2.7.2. Fixed parameters: • cladding type: irradiated E110 cladding made from commercial fuel rods with burnup ~50 MWd/kg U • coolant (oxidation medium): water steam • oxidation type: double-sided • parameters of mechanical tests: – 20, 135 C – 1 mm/min	• The preliminary data base obtained in these tests will allow to estimate high burnup fuel effects in the context of embrittlement phenomena of the E110 cladding

3.2. Methodological aspects of oxidation and mechanical tests

3.2.1. Oxidation tests

In accordance with the review results discussed in Chapter 2 oxidation tests have a long historical tradition based on the following approach:

- oxidation is performed under indirect heating of a cladding sample;
- cladding samples are oxidized and the same samples are used in the mechanical tests;
- oxygen weight gain is determined by weighing the sample during the oxidation process or by weighing the sample before and after the test.

However, the analysis performed on preparing this paper has shown that this approach has several disadvantages, the following two of which are the basic ones:

1. Oxidation of the cladding samples of any length is accompanied by the occurrence of end-effects caused by oxygen (hydrogen) absorption at the end-faces of the cladding sample. These end-effects lead to two consequences of importance:

1.1. These parts of the cladding sample are characterized by a higher tendency to the embrittlement caused by: a) a higher ECR and b) additional stresses in the ZrO_2 layer resulting in an early initiation of the breakaway oxidation;

1.2. The ECR (weight gain) of the oxidized cladding sample is overestimated as the area of the cladding end-faces is not taken into account in the ECR (weight gain) calculations.

It is evident that the results of oxidation and mechanical tests are the more sensitive to the end-effects, the less is the length of the cladding samples. This approach is especially unacceptable for E110 claddings as the end-effects intensify the development of the breakaway phenomena.

Besides, the employment of short cladding samples extends the duration and labour-intensiveness of the investigation, on the one hand, and restricts the opportunity to perform other types of tests (except for mechanical ones) with oxidized samples, on the other hand.

2. Determination of the weight gain by measuring the difference in the sample weight before and after oxidation is quite an undesirable procedure for alloys susceptible to such effect as spallation of ZrO_2. This method application for such alloys leads to the underestimation of the actual weight gain.

Basing on this analysis results, on technical requirements presented in Table 3.1, the following major methodical problems have been formulated:

1. To develop the facility and procedure necessary for oxidation of the cladding sample 100 mm long;
2. To develop the experimental procedure independent of end-effects and ZrO_2 spallation and flaking off to determine the ECR (weight gain).

A brief description of this work results is presented in the following sections.

3.2.1.1.Test samples and oxidation apparatus

Fig. 3.1 illustrates the appearance of test samples developed for this program.

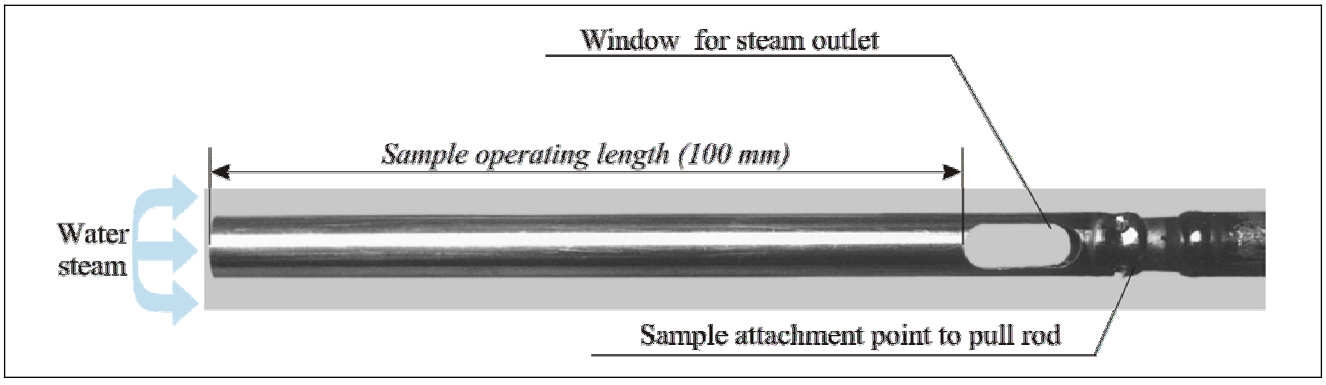

Fig. 3.1. Schematics of the cladding sample

The sample shown in Figure is intended for the double-sided oxidation. The sample for single-sided oxidation had no window for steam outlet and, besides, the sample bottom end was plugged. The sample was oxidized in the facility the basic diagram of which is demonstrated in Fig. 3.2.

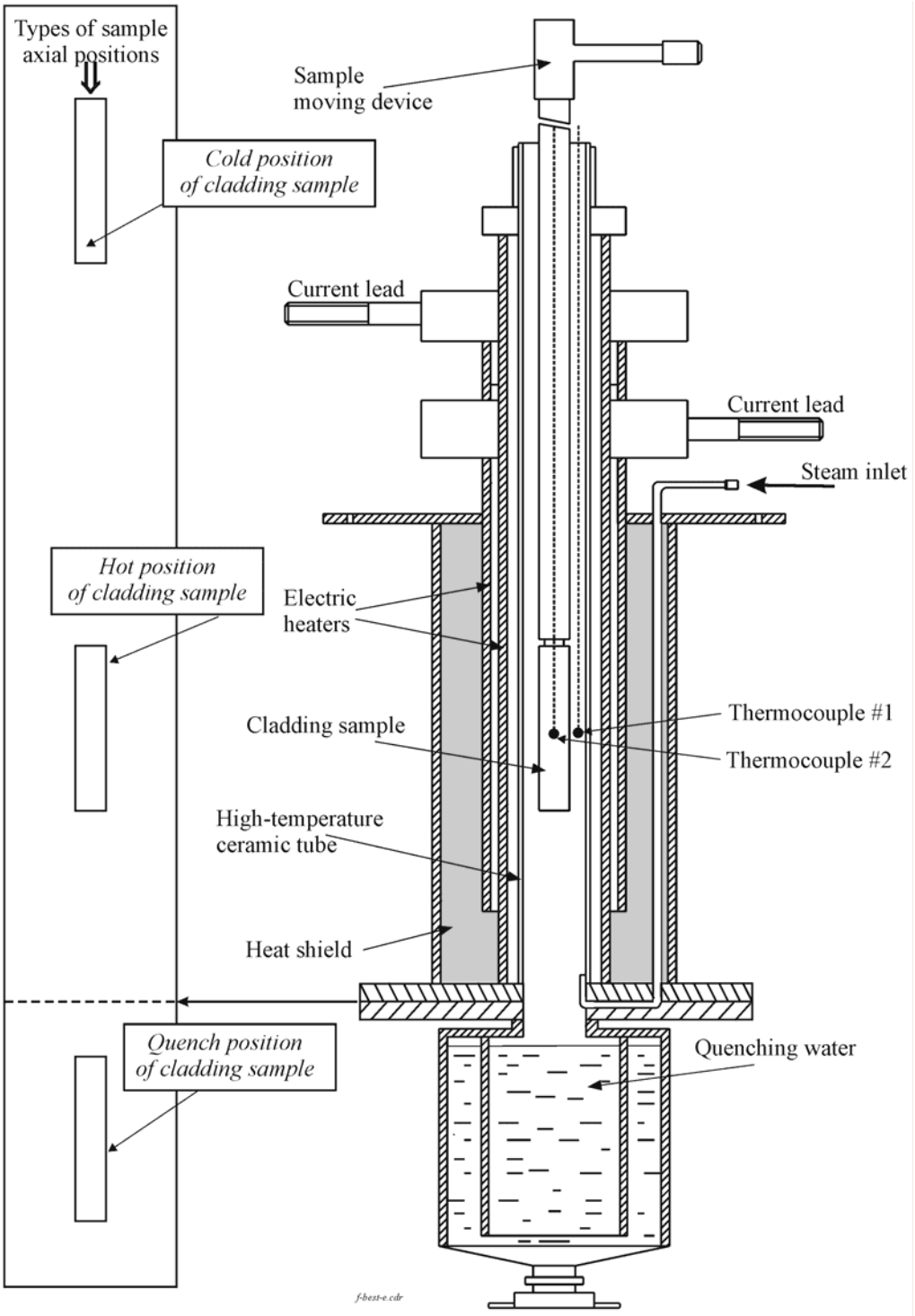

Fig. 3.2. Oxidation test apparatus

Description of the facility and procedures employed for the oxidation of samples are described in more detail in Appendixes A–1, A–2. Parameters of all types of the cladding samples used in this work are presented in Appendix A–3. Results of scoping tests performed to characterize the temperature distribution in the cladding sample are given in Appendix A–4. In accordance with the Program of research, the oxidation facility provided for the following combinations of heating and cooling rates: S/S, S/F, F/S, F/F, F/Q, where S is slow, F is fast, and Q is quench. Fig. 3.3 demonstrates typical examples for the temperature histories for these combinations. p.3.8. It should be noted also, that the preliminary heating of cladding samples to 150 C was performed with the argon flow, and the further heating was performed with the water steam flow.

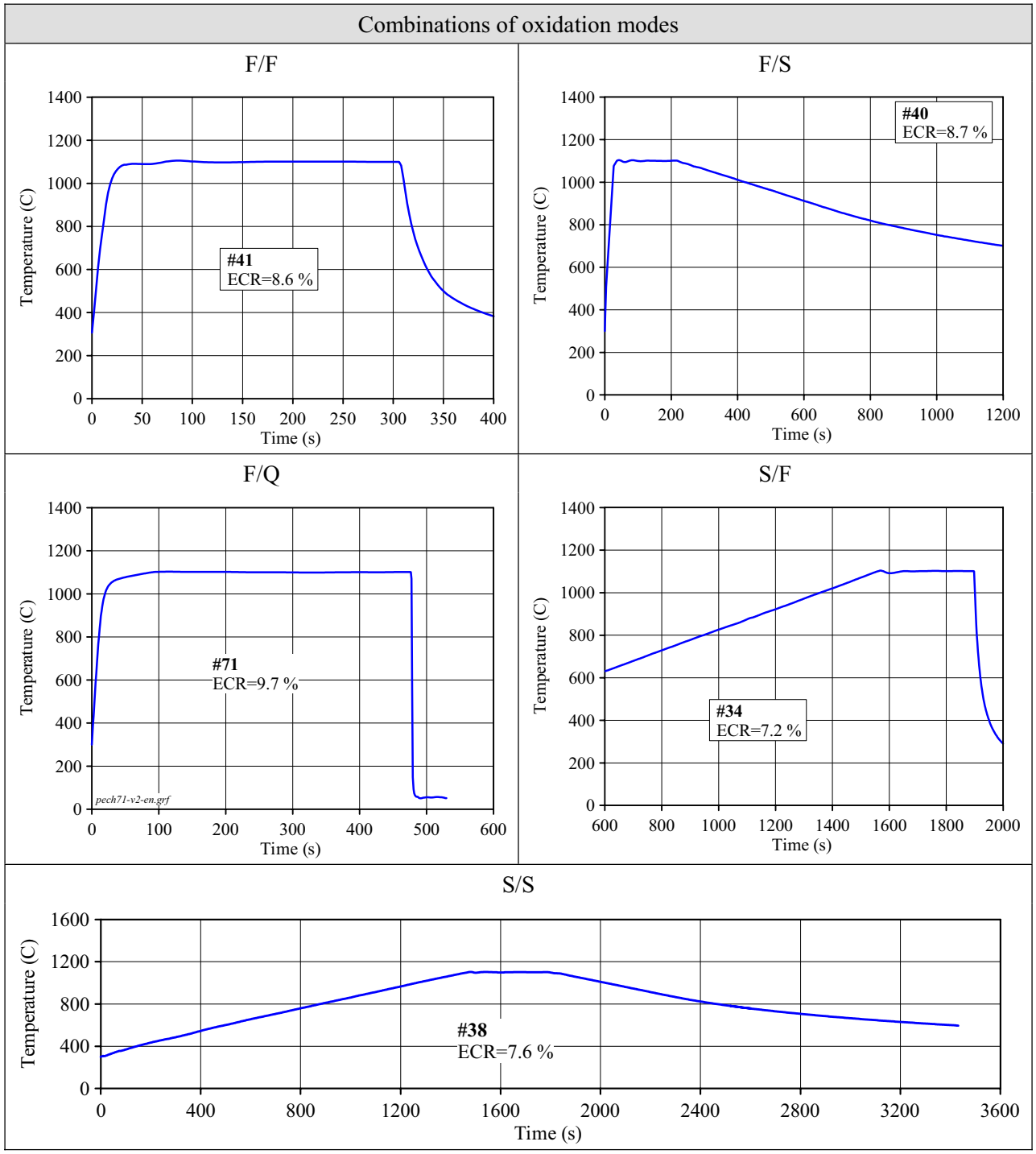

Fig. 3.3. Types of temperature histories for different combinations of heating and cooling rates

Appendix A–5 contains the description of the method for the ECR determination. Major provisions of the method developed in the frame of this work may be characterized by the following way:

$$\Delta W_o = \Delta W_\infty - \Delta W_e,$$

where ΔW_o – the cladding oxygen weight gain obtained during the oxidation test (mg/cm^2);

ΔW_∞ – the oxygen weight gain calculated for the case with the cladding oxidation during the infinite time (full transformation of Zr-1%Nb to ZrO_2 and Nb_2O_5 oxides) (mg/cm^2);

ΔW_e – the oxygen weight gain necessary to oxidize the metallic part of the cladding remaining

after the oxidation test to the stoichiometric oxide.

The concept of this method consists in the fact that a new experimental procedure named the "extra oxidation" is introduced in addition to the oxidation test. This procedure includes the following stages:

- a ring sample (with the measured length) cut out from the oxidized cladding sample of the initial length 100 mm is located into the crucible of the oxidation facility;
- the crucible with the ring sample is weighed;
- the extra oxidation of the ring sample is carried out up to the complete oxidation of a metallic phase and the generation of a stoichiometric oxide;
- the crucible with the extra oxidized ring sample is weighed and oxygen weight gain obtained during the extra oxidation (ΔW_e) is determined.

Thus, the oxygen weight gain during the oxidation test is determined as the difference between the theoretical value of weight gain necessary for the complete oxidation of Zr-1%Nb ring sample (ΔW_∞), and the measured weight gain after the extra oxidation procedure (ΔW_e). The introduction of this procedure for the weight gain determination and employment of a long (100 mm) cladding sample for the oxidation tests allowed to solve the following urgent investigation problems:

- to fabricate several ring samples for mechanical tests from one oxidized sample;
- to perform mechanical tests of ring samples at different temperatures;
- to fabricate special samples from the same oxidized sample for metallographic investigations, fractography research, hydrogen content measurement, scanning electron microscopy examination (SEM), transmission electron microscopy examination (TEM).

Fig. 3.4 presents the major provisions for experimental procedures with cladding samples.

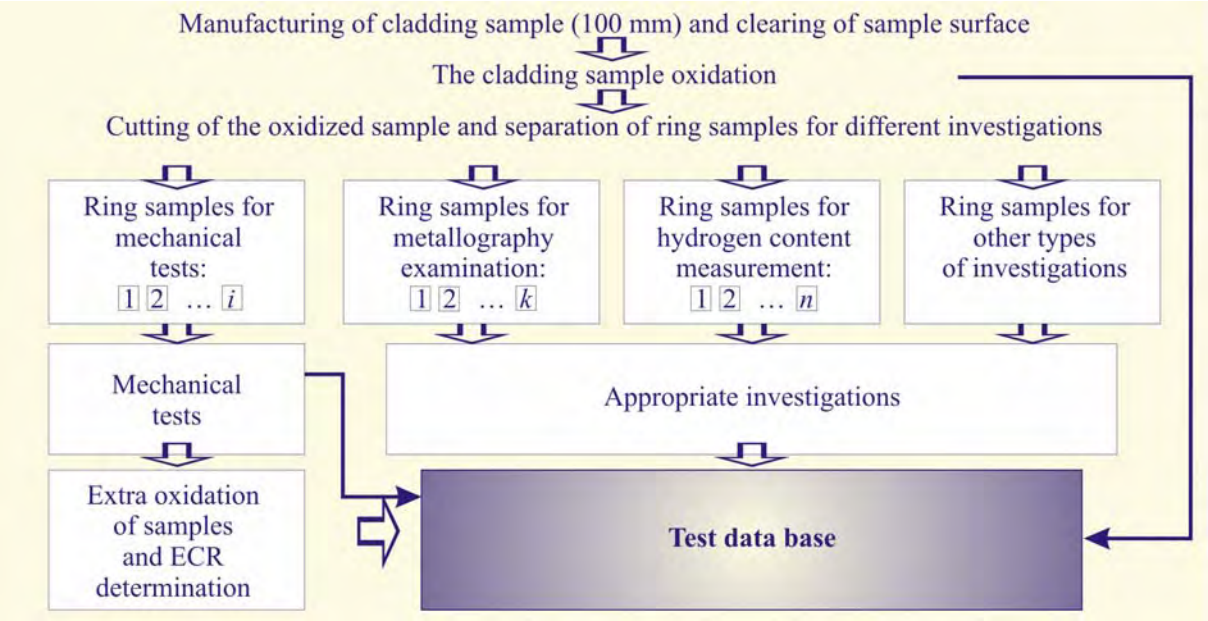

Fig. 3.4. Development of the data base with test results

The procedure developed for mechanical tests is described in the following paragraph. Other special procedures are characterized in Appendix A–6.

3.2.2. Mechanical tests

In accordance with the program, three types of mechanical tests were provided to assess the mechanical behavior of the E110 oxidized cladding:

1. Ring compression tests.
2. Ring tensile tests.
3. Three-point bending tests.

In this case, ring compression tests were considered as the basic type of mechanical tests. And two other types of tests were intended to assess the representativeness of the obtained data base.

3.2.2.1. Ring compression tests

The procedure of ring compression tests may be schematically described in the following way (see Fig. 3.5):

- an oxidized ring sample is located in the test machine;
- a ring sample is compressed at the constant rate of cross-head displacement;
- the load-displacement diagram is noted during the test.

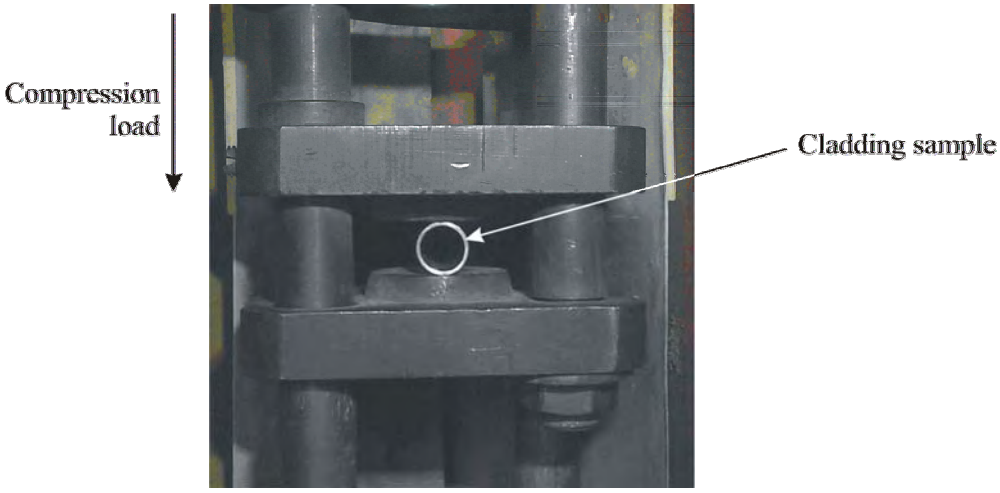

Fig. 3.5. Test machine for ring compression tests of oxidized cladding samples

As it was already mentioned above, this method is not used (as a rule) for the measurement of mechanical properties. However, it allows to determine that the threshold state of oxidized metal at which the cladding failure takes place without macroscopically significant plastic strain. This cladding material may be considered brittle. Accordingly, the ECR of this material is regarded as the cladding embrittlement threshold.

The analysis of previous approaches used to determine the embrittlement threshold of zirconium claddings on the basis of ring compression tests (see Chapter 2) allowed to reveal the following general problems:

- cladding samples of different length (6–30 mm) were used for these tests;
- the standard procedure for the processing of load-displacement diagrams was not developed;
- the cladding embrittlement threshold was estimated by different methods basing on results of ring compression tests;
- the organization of previous data into the summarized data base is not possible for any tested alloys (see the additional information presented in section 3.3.2).

Therefore, thorough development and validation of the procedure for ring compression tests were the most important tasks in this work.

A real load-displacement diagram based on the ring compression test of the E110 oxidized cladding allows to illustrate the above mentioned problems more obviously (see Fig. 3.6)

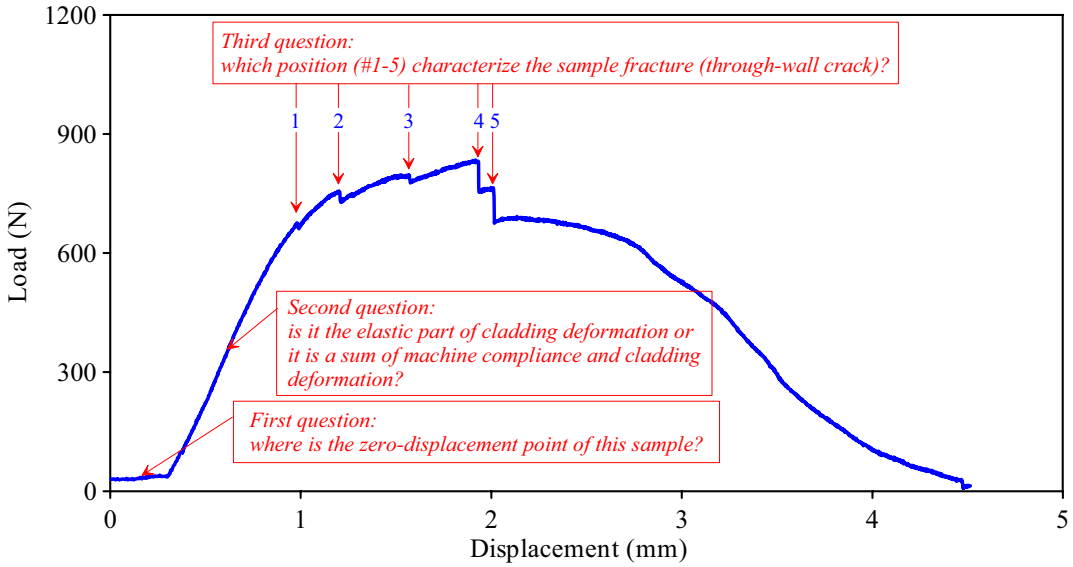

Fig. 3.6. The as-measured load-displacement diagram of the E110 oxidized cladding sample

The list of three questions formulated in Fig. 3.6 should be added with the fourth one: what is the impact of the ring sample length on the parameters of the load-displacement diagram? To find answers to these questions, the program of scoping mechanical tests was worked out the major tasks of which were as follows:

- the determination of an effective elasticity modulus for the ring sample;
- the development of the processing procedure for as-measured load-displacement diagrams;
- the sensitivity studies to validate a standard length of the ring sample;
- the development of a special data base necessary to determine the relationship between the cladding fracture and load-displacement response.

The first step of this work was devoted to the transformation of the as-measured load-grip displacement diagram into the standard form using (for each tested ring sample) the procedure of the zero-displacement point determination in accordance with the approach presented in Fig. 3.7.

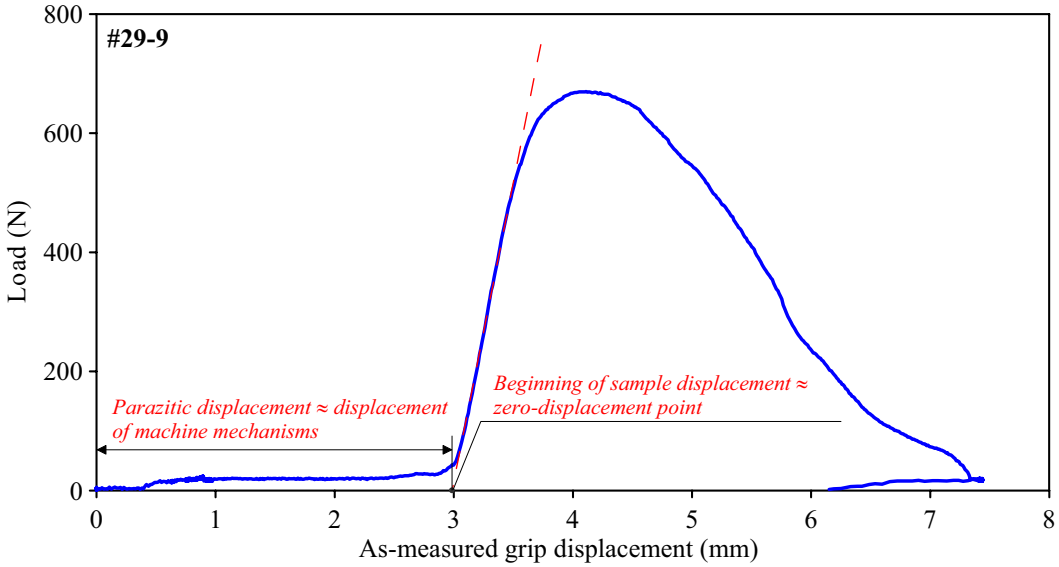

Fig. 3.7. Procedure for the determination of the sample zero-displacement point

After that, special scoping tests were performed to determine the verification data characterizing Young's modulus of the cladding ring sample. It should be noted that the compression diagram consists of two portions:

1. The portion of the sample elastic deformation with the linear relationship between the load and displacement.
2. Nonlinear portion characterizing the plastic component accumulated in the total deformation of sample. The effective modulus of elasticity is employed in the uniaxial mechanical tests to determine the plastic component of a total elongation.

However it is known that the ring sample compression induces not only the compression and tensile stresses but also bending stresses that are distributed along the sample perimeter in the compound way. In this case, it should be pointed out that the investigation of the similar issue performed earlier allowed to develop the procedure of comparison of the effective elastic modulus and the load relief lines [11]. Fig. 3.8 illustrates the results of appropriate scoping compression tests.

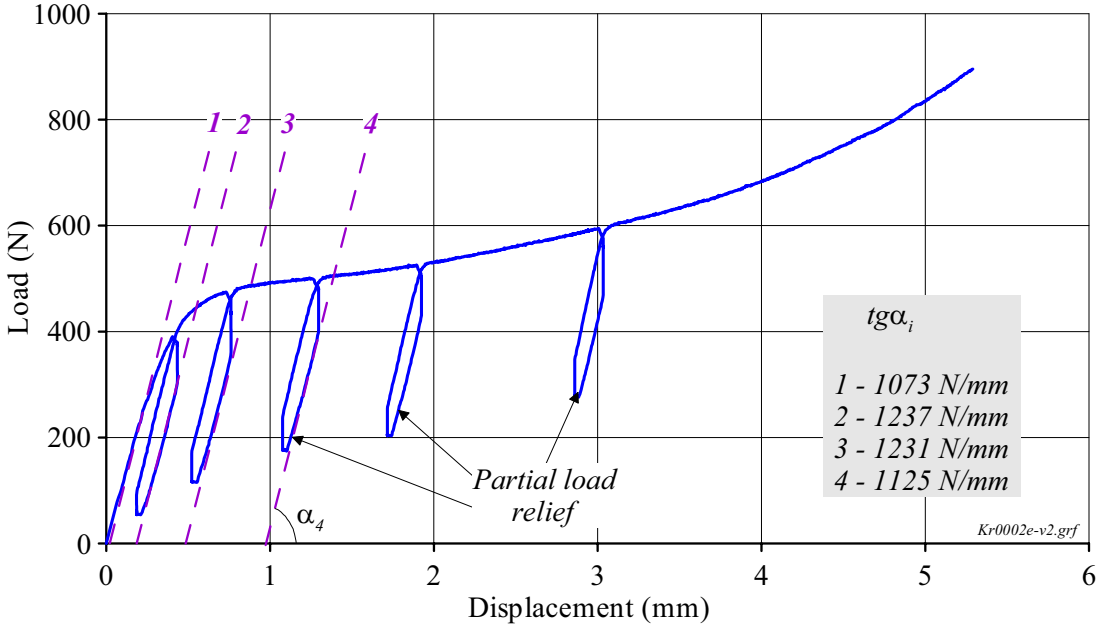

Fig. 3.8. Determination of effective modulus of elasticity basing on the results of scoping compression tests

The procedure of this test included the compression of the ring sample with the load reduction in several points of the diagram (partial load relief). It is known that the process of the load reduction in the elastic deformation area is described by the similar straight line as that describing the sample compression process. The comparative analysis of the obtained data has shown that the linear portion of the load-displacement diagram characterizes the real elastic deformation of the sample ($tg\alpha_1 \approx tg\alpha_{2...i}$). Thus, this part of the diagram can be used to determine the plastic component of the deformation on the diagram processing.

The next step of the procedure development was devoted to the determination of the parameter characterizing the margin of residual ductility in the oxidized cladding. Fig. 3.9 presents the major provisions of the procedure proposed for this work.

In accordance with this procedure, the cladding strain at the compression was assessed by two parameters:

1. Relative displacement at failure (S_f).
2. Plastic component of relative displacement at failure (S_{pl}).

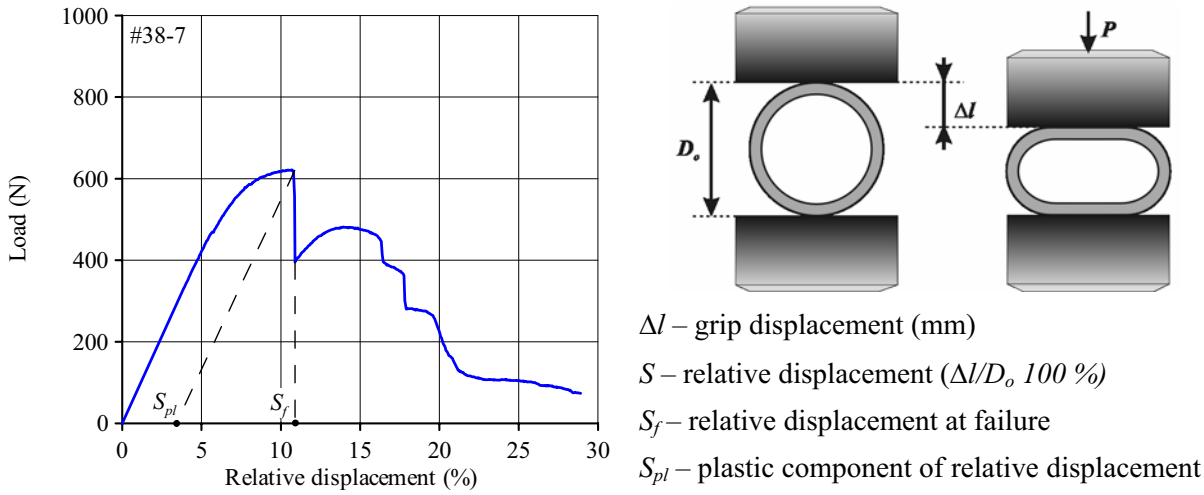

Fig. 3.9. The processing procedure for the load-displacement diagram of the ring compression test of the E110 oxidized cladding

The first of these parameters was used in some of the early ring compression tests [2, 12, 13, 14, 15, 16, 17, 18]. However this approach has several essential weak points:

- the sensitivity of this parameters to the deformation plastic component is reduced as the cladding embrittlement is progressing;
- this parameter does not tend to zero as the cladding approaches the zero-ductility threshold;
- it is impossible to determine the zero-ductility threshold on the basis of the cladding relative displacement as a function of the ECR without an additional relationship connecting these two parameters.

Data presented in Fig. 3.10 illustrate these problems obviously.

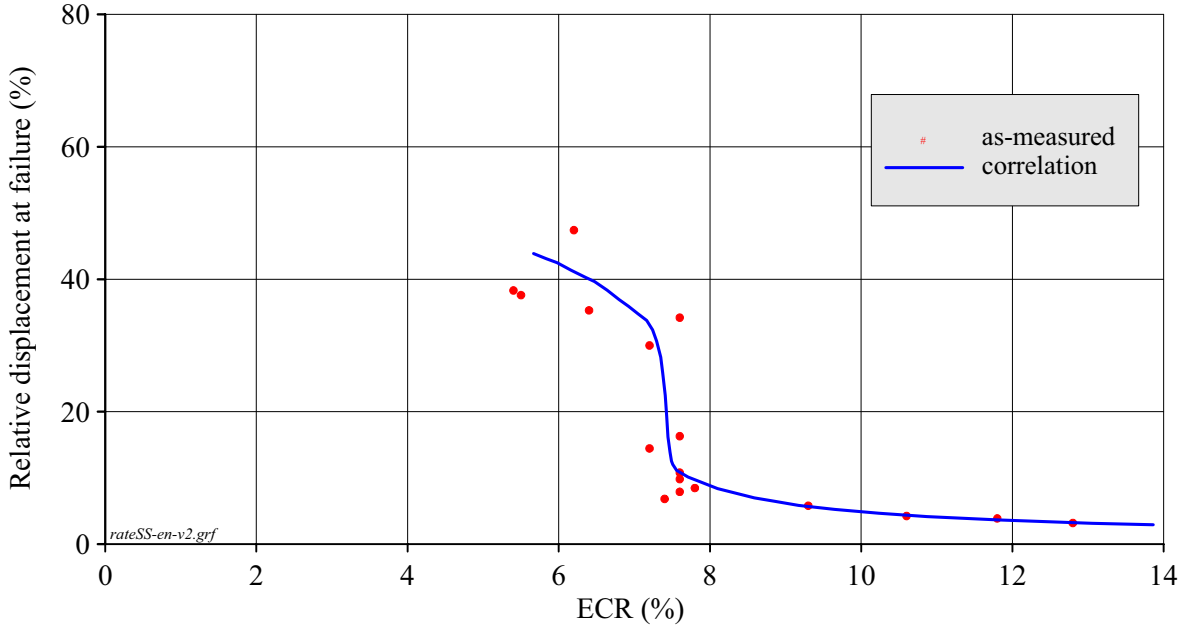

Fig. 3.10. Relative displacement at failure of the E110 cladding after a double-sided oxidation and S/S combination of heating and cooling rates as a function of the ECR

The analysis performed by the report authors to solve these problems has shown that from the physics point of view the macroscopic zero-ductility threshold or, in other words, the macroscopic cladding embrittlement threshold may be defined as such ECR critical value at which the plastic component of the cladding strain at ring compression tests tends to zero. Fig. 3.11 presents the graphic interpretation of this approach for the same data base demonstrated in Fig. 3.10.

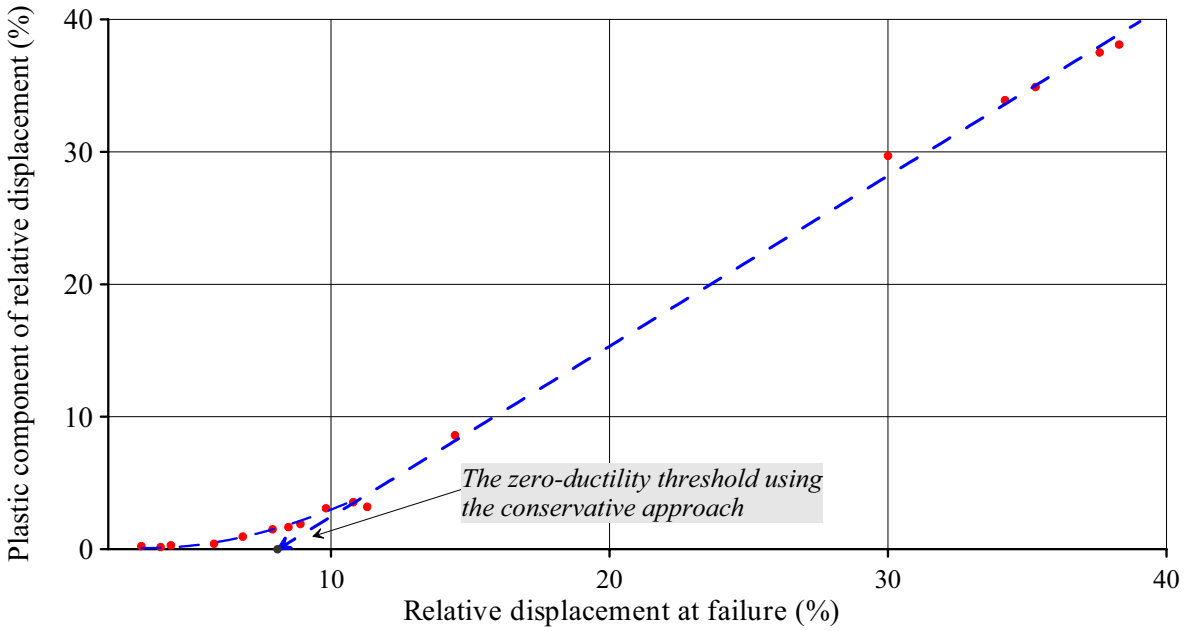

Fig. 3.11. The validation of the procedure for the zero-ductility threshold determination

It should be noted that the term "the plastic component of relative displacement at failure" reflects clearly the physics sense of the appropriate parameter, however, the understanding of this term requires the knowledge of the ring compression test procedure in detail. Therefore, to provide for the understanding of the investigation results by a wide circle of specialists interested in this work, it was decided to replace this term by the term "residual ductility". The term "residual ductility" adequately reproduces the sense of the subject of investigation, on the one hand, and does not require a special study of the procedure for mechanical tests, on the other hand.

The next task of scoping mechanical tests was devoted to the development of the comparative data base for the assessment of sensitivity of the test results to the sample length. The appropriate tests were performed with ring samples the length of which was varied from 8 up to 25 mm. Two oxidized samples 100 mm long were selected for these tests:

- the first sample was characterized by a high margin of residual ductility;
- the second sample was practically brittle.

Fig. 3.12, Fig. 3.13 show the results of these scoping tests.

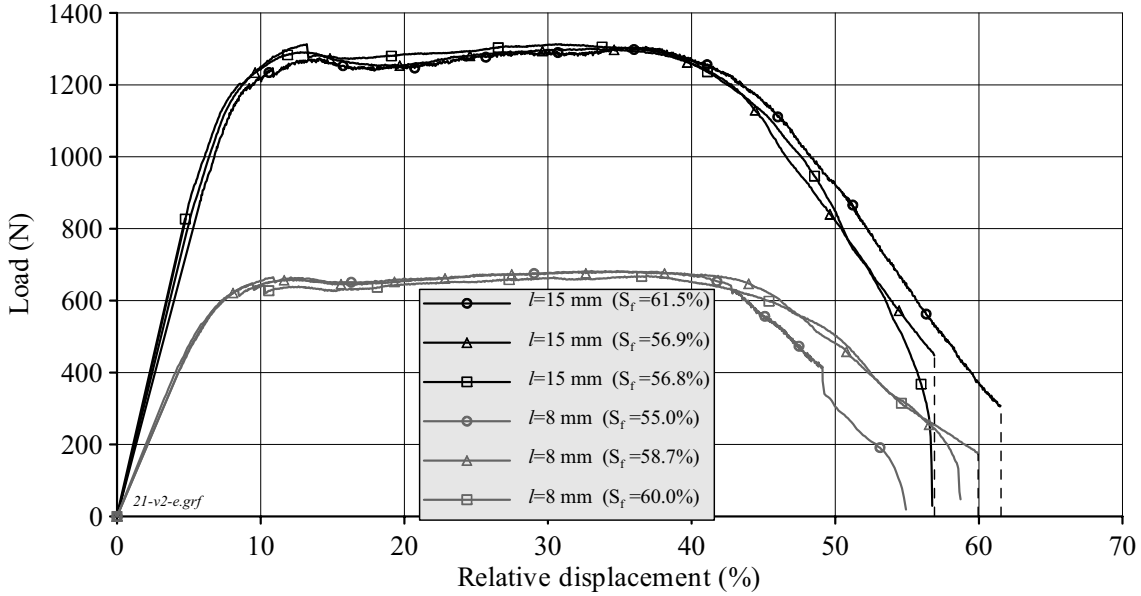

Fig. 3.12. Sensitivity of a relative displacement at failure to the ring sample length for the ductile sample

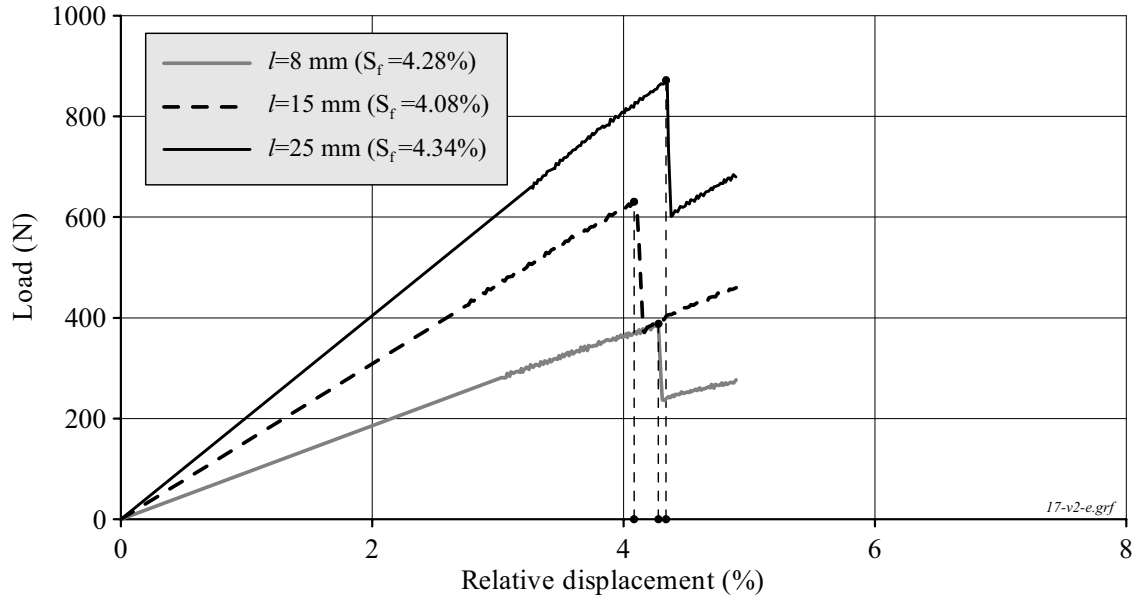

Fig. 3.13. Sensitivity of a relative displacement at failure to the ring sample length for the brittle sample

The analysis of obtained data has allowed to make the following practical conclusion: the relative displacement at failure is independent of the ring sample length. In this case, the increase of the effective modulus of elasticity and maximum load with the sample elongation is quite natural because this effect is explained by a higher stiffness of longer samples. However, it should be pointed out that this conclusion might not be applied to the case when samples of different length were oxidized. As it was already stated, the mechanical behavior of these samples is complicated by the occurrence of end effects (if end parts of oxidized sample were not cut).

The final task of this stage of work was formulated as follows: to develop the experimental data necessary to identify the cladding fracture in load-displacement diagrams obtained from ring compression tests. The appropriate analysis showed that in spite of the evident importance of this issue, the purposeful studies of this subject were performed in neither of the previous programs. The main point of the problem under discussion may be illustrated by the examples presented in Fig. 3.6 and Fig. 3.14.

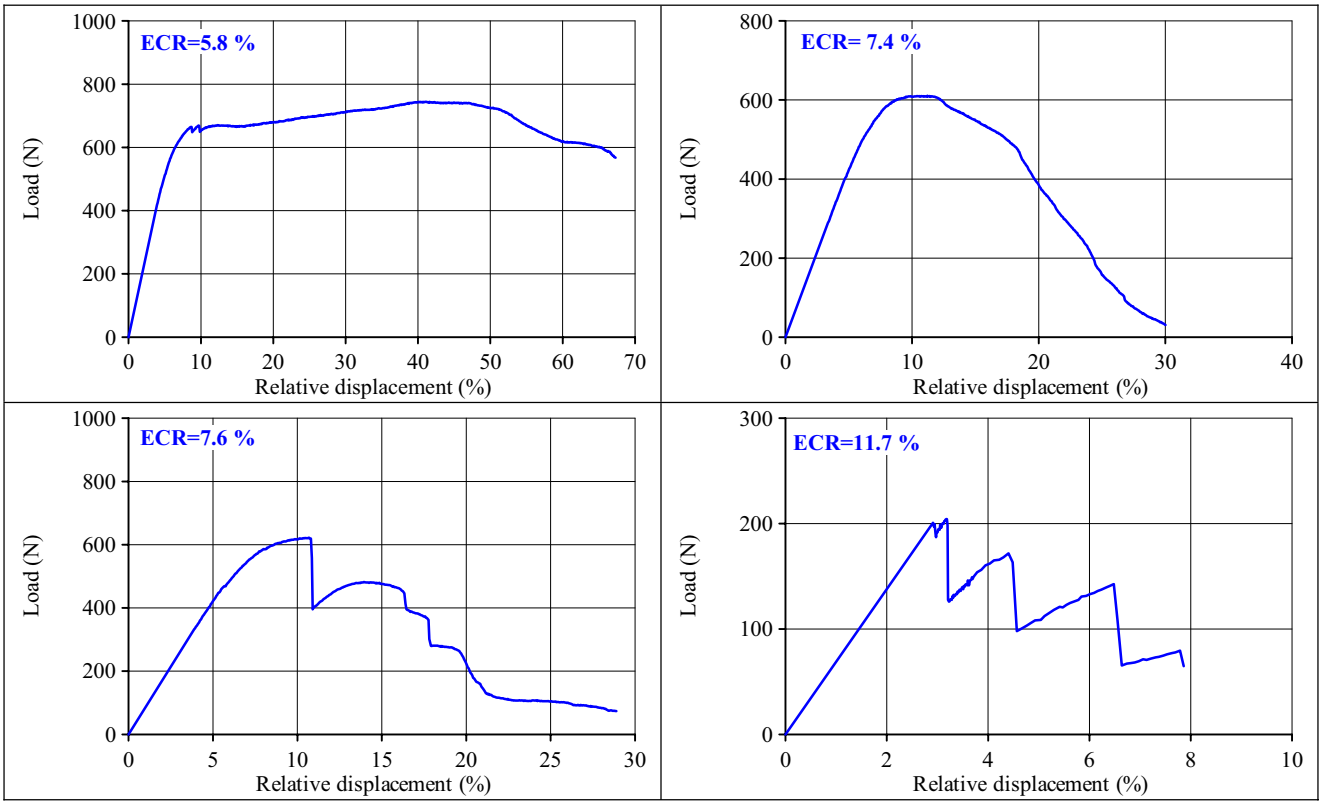

Fig. 3.14. Typical E110 load-displacement diagrams for different oxidation

The obtained results may be divided into two groups:

1. Diagrams with relatively smooth load variation (two upper diagrams in Fig. 3.14).
2. Diagrams with a sharp drop (20% and more) of load with 2–15 % relative displacement (two lower diagrams in Fig. 3.14 and diagram in Fig. 3.6).

Several special tests were performed to interpret sufficiently diagrams of different types. Metallographic cross-sections were prepared from the samples of high residual ductility (a smooth diagram load-displacement). Besides, reference oxidation tests were performed with the ECR two characteristic levels:

3. ECR=5.8 %. The sample with this ECR has a high margin of ductility.
4. ECR=9.9 %. The sample with this ECR is brittle.

Several ring samples were fabricated from each oxidized sample 100 mm long. After that, ring compression tests were performed in accordance with the following outline:

- the ring sample loading up to the occurrence of the first drop of load in the diagram and termination of this sample test;
- the test of the next sample from this batch up to the occurrence of the second drop of load in the diagram and termination of the test;
- and so on.

This approach allowed to visualize the state of the cladding sample in all characteristic points of load-displacement diagrams. Fig. 3.15 demonstrates a typical appearance and cross-section of tested ring samples with a high ductility margin.

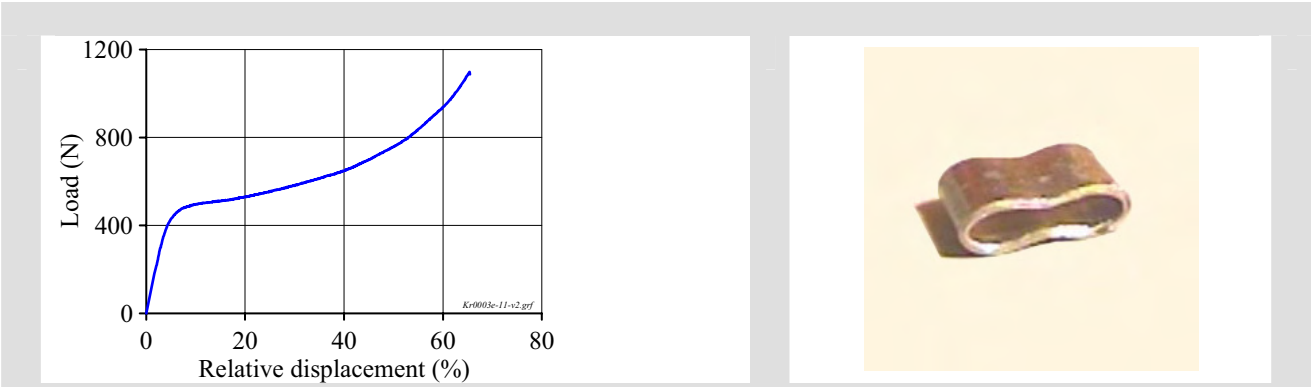

a) unoxidized cladding (appearance of a ring sample after mechanical tests)

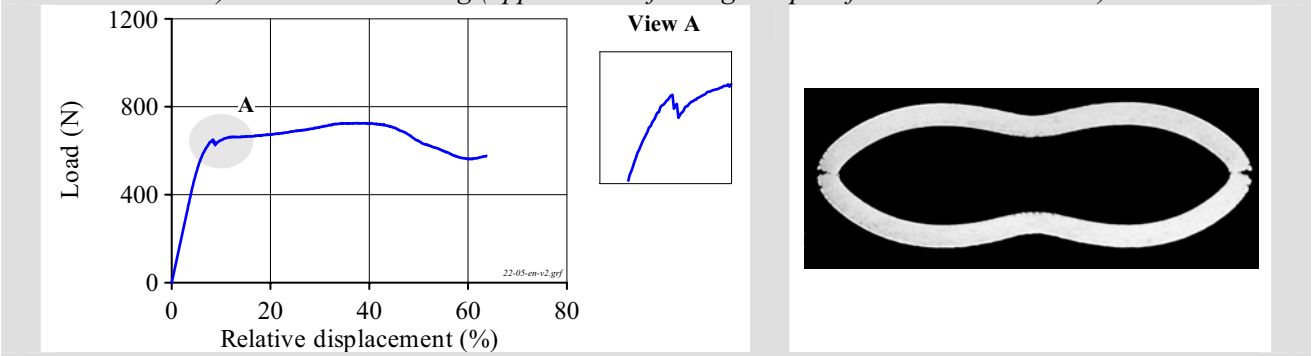

b) oxidized cladding (cross-section of a ring sample after mechanical tests)

Fig. 3.15. Demonstration of the state of ductile claddings after ring compression tests

In accordance with the obtained data, the compression of the unoxidized cladding sample results in its plastic deformation with no indications of failure. The shape of deformed oxidized sample with a high margin of ductility is practically the same as that of the unoxidized sample. However, the comparative analysis of such two phenomena as the drop of load after approximately 40 % displacement and the cross-section view allows to state that two nonthrough sample ruptures appeared in the areas of the maximum tensile stresses. Thus, the low in value and smooth decrease of load indicates the occurrence of a local rupture in the cladding outer layer prior to the β phase. The analysis of the oxidized cladding diagram presented in Fig. 3.15 allows to formulate one more question: what means the local drop of load noted in the diagram on the transfer from the elastic deformation to the plastic deformation (see view A). This question is of sufficient importance because this characteristic area was present in the majority of the load-displacement diagrams.

To answer this question, a series of tests was performed with two rings fabricated from the same sample as the ring shown in Fig. 3.15. Fig. 3.16 presents the results of these tests. The analysis of obtained data shows that the observed load peak is not associated with the cladding failure. This peak indicates the process of formation of microcracks on the cladding surface in the areas of concentrated tensile stresses. The length of these cracks corresponds to ZrO_2 and α-Zr(O) layer thickness. Cross-sections of the ring compressed up to the maximum load (Fig. 3.16b) demonstrate that a growth and some opening of these cracks take place, however, the cladding metal part (the prior β-phase) continues to be deformed plastically.

The next stage of this study was dedicated to the interpretation of load-displacement diagrams having segments with a sharp drop of load. The first type of these diagrams reflects the behavior of oxidized samples with a definite ductility margin (see Fig. 3.6, Fig. 3.14 The lower left diagram). The second type of diagrams characterizes the behavior of a brittle cladding (Fig. 3.14 The lower right diagram). In accordance with this classification, the failure of the following two samples was investigated:

- Zry-4 sample #43;
- E110 sample #25.

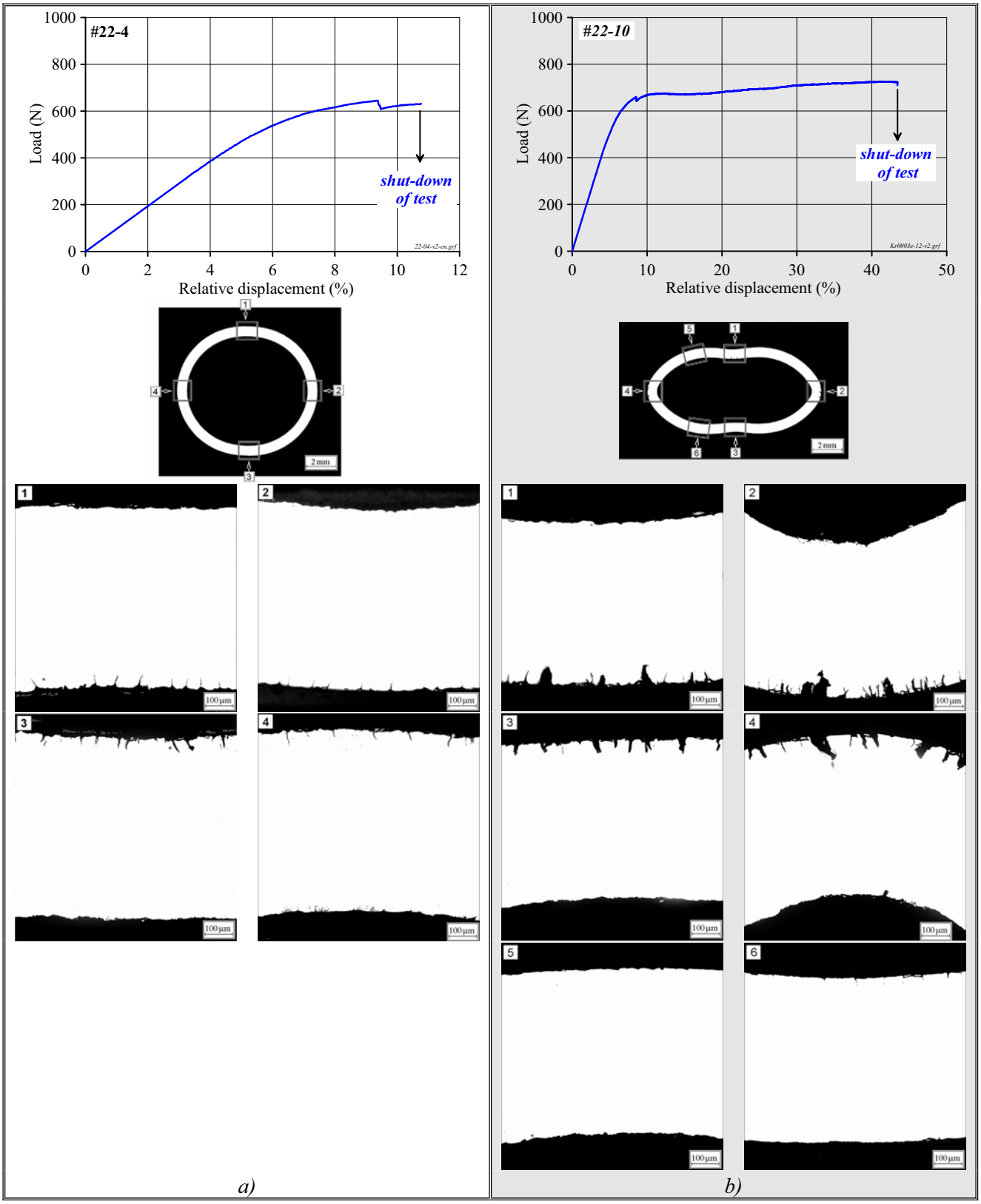

Fig. 3.16. The data base for the interpretation of load-displacement diagrams for oxidized samples with a high ductility margin

The load displacement diagram of Zry-4 samples oxidized up to 11.3 % ECR at S/S combination of heating and cooling rates is shown in Fig. 3.17.

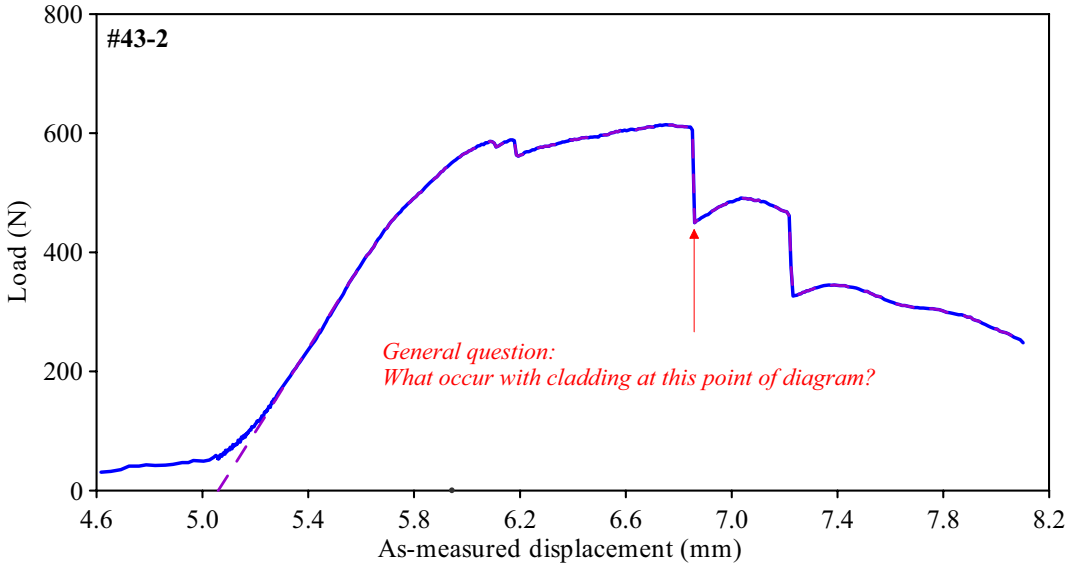

Fig. 3.17. The load-displacement diagram of Zry-4 cladding sample with a partial ductility margin

To get the answer to the question put in Fig. 3.17, additional mechanical tests of two ring samples cut out of the oxidized sample were performed. Fig. 3.18, Fig. 3.19 demonstrate the results of these tests.

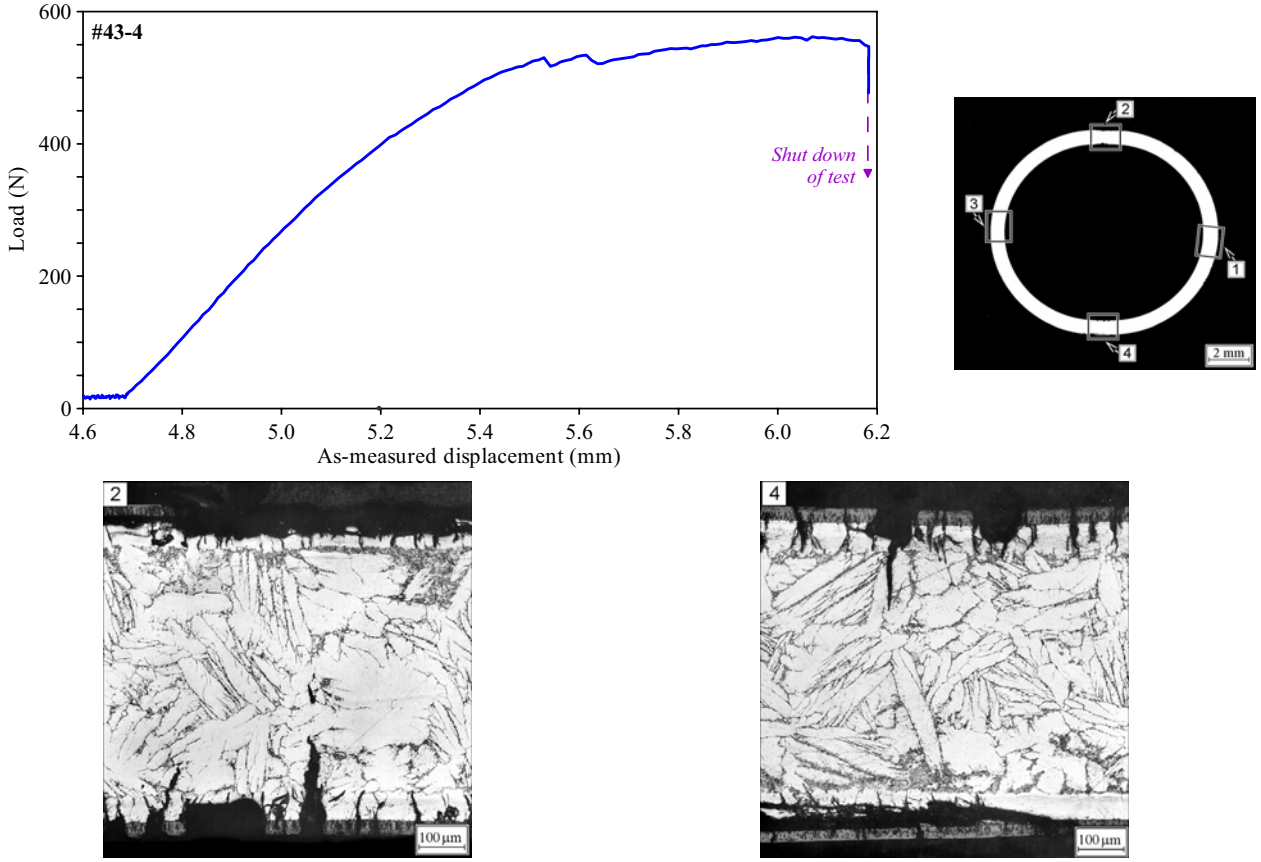

Fig. 3.18. The data base to characterize the mechanical behavior of the cladding sample with a partial residual ductility before the fracture

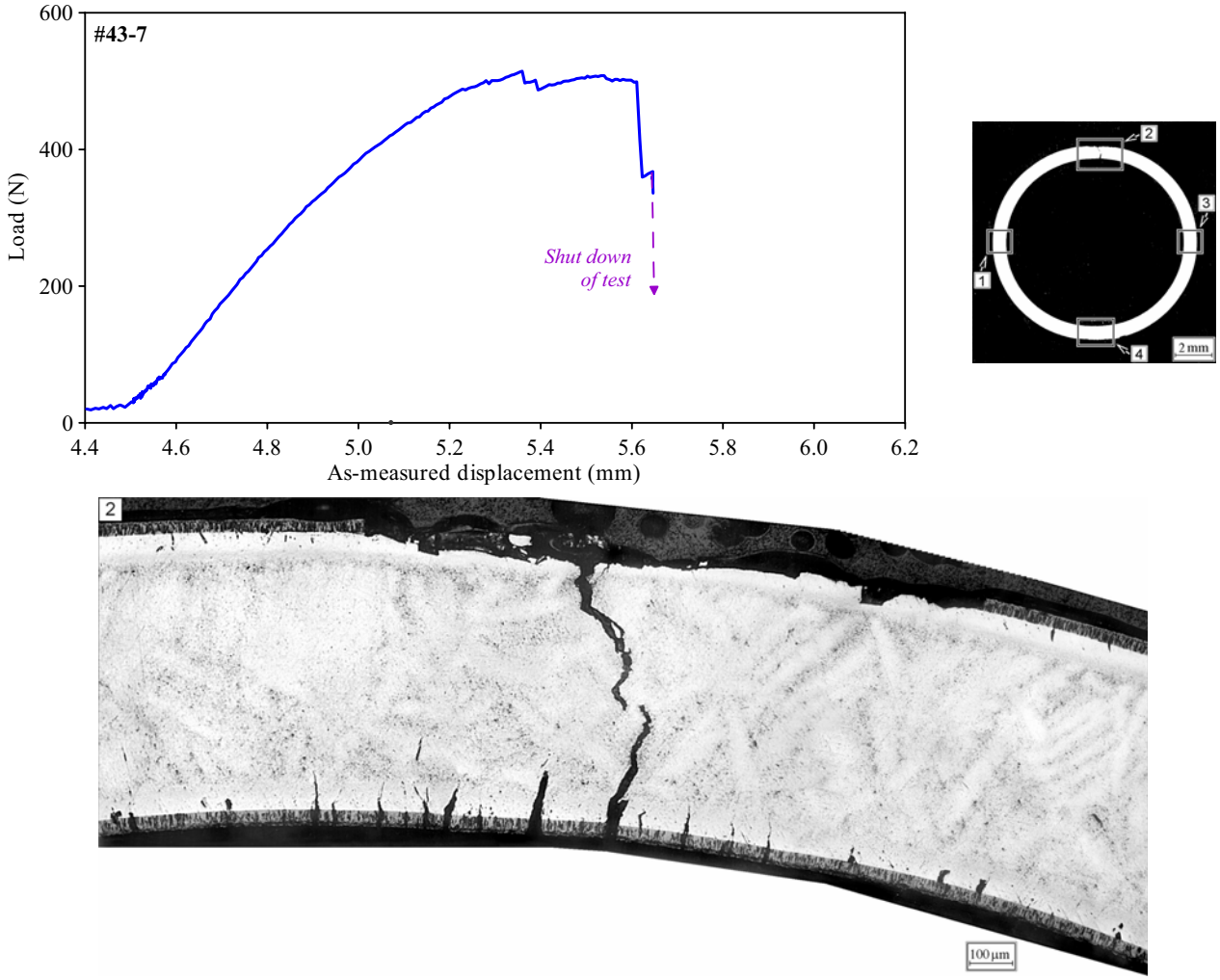

Fig. 3.19. The data base to characterize the mechanical behavior of cladding sample with the partial residual ductility at failure

The compression of the ring sample tested in the first case (Fig. 3.18) was terminated immediately after the sharp load drop was noted. The corresponding sample cross-section made from this ring sample demonstrated that two cracks in prior β-phase were formed on the inside of the sample (that is, on that side which underwent a tensile stress). However, these cracks were not classified as through-wall cracks and, therefore, this test was not accompanied with the cladding failure. The next test was performed with a new ring sample. In this case, the test was terminated at the moment when the load drop not only stopped but the load began to increase again. The analysis of data obtained in this test (see Fig. 3.19) showed that the cladding failure was practically noted. Two cracks formed on the outer and inner sides of the cladding practically joined into the through-wall crack (though, in this cross-section a diminutive bridge of underformed material remained between two cracks).

To supplement the data base necessary to work out the final conclusions on this issue, one more test with the E110 brittle ring sample was performed (see Fig. 3.20).

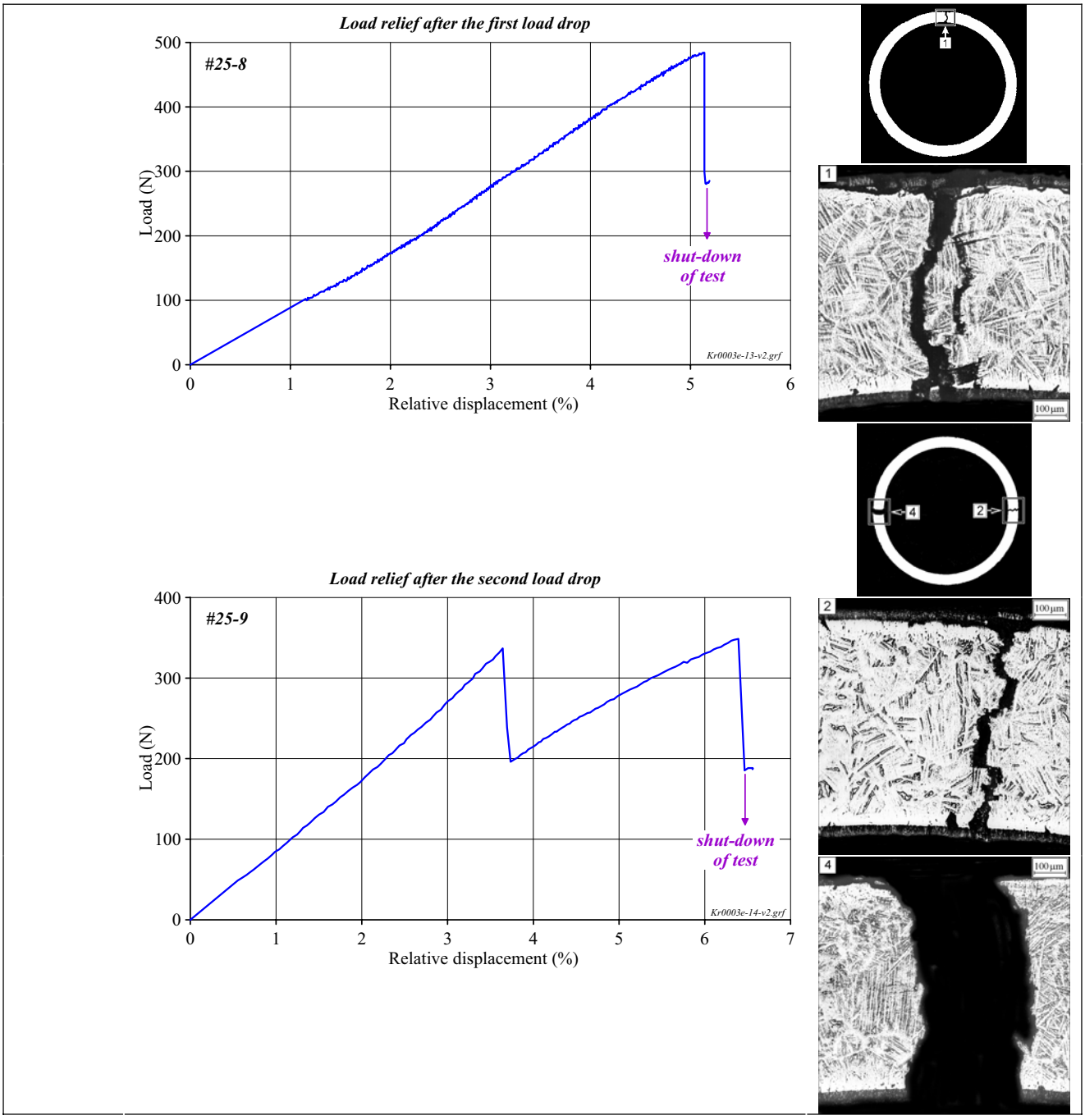

Fig. 3.20. The data base to characterize the mechanical behavior of the brittle ring sample

The analysis of obtained data shows that the first load sharp drop is associated with the formation of the through-wall crack, that is, this point should be qualified as the cladding failure. The second (and the following) load drop indicates the formation of new through-wall cracks in the cladding up to the complete sample fragmentation.

The generalization of all performed investigations allows to make the following conclusions:

- the load displacement diagrams with the monotonic change in the load during the tests (samples with a high residual ductility) are processed using two approaches:

– if the maximum relative displacement is higher than 60 % (see the upper left diagram in Fig. 3.14) it is considered that the sample failure takes place in the point of the sample compression termination (thus, the sample may remain actually unfailed);

– if the maximal relative displacement is less than 60 % (see the right diagram in Fig. 3.14) it is considered that the sample failure takes place at the moment of the load sharp drop.

- the load-displacement diagrams of brittle samples with the low ductility margin (see two lower diagrams in Fig. 3.14) are processed using the following method:

– a local drop of the load (with the value not higher than several tens of newtons) is neglected;

– the moment of the sample failure is determined in the point of the load sharp drop (with the value higher than 100–150 N).

3.2.2.2.Ring tensile tests

Simple ring specimens cut out of the oxidized E110 cladding samples were used for ring tensile tests. Major provisions of these tests were described in [11, 19, 20]. It should be noted that scoping tests necessary to certify the procedure as applied to the oxidized cladding were not provided for in the present research program. Therefore, the obtained results should not be considered as a set of standard mechanical properties for the cladding material. These tests were aimed at the obtainment of a set of experimental data characterizing the tendency towards the cladding ductility reduction as a function of the ECR and at the determination of the zero ductility threshold (the critical ECR). The plastic component of relative displacement (S_{pl}) was determined for each tested specimen in accordance with the procedure presented in Fig. 3.21.

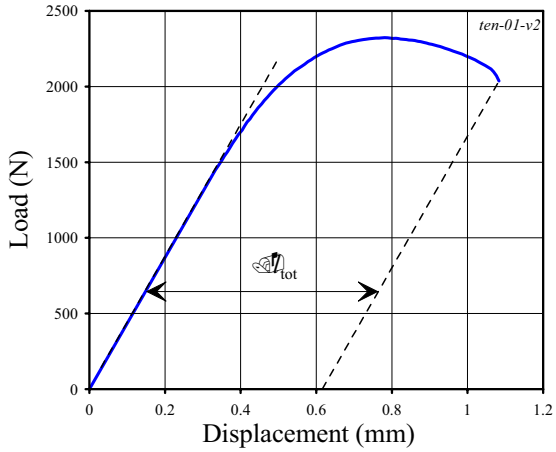

$$S_{pl} = \frac{\Delta l_{tot}}{l_g} 100\ \%,$$

where

S_{pl} – plastic component of relative displacement at failure (%);

Δl_{tot} – total displacement at failure (mm)

l_g – gauge length of a ring specimen (7.85 mm)

Fig. 3.21. Processing of the load-displacement diagram obtained in the ring tensile test of a simple ring sample manufactured from the oxidized E110 cladding tube

3.2.2.3.Three-point bending tests

Three-point bending tests of the oxidized E110 claddings were performed in the universal test machine (1794Y-5) equipped with the device shown in Fig. 3.22.

The oxidized E110 cladding sample 80 mm long was placed on two cylindrical supports of the roller type 5 mm in diameter. The distance between the supports was 70 mm. The third cylindrical roller bearing provided for the impact of the bending load on the cladding sample with the rate of about 1 mm/min. All these tests were performed at 20 C. The load-displacement diagram was recorded during the tests. It should be noted that three-point bending tests of tubular samples were not of the standard type of mechanical tests. Therefore, the experience gained previously in similar tests was specially analyzed [21, 22]. The analysis allowed to formulate the following general requirements imposed on three-point bending tests:

- a roller bearing should be employed as a support and a loading tool to minimize friction during the process of cladding bending;
- the distance between supports must exceed the sample diameter not less than 8–10 times.

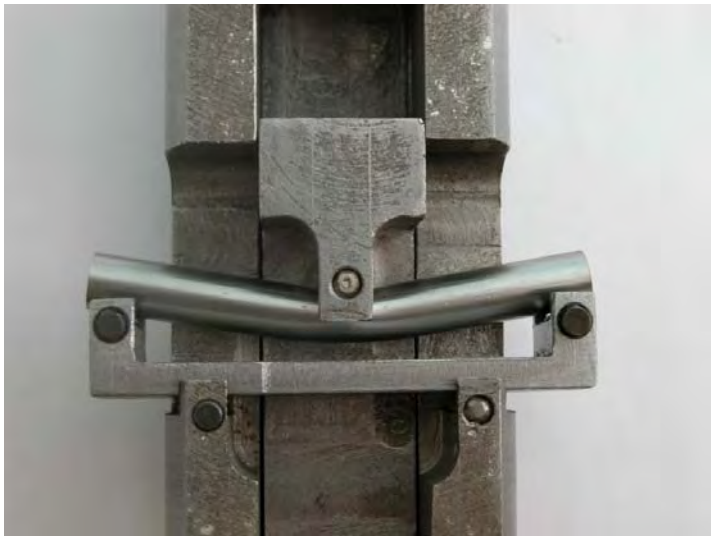

Fig. 3.22. Three-point bending test apparatus

The test apparatus illustrated in Fig. 3.22, complies completely with these requirements. Besides that, this approach is in a good agreement with the configuration of similar tests performed with the M5 alloy samples [23].

The major provisions of the result processing procedure for three-point bending tests are shown in Fig. 3.23.

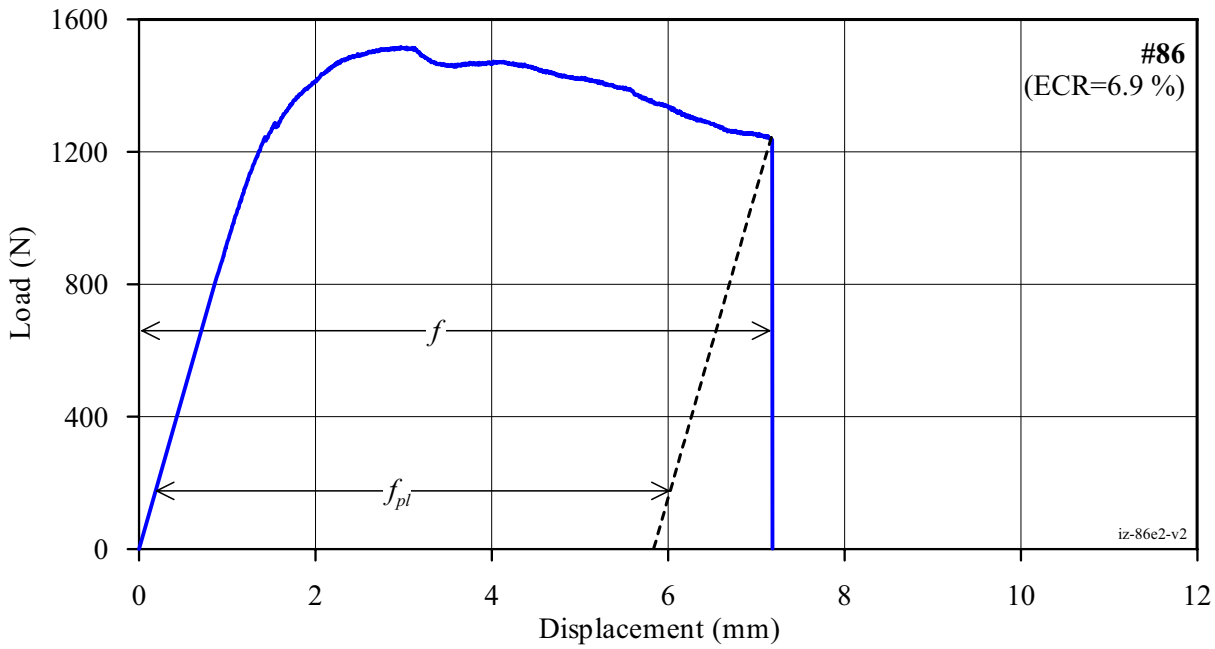

Fig. 3.23. Schematic for the processing of the load-displacement diagram after three-point bending tests

In accordance with the presented scheme, the residual deflection at failure (D_{pl}) as a function of the ECR was used as a result of each three-point bending test.

3.3. Discussion of test results and working out of preliminary conclusions

3.3.1. Reference tests

The goal of reference tests was to determine the dependence of cladding residual ductility on such parameters of the oxidation mode as heating and cooling rates, following which to develop recommendations concerning the oxidation conditions for other stages of the research program. The background of this stage of the work was the following:

- the heating rate defines such processes as the phase transformations ($\alpha \rightarrow \alpha+\beta \rightarrow \beta$) and the diffusion redistribution of alloying and impurity elements in the cladding material, that in its turn predetermines the oxide type (monoclinic, tetragonal) formed on the cladding surface, his protective properties and, as a consequence, H_2 uptake by the cladding material;
- the cooling rate determines specific features of such processes as transition of a high temperature β-phase into low temperature α'-phase as well as the size and distribution of solid hydrides in the prior β-phase of oxidized cladding.

In spite of the fact that the above listed effects were subjected to the attention of many researchers performing similar works, the analysis showed that systematical studies to estimate these effects in the aggregate were not performed. Therefore, the appropriate reference tests were included in this research program in accordance with the following test approach:

- cladding type: as-received E110 tube;
- oxidation type: double-sided;
- isothermal oxidation: 1100 C;
- temperature of mechanical tests: 20 C;
- combination of heating and cooling rates during the oxidation:
  - F/F (fast heating at 25 C/s and fast cooling at 25 C/s);
  - F/Q (fast heating at 25 C/s and quench cooling at 200 C/s);
  - S/S (slow heating at 0.5 C/s and slow cooling at 0.5 C/s);
  - S/F (slow heating at 0.5 C/s and fast cooling at 25 C/s);
  - F/S (fast heating at 25 C/s and slow cooling at 0.5 C/s).

The whole scope of test results obtained due to these tests is presented in Appendixes B, C, D; the organized test results are shown in Fig. 3.24.

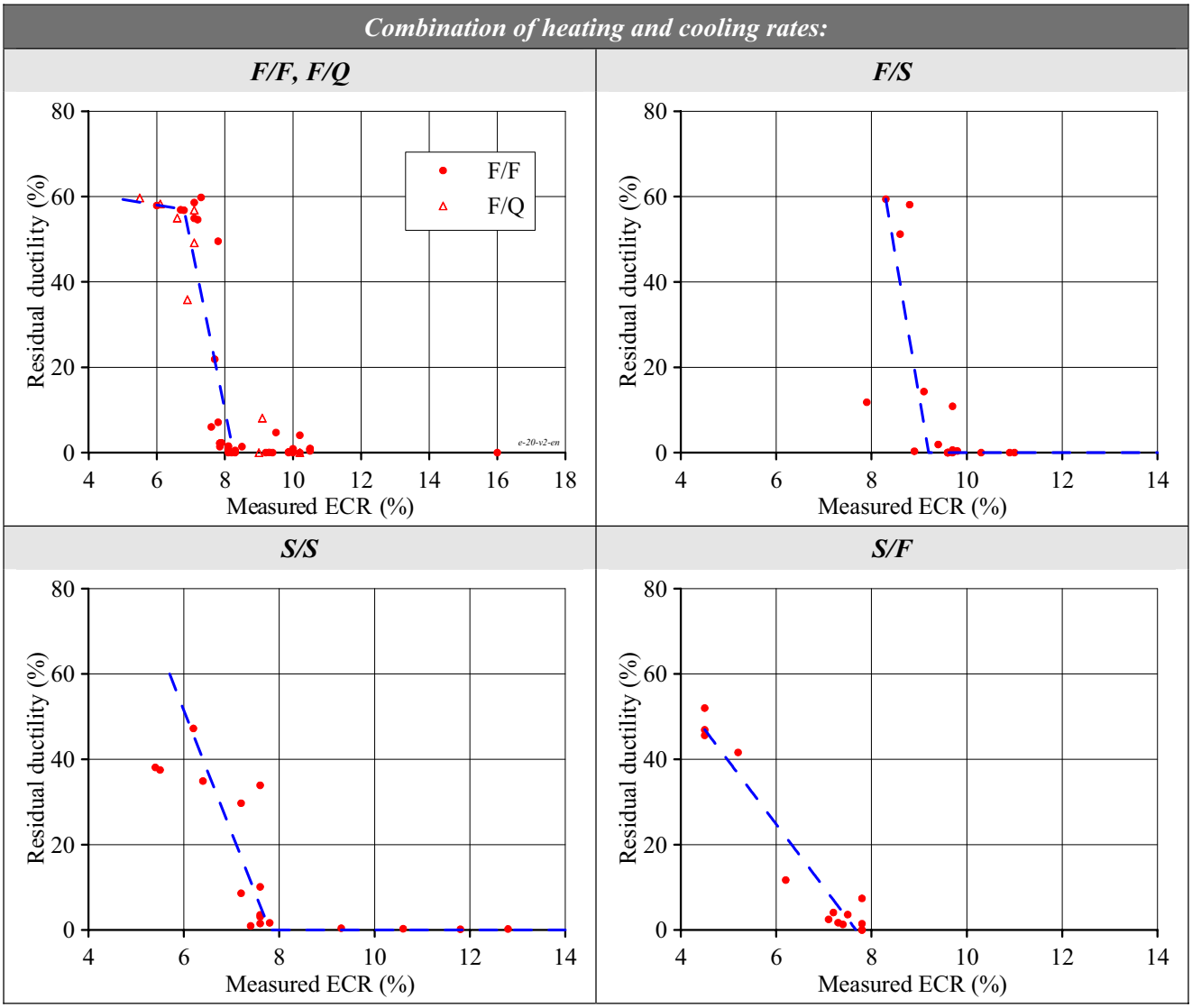

Fig. 3.24. Results of reference tests

The comparative analysis of the mechanical behavior of oxidized E110 claddings after reference tests allowed to reveal the following (see Fig. 3.25):

- the higher the ductility margin in the oxidized cladding, the greater the extent for this margin to be a function of oxidation conditions;
- the less the cladding heating rate and higher the cladding cooling rate, the less degree of oxidation for the proportional decrease of the cladding residual ductility; thus, the decrease of residual ductility down to 40% (approximately 2 times in comparison with the unoxidized cladding) takes place in the following consecution:

– S/F test mode: ECR=5%;

– S/S test mode: ECR=6.3%;

– F/F, F/Q test modes: ECR=7.1%;

– F/S test mode: ECR=8.5%;

- the mechanical behavior of oxidized claddings cooled at 25 C/s and 200 C/s (F and Q) does not differ;
- the closer the cladding is approaching the brittle state, the less its mechanical behavior depends on the studied parameters of the oxidation scenario (see Fig. 3.26) because, apparently, the alloy type is that key factor on which the zero ductility threshold depends.

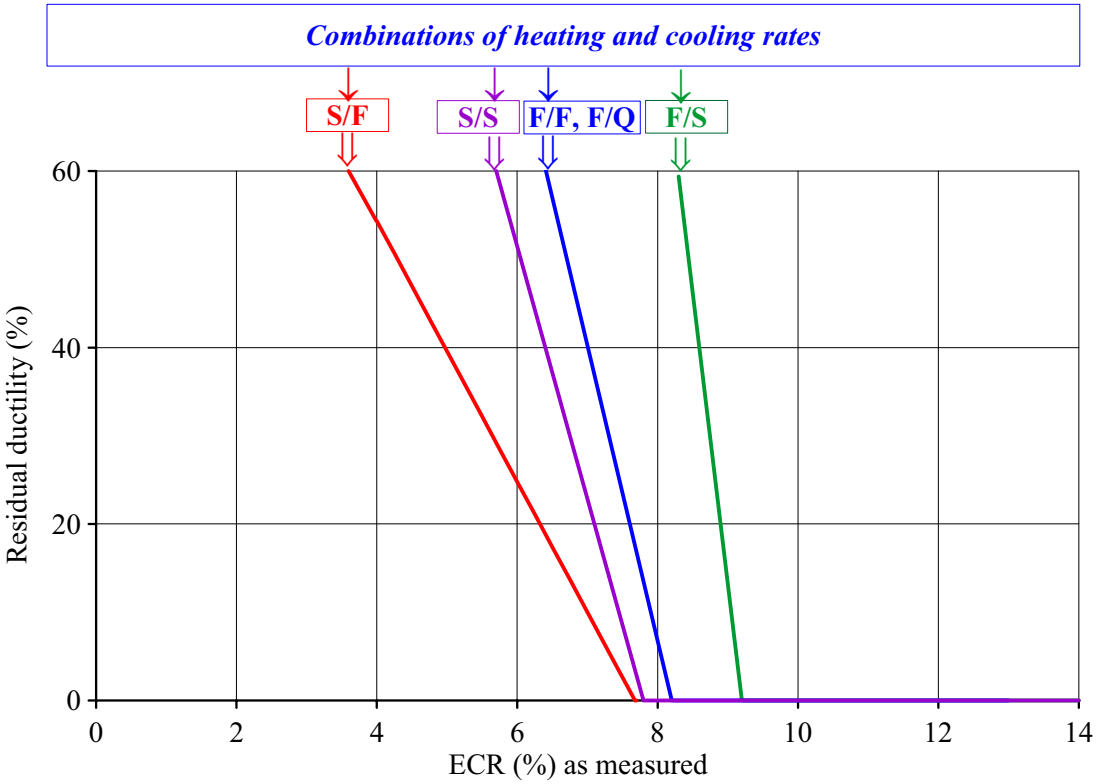

Fig. 3.25. The residual ductility of the E110 cladding vs heating and cooling rates

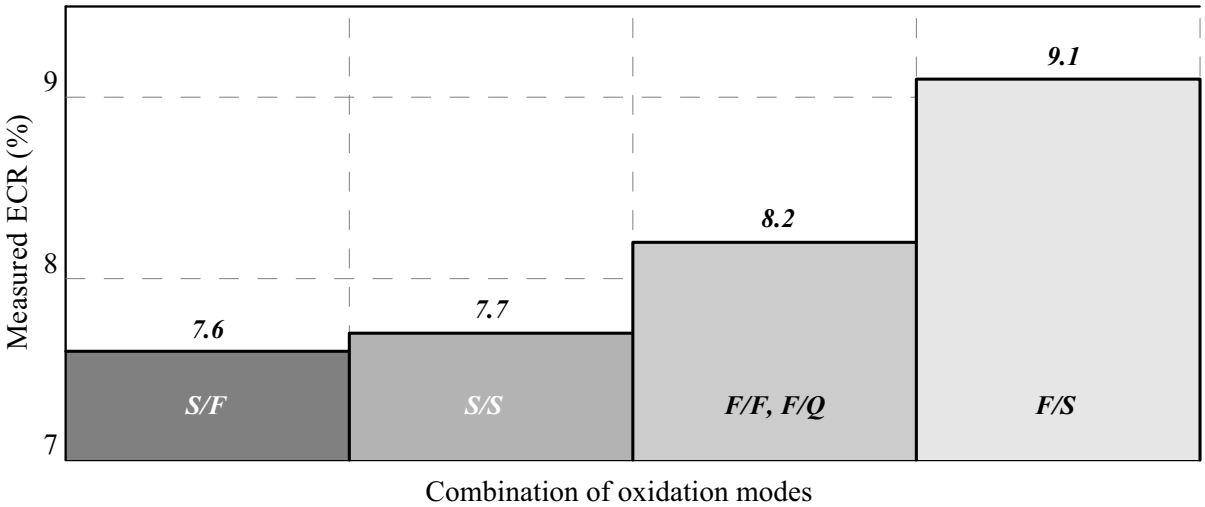

Fig. 3.26. The zero ductility threshold of the E110 cladding vs heating and cooling rates

Thus, the performed reference tests have demonstrated that in spite of the wide range in the variation of heating and cooling rates, the zero ductility thresholds of the oxidized E110 cladding are in the narrow range of ECR (7.9–9.1%). Taking this circumstance into account as well as the fact that slow heating and cooling conditions (used in these tests) are not prototypical for the LOCA analysis and in addition the fact that the difference between the fast cooling and quench cooling was not observed, the following general recommendation was worked out on the basis of reference tests: to perform the oxidation of cladding samples at other stages of the research program at the F/F combination of heating and cooling rates.

3.3.2. The comparative analysis of E110 and Zry-4 oxidation and mechanical behavior

Two cladding samples of Zry-4 alloy were oxidized at 1100 C and F/F, S/S combinations of heating and cooling rates. The oxidation mode with a slow heating and slow cooling was employed to reveal peculiar features in the oxidation of Zry-4 claddings under the most adverse test conditions. The general goals of tests with the Zry-4 cladding were as follows:

- to verify the test procedures and test equipment using the previous test data obtained for the Zry-4 claddings;
- to clarify the major differences in the behavior of the E110 and Zry-4 claddings.

The initial characterization of the Zry-4 cladding and obtained test results are presented in Appendixes A-3, B, G.

3.3.2.1. The verification of test procedures

In spite of the fact that significant efforts have been put into the development and validation of test procedures used for this research, the practical experimental experience shows that the risk of systematical (unaccounted) errors is never too low. Therefore, the only reliable assurance of the fact that these errors are of the acceptable value may be found in the comparison of results obtained in different laboratories employing different experimental apparatus and experimental methods.

The test programs performed in the following countries were selected to compare Zry-4 test results:

- Russia, VNIINM [15];
- Germany, NC Rossendorf [24];
- Hungary, KFKI [25];
- Czech Republic, SCODA-UJP [26];
- France, Framatom [23];
- USA, ANL [27, 28].

The data published for the appropriate tests (table data and numbered graphical output) were used to develop the regression correlations for these six test sets (see Fig. 3.27). The obtained regression correlations are presented in Fig. 3.28.

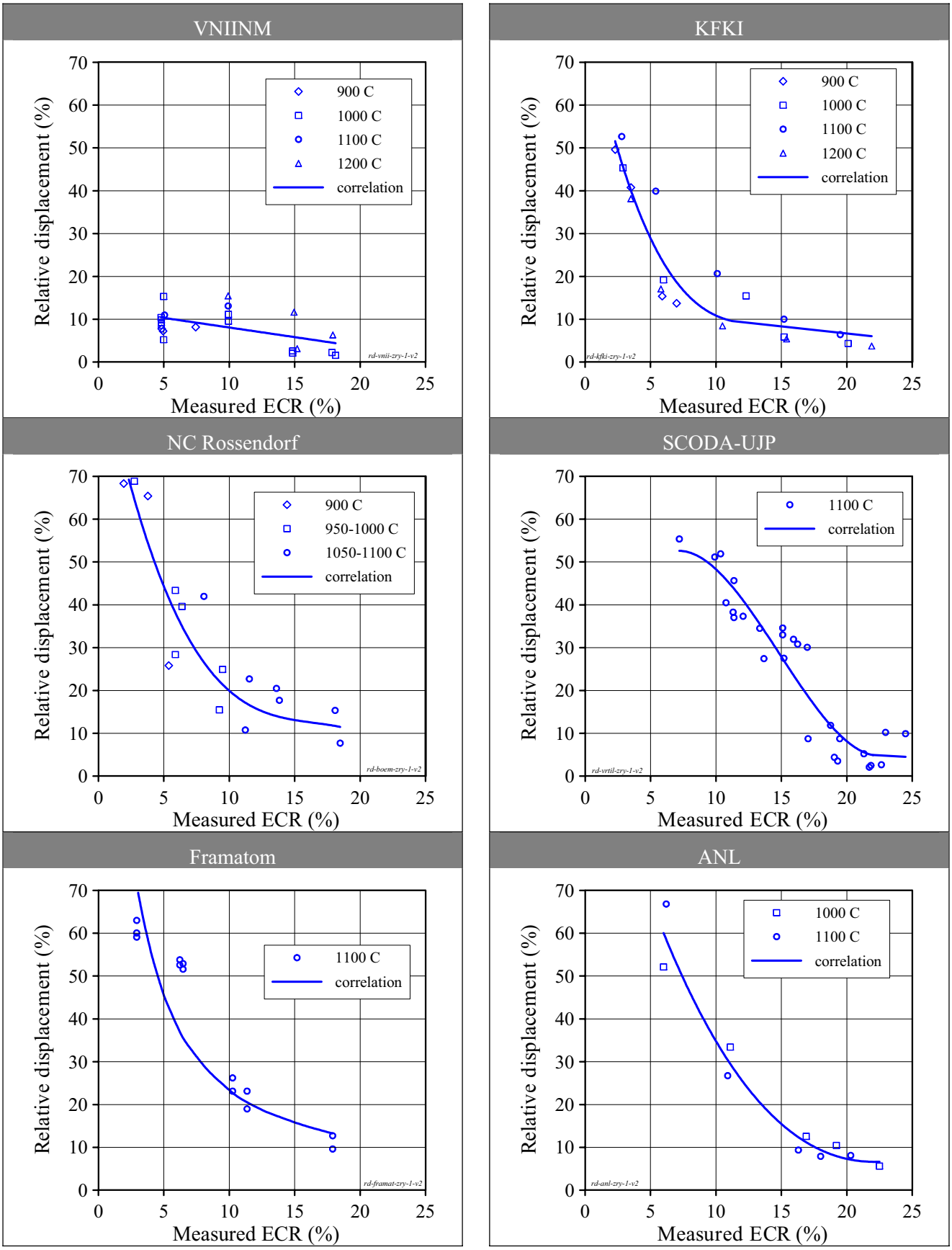

Fig. 3.27. Summary of the ring compression test results performed in different laboratories with the Zry-4 oxidized cladding

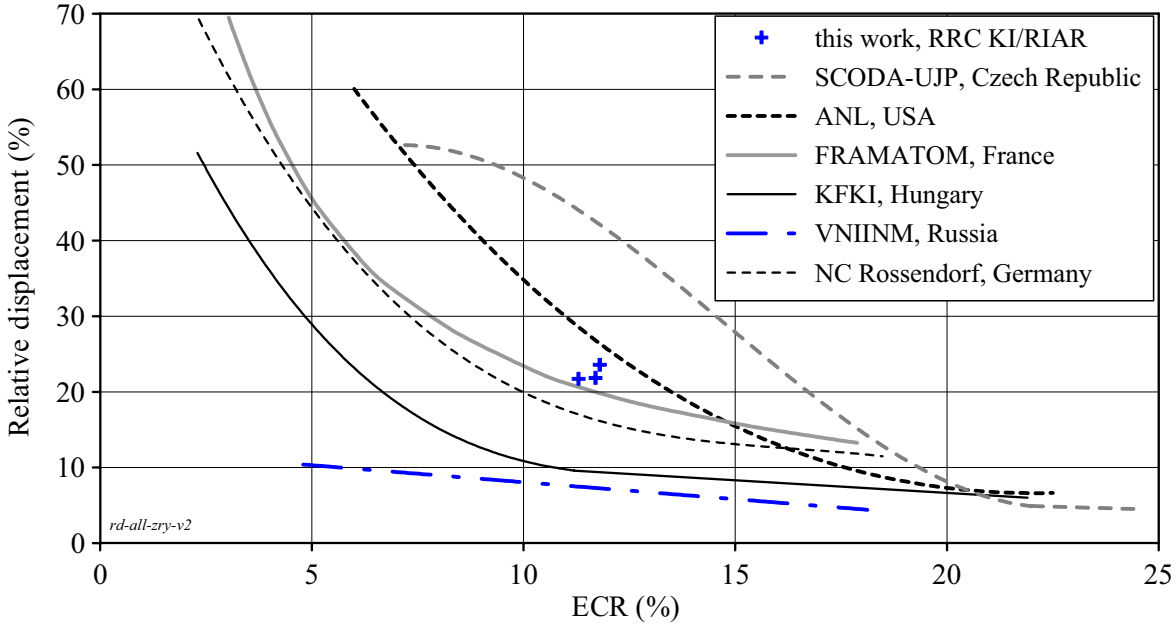

Fig. 3.28. The comparative test data characterizing the ductility of Zry-4 oxidized cladding vs ECR

The comparison of these data with the data obtained by RRC KI/RIAR allows to conclude that:

- the previous VNIINM data [15] must be eliminated from the consideration and, probably, KFKI data [25], also (the motivation to this position will be discussed in the next sections of this Chapter);
- the analysis of the data base confirms the conclusion developed in the section 3.3.1 of this report: "the higher the ductility margin in the oxidized cladding, the greater the extent for this margin to be a function of oxidation conditions". Besides, in this case this margin is a function of the zircaloy type (because the test data base covers more than a twenty-year period, and, accordingly, it cannot be considered that characteristics of tested zircaloy types have been completely identical);
- taking into account the preceding conclusion, different test data in the range 0–10% of the ECR were not compared; as for the presented range of the ECR (10-20%) then everybody can see that the RRC KI/RIAR test data are in the middle of the range for the experimental dispersion of results.

One more proof of the RRC KI/RIAR test data representativity was performed basing of the comparison of data characterizing the Zry-4 oxidation kinetics (see Fig. 3.29).

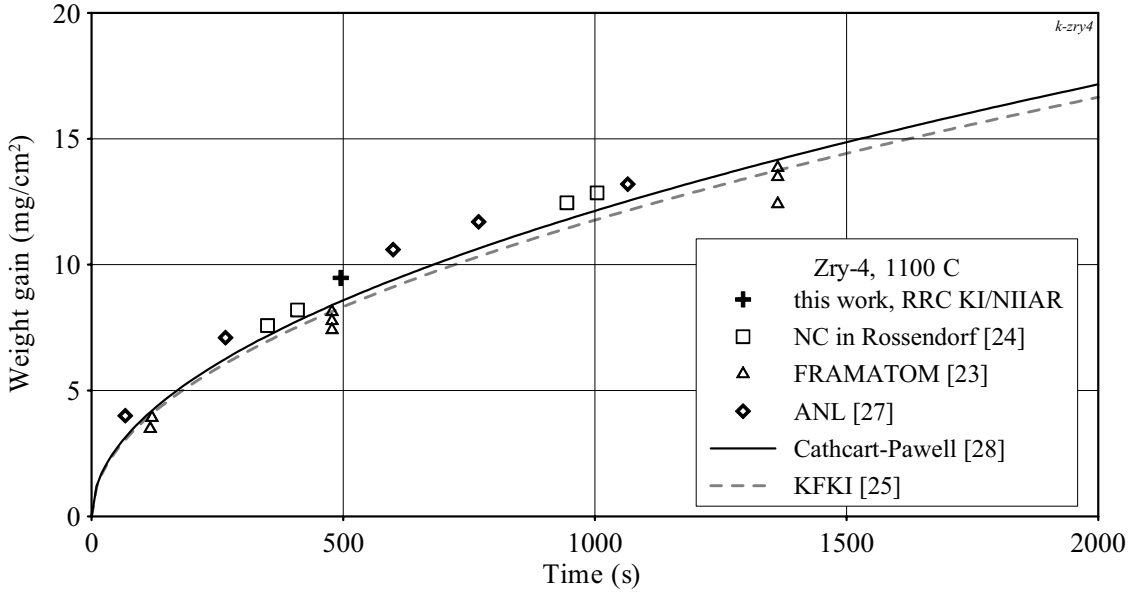

Fig. 3.29. The comparative data obtained in different laboratories to characterize the Zry-4 oxidation kinetics

The analysis of comparative data shows that RRC KI/RIAR data are in a good agreement with the data obtained by other researchers. Consequently, the integral verification the RRC KI/RIAR test approach showed that possible systematical errors connecting with experimental and processing procedures do not exceed reasonable values.

3.3.2.2.The comparison of the E110 and Zry-4 oxidation and mechanical behavior

The comparison of the E110 and Zry-4 residual ductility* as a function of the ECR is presented in Fig. 3.30.

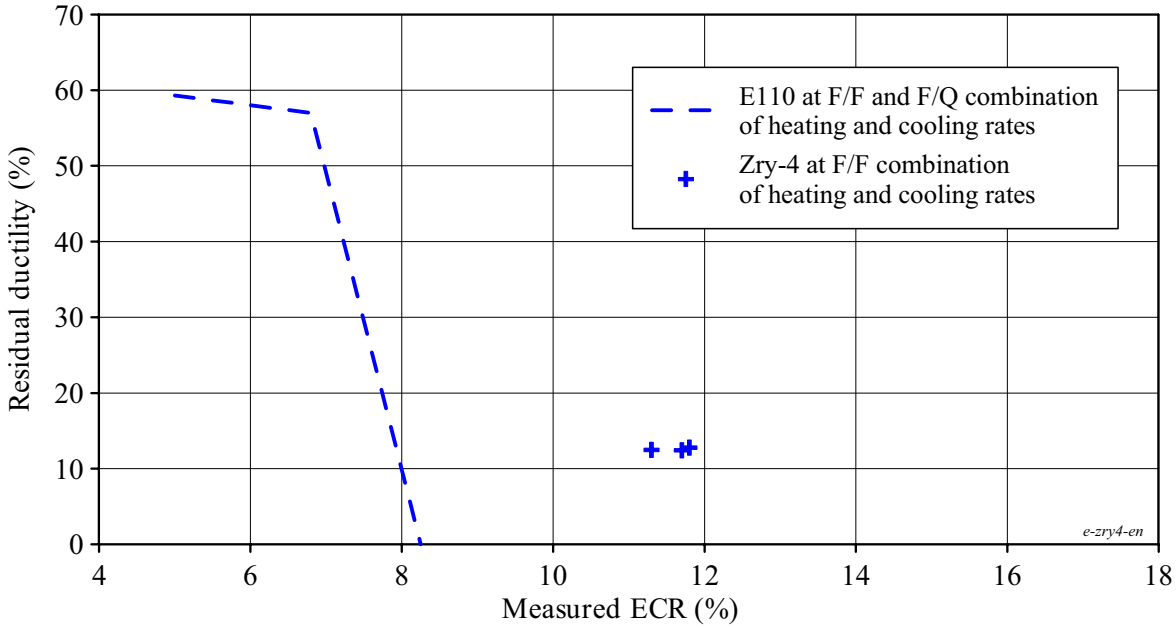

Fig. 3.30. The comparison of E110 and Zry-4 cladding behavior in accordance with RRC KI/RIAR test data

* The characterization of the E110 cladding and test results obtained at 1100 C and F/F, F/Q combinations of heating and cooling rates are presented in Appendixes A–3, B, D

The analysis of these data allowed to state the following:

- the zero ductility threshold of the E110 cladding is 8.3% ECR;
- a sharp decrease of the E110 cladding ductility (from 60% down to 0) occurs in a very narrow range of ECRs (6.7–8.3%) that indicates that some new physical phenomenon takes place in the mechanism of the E110 alloy oxidation;
- in accordance with the data presented in Fig. 3.28 the ductility decrease of the Zry-4 cladding is of a monotonic character, that is, one and the same mechanism accompanies the Zry-4 oxidation in the whole studied range of the ECRs;
- the Zry-4 oxidized cladding has the residual ductility 14.3% (22.4% of the relative displacement) at 11.5% of the ECR.

To clarify the physical phenomena, which are responsible for the revealed differences in the E110 and Zry-4 oxidation behavior, the analysis of data characterizing the appearance of these cladding types was performed first of all (see Fig. 3.31).

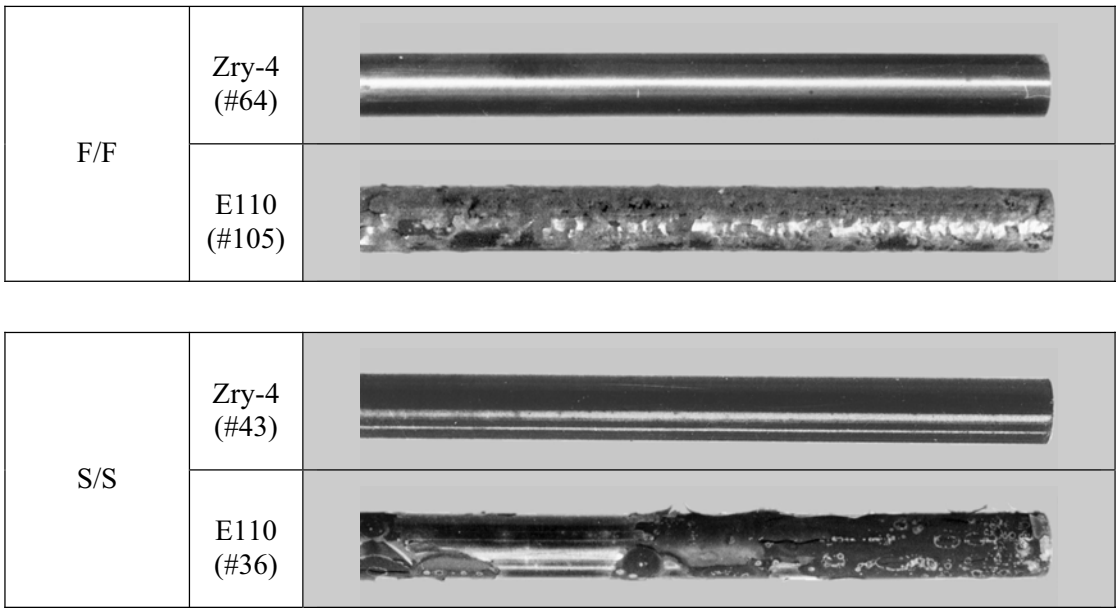

Fig. 3.31. Appearance of the E110 and Zry-4 claddings after the oxidation at 11.3–11.8% ECR and F/F, S/S combinations of heating and cooling rates

These first observations have shown the following:

- the Zry-4 cladding is covered with the lustrous black ZrO_2 oxide in both variants of heating and cooling rates;
- the E110 cladding oxidized at F/F combination of heating and cooling rates has the spalled white oxide on the surface;
- the E110 cladding oxidized at S/S combination of heating and cooling rates has the remains of the lustrous black oxide (outer layer) and very spalled oxide (inner layer).

The noted peculiar features of the oxide state on the E110 cladding surface indicated that the breakaway mechanism of the cladding oxidation took place. In accordance with the data presented in Fig. 3.32, the beginning of this type of oxidation is observed at 6.5% ECR in the form of local white spots on the cladding surface. On the ECR increase, the number of white spots is increased also right up to these white spots joining and producing the outer layer of the spalled oxide.

ECR=6.5%	ECR=7.6%	ECR=7.9%	ECR=14%
#46-9	#65-10	#82-7	#110-4

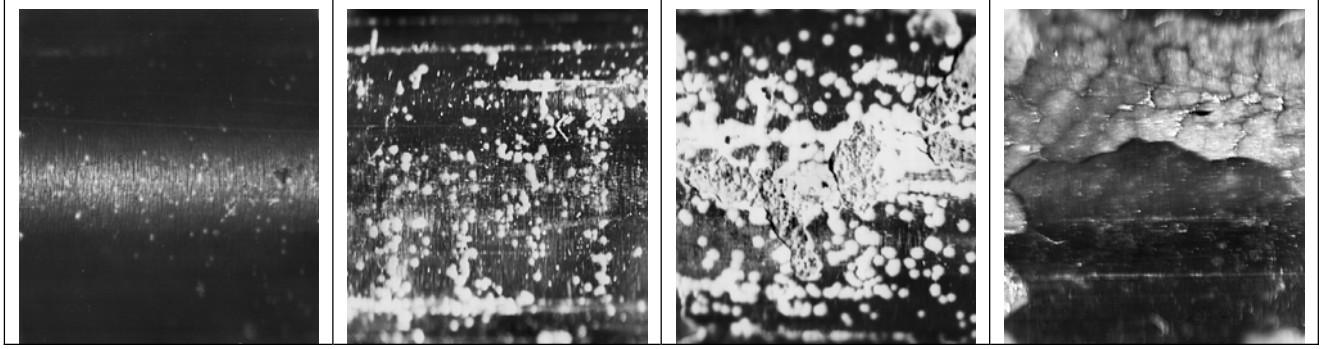

Fig. 3.32. The appearance in detail of the E110 oxidized surface vs the ECR

The additional illustration of this effect presented in Fig. 3.33 shows that two oxide layers are formed on the E110 cladding surface during the oxidation at the ECR higher than 7-8%.

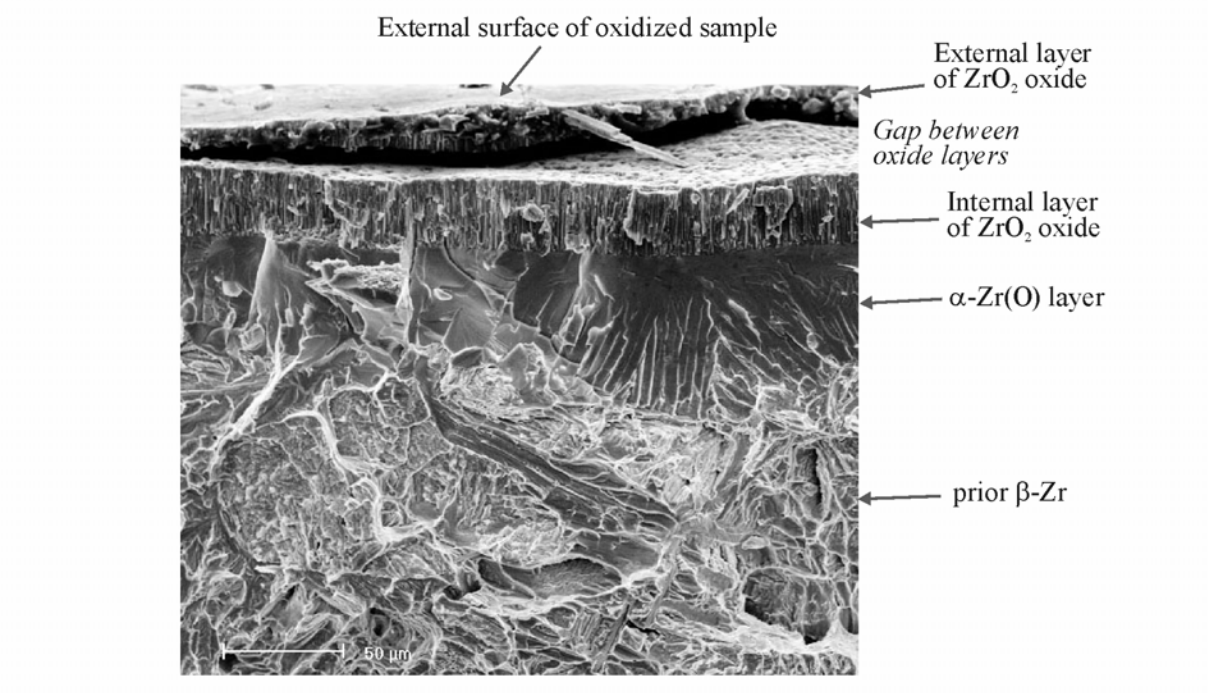

Fig. 3.33. Demonstration of two layers of ZrO_2 oxide on the outer surface of the E110 oxidized standard as-received tube using fractography results

Thus, this stage of the analysis of the E110 specific behavior allowed to determine that the breakaway oxidation occurs in the E110 cladding where breakaway oxidation is not observed in the Zry-4 cladding at 1100 C [13]. Taking into account that the breakaway oxidation may be realized in the form of two different mechanisms (the uniform oxidation and nodular oxidation), additional examinations were performed to study these effects using the metallographic cross-section samples of oxidized claddings (see Appendixes C, D, G).

In parallel with the RRC KI/RIAR studies, several cross-sections of E110 oxidized claddings were prepared in the ANL. The interpretation of the ANL data was made by H.Chung (see Fig. 3.34). In accordance with his position, the nodular type of the breakaway oxidation was observed on the tested E110 cladding samples. The combination of phenomena during the oxidation may be described in the following way [29]:

- "initial development of white nodules;
- coalescence and interconnection of nodules;

- flake-of of gray-white continuous oxide layer".

This point of view was taken as the basis in our previous analysis of this program results [30]. But a more careful analysis of this approach based on the metallographic studies performed by the RRC KI/RIAR has shown that there are some contradictions between this position and the experimental data. To demonstrate the revealed contradictions, the appearances of several oxidized E110 cladding samples are presented in Fig. 3.35.

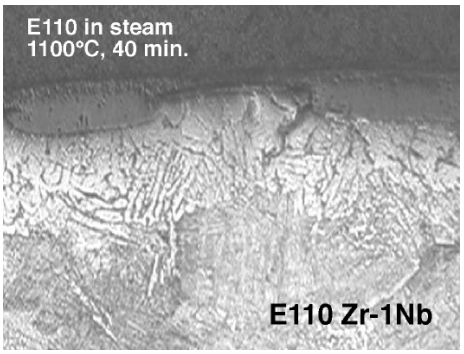

Fig. 3.34. Cross section of the oxide nodule in the E110 cladding

ECR=6.5%	⇒	The microeffects of breakaway oxidation	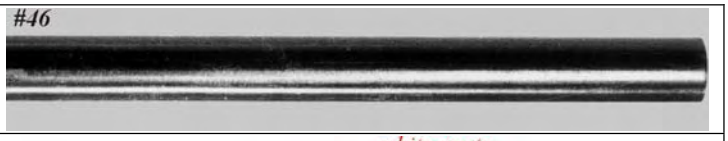
ECR=7.9%	⇒	The macroeffects of breakaway oxidation	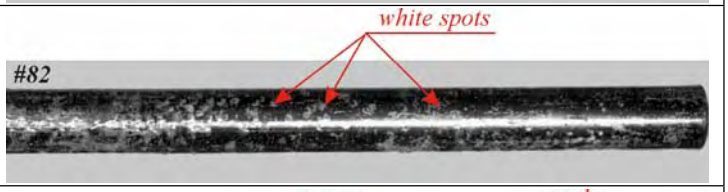
ECR=10.5%	⇒	The heaving of large parts of oxide in the crater form, cracking of oxide	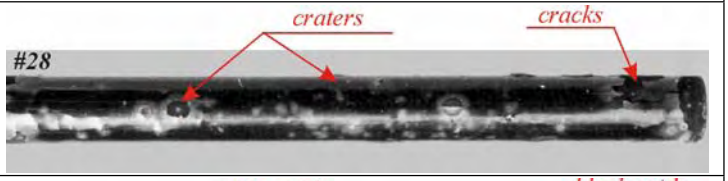
ECR=14%	⇒	The oxidation of previous separated parts into the stoichiometric white oxide	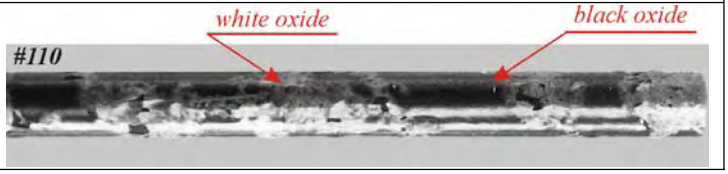

Fig. 3.35. The characterization of the oxidized E110 claddings vs ECR

Thus, if we are based on the concept of the nodular corrosion as the only mechanism determining the E110 cladding behavior as a function of the ECR then it should be expected that the cladding samples will be so much more white the higher is the ECR value. However, analyzing the appearance presented in Fig. 3.35 it can be seen that this thesis is confirmed while turning from the sample #46 to the sample #82 and is not confirmed if to turn from the sample #82 to the sample #28 (as the major part of the sample #28 is covered by the lustrous black oxide having several separate big defects of the crater type, microcracks and the explicit tendency to the whole oxide layer exfoliation from the cladding surface). On the further ECR increase (the sample #110) it may be observed that these sections (separated earlier) of the tetragonal oxide layer located under the stoichiometric oxide are oxidized into the white stoichiometric oxide, while the oxide sections retaining the adhesion with the cladding material remain lustrous and black.

To investigate these processes in more detail, metallographic samples of oxidized cladding were studied. The general tendency of processes, which take place in the E110 cladding as a function of ECR, may be characterized using the data presented in Fig. 3.36.

The consideration of these data confirms that:

- the uniform oxide layer is formed on the E110 cladding surface at the ECR<6.5%;
- at the ECR=8.9% the formation of local parts is observed in which oxide is separated into individual layers due to cracking. In this case, at least the upper layers are of the stoichiometric oxide and are perceived as white spots on the visual inspection.

Thus, the preliminary consideration of the nature of the E110 high temperature oxidation allows to determine that the beginning of the E110 oxidation process is accompanied by the initiation of the breakaway oxidation in small local points of the cladding surface, and this oxidation stage can be characterized as the nodular breakaway oxidation. But the analysis of a number of metallographic samples prepared to observe this process (see Appendixes C, D) has shown that on the ECR increase up to approximately 7% these primary effects remain on the oxide outer surface but are not developed into the depth. Therefore, a typical view of a developed stage for the nodular breakaway oxidation presented for the comparison in Fig. 3.37 is not observed in the tested cladding samples. Moreover, a special set of metallographic samples prepared to reveal the space geometry of oxide layers (see Fig. 3.38) allows to reveal that quite an even boundary separates the α-Zr(O) from the outer and inner oxide layers.

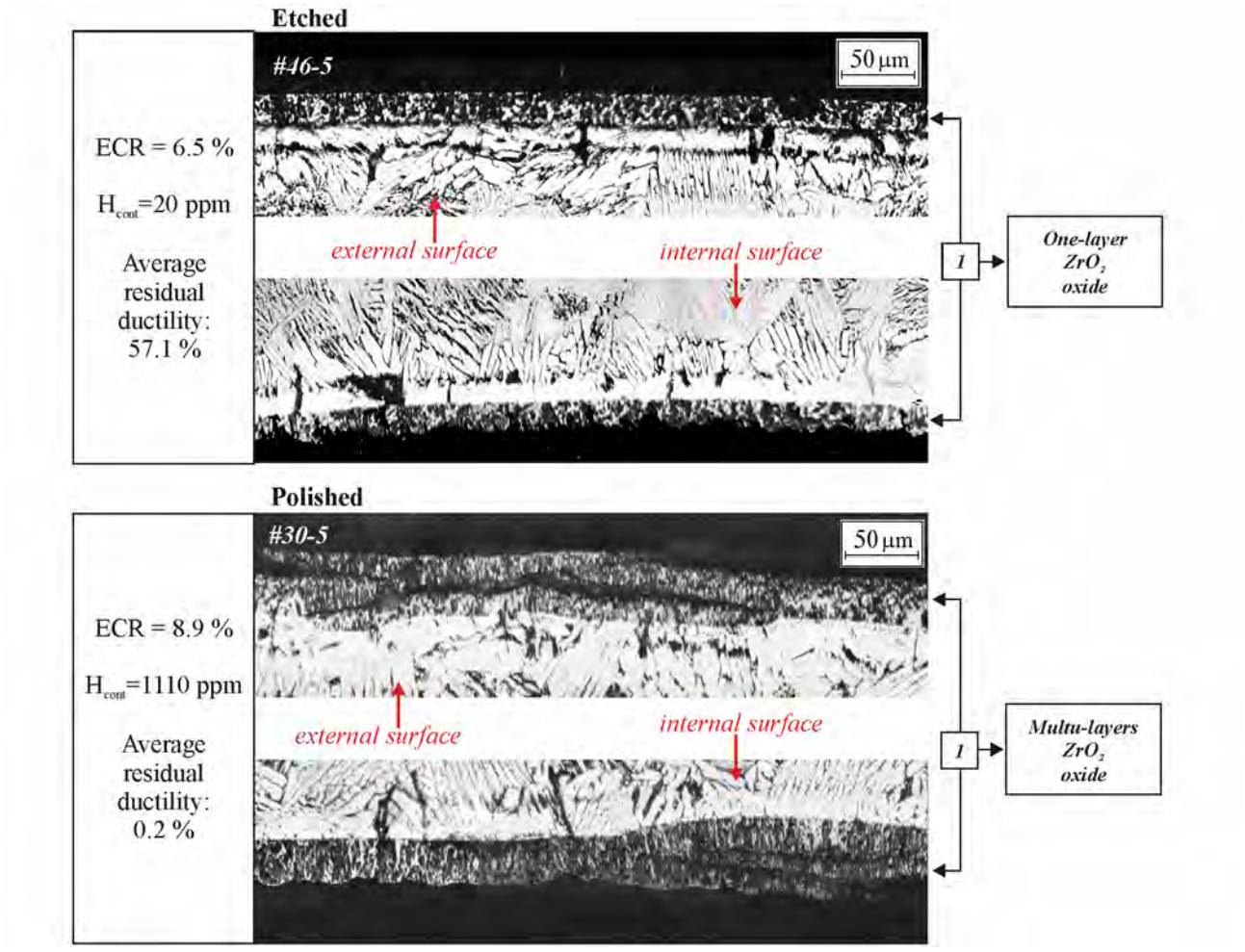

Fig. 3.36. Visualization of ZrO_2 oxide behavior as a function of the ECR after the double-sided oxidation at 1100 C (F/F combination of heating and cooling rates) of E110 standard as-received tubes

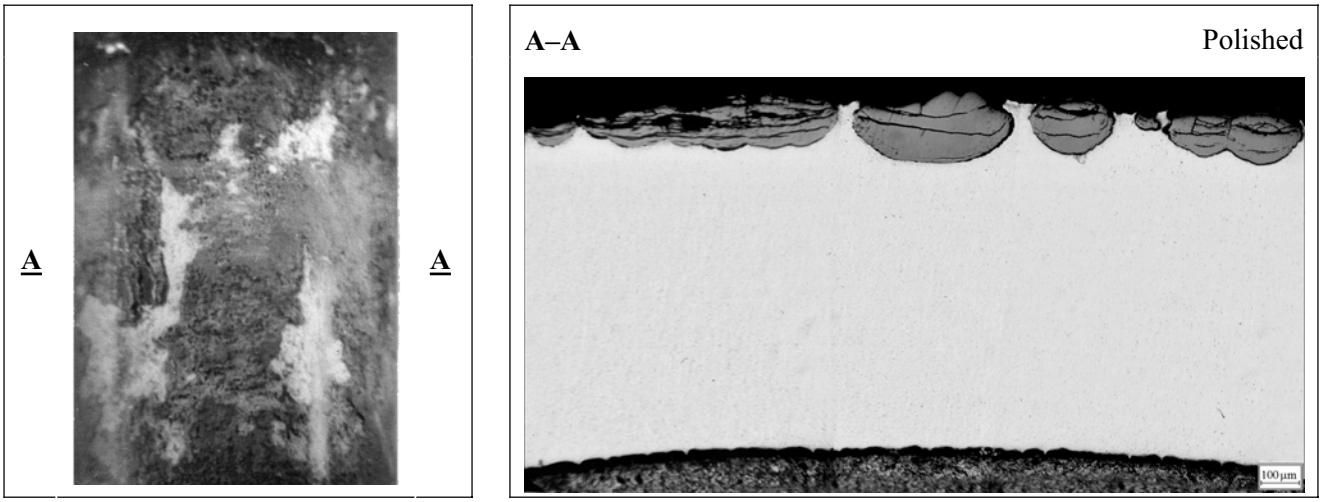

Fig. 3.37. The appearance and microstructure of Zr-Nb oxidized cladding after the operation with the surface boiling (RBMK cladding type)

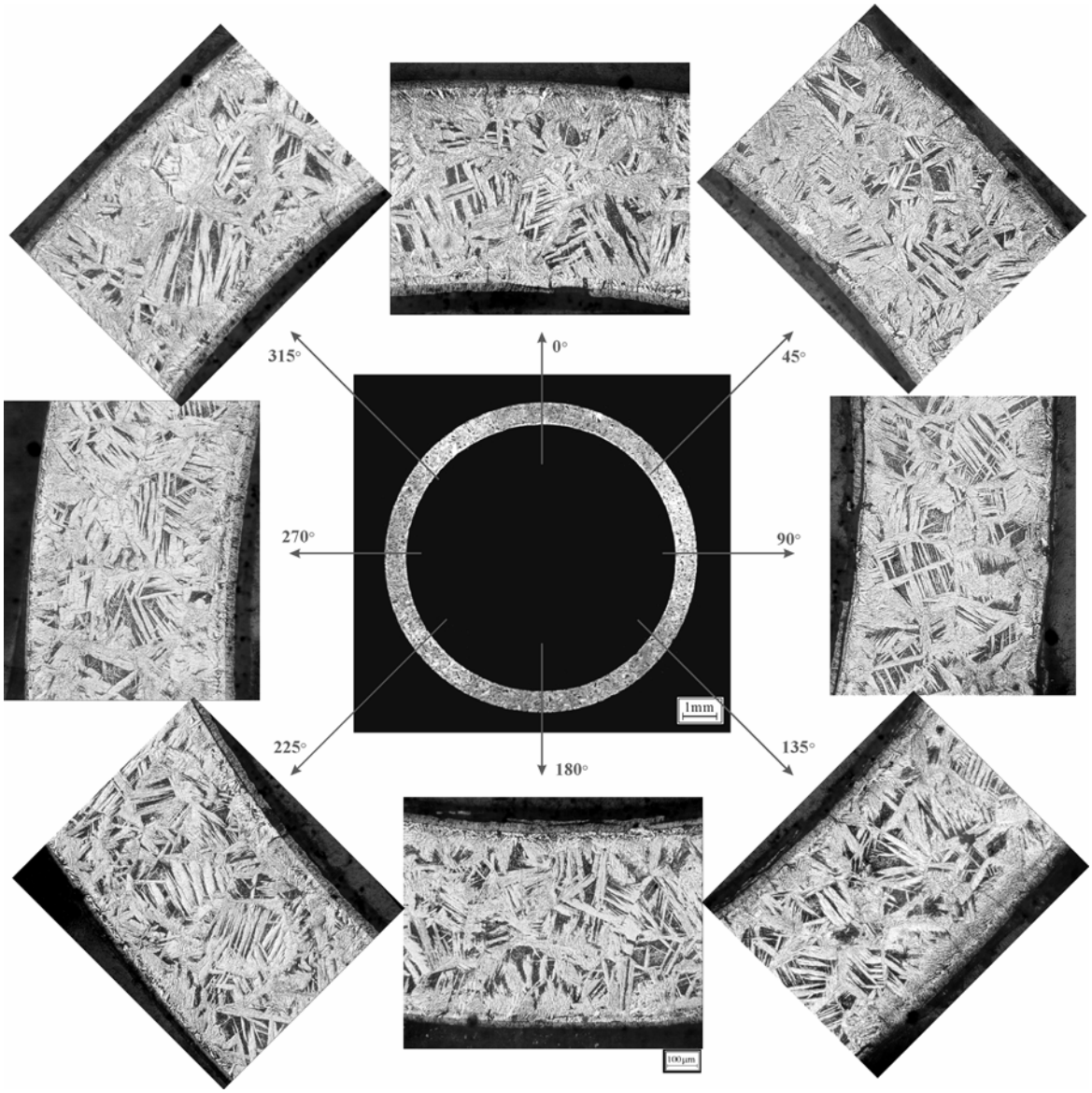

Fig. 3.38. Angular variations of the E110 standard as-received tube microstructure after a double-sided oxidation at 1100 C and 10% ECR (sample #17)

The analysis of the E110 breakaway oxidation nature will be continued in other sections of the report. But to complete the comparison of the E110 and Zry-4 oxidation and mechanical behavior, several other important phenomena are considered in this paragraph:

- oxidation rate;
- the α-Zr(O) thickness;
- oxygen absorption and distribution in the prior β-phase;
- hydriding of prior β-phase.

As for first position of the list, this research confirms that the E110 oxidation rate is somewhat less then that of zircaloy. However, for the objectives of this research it may be considered that the E110 and Zry-4 oxidation kinetics are comparable.

The next important factor influencing the mechanical behavior of the oxidized cladding is the α-Zr(O) phase thickness. A typical feature for the Zry-4 cladding oxidation behavior at high temperatures is the formation of three concentric layers in the oxidized cladding (see Fig. 3.39): ZrO_2, α-Zr(O), prior-β phase.

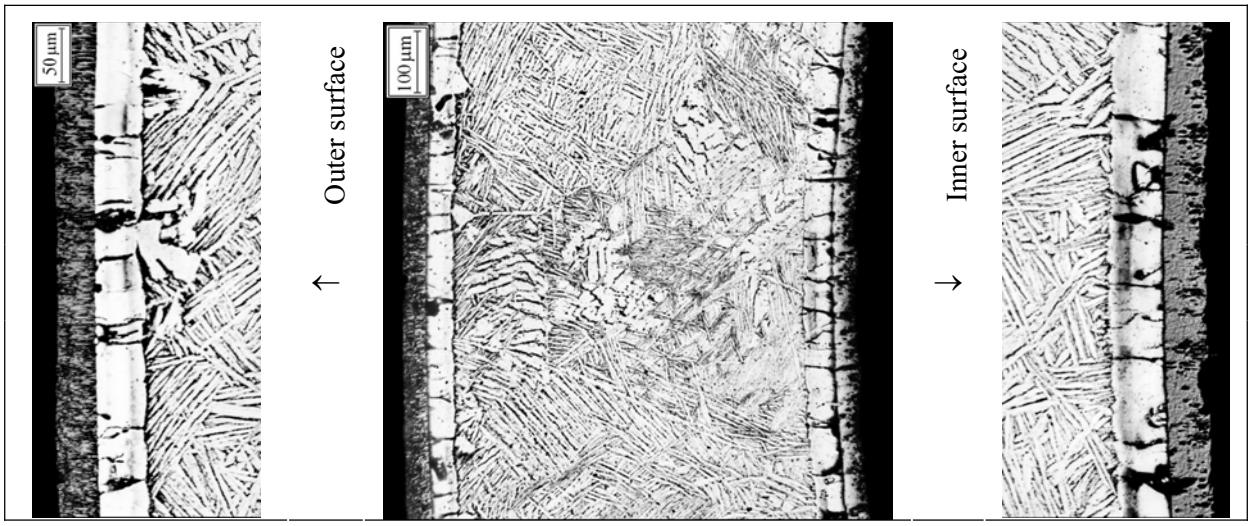

Fig. 3.39. The microstructure of the Zry-4 cladding (sample #64) oxidized at 11.5% ECR at F/F combination of heating and cooling rates

In the Zr-Nb claddings (in contrast to Zry-4), the α-Zr(O) phase (in the form of needles) penetrate deeply into the prior-β phase producing an irregular boundary between these phases. Moreover, as a rule, the boundary line in these phases cannot be legibly determined (see Fig. 3.40).

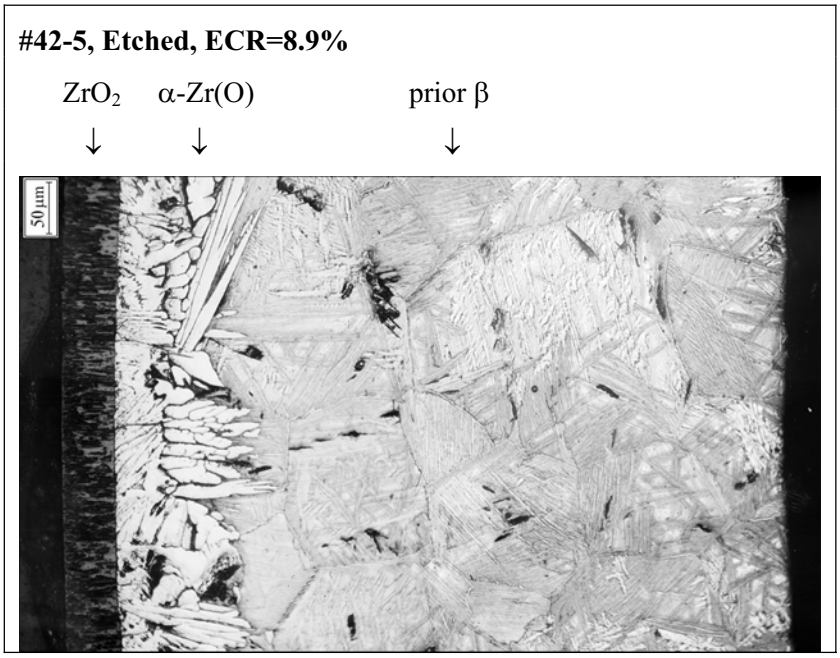

Fig. 3.40. The microstructure of the E110 cladding after a single-sided oxidation at 1100 C

This peculiar feature of the Zr-Nb claddings is supplemented with the fact that the α-Zr(O) layer in the E110 cladding is noticeably thicker then that in the Zry-4 one (see Fig. 3.41).

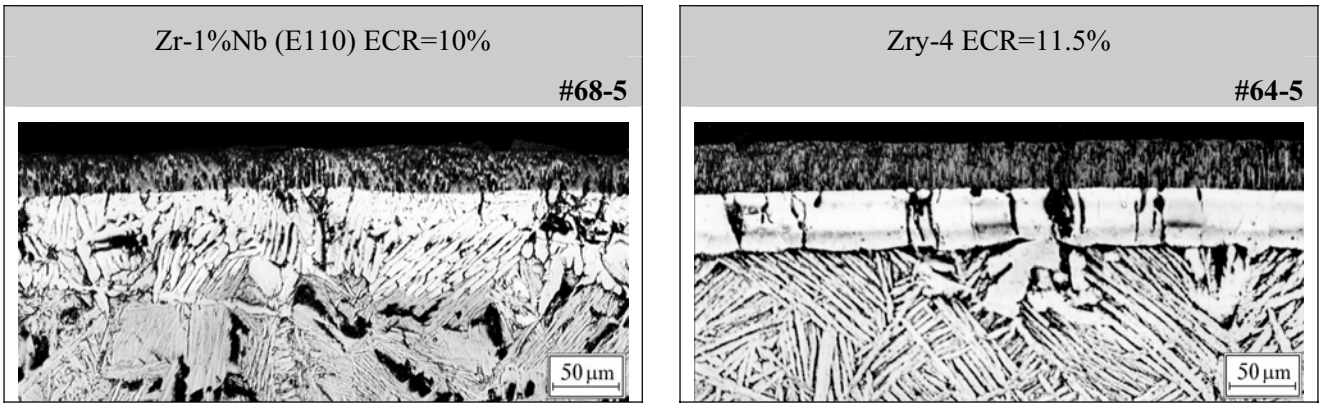

Fig. 3.41. The comparative data characterizing the ZrO_2 and α-Zr(O) thickness

To clarify oxygen absorption by the E110 cladding under oxidation conditions, several special investigations were performed including such methods as:

- the measurement of microhardness across the cladding thickness;
- the measurement of oxygen concentration across the cladding using the Auger spectrometry;
- the determination of oxygen concentration across the cladding using the SEM (scanning electron microscopy) technique.

The comparative data characterizing the microhardness and oxygen distributions in the cladding sample #41 presented in Fig. 3.42 confirm the known thesis that the microhardness distribution corresponds to the oxygen distribution. Besides, both types of test data allow to support the following conclusion formulated earlier [24]: oxygen is uniformly distributed in the prior β-phase of the E110 cladding in contrast to the Zry-4 cladding.

To reveal the character of oxygen distribution in the ZrO_2, α-Zr(O) and prior β-phase of the E110 oxidized cladding, the SEM examinations of the reference cladding sample were performed using the XL 30 ESEM-TMP scanning electron microscope (FEI/Philips Electron Optics) equipped with INCA Energy

300 (Oxford Instruments) EDX (energy dispersion x-ray analyzer). Those allowed to formulate several observations concerning oxygen behavior in the E110 claddings (see Fig. 3.43):

- oxygen concentration in the α-Zr(O) phase of the niobium-bearing cladding is monotonically decreased from the metal-oxide interface down into the depth of α-Zr(O) layer;
- non uniform distribution of oxygen concentration across the ZrO_2 layer has been revealed using the electron probe microanalysis, besides, the secondary electron image of zirconium dioxide has shown that two different types of ZrO_2 are observed on the surface of the reference cladding sample;
- in accordance with the results of investigations performed to interpret similar processes taking place in zircaloy claddings during the base irradiation (see, for illustration [31]), the oxide of this type consists of the outer layer, in which the monoclinic phase (stoichiometric white oxide with the maximum oxygen concentration) of zirconium dioxide prevails, and of the inner layer which represents the tetragonal modification (understoichiometric oxide with lower oxygen concentration).

Appearance of the E110 cladding after the oxidation at 8.2% ECR	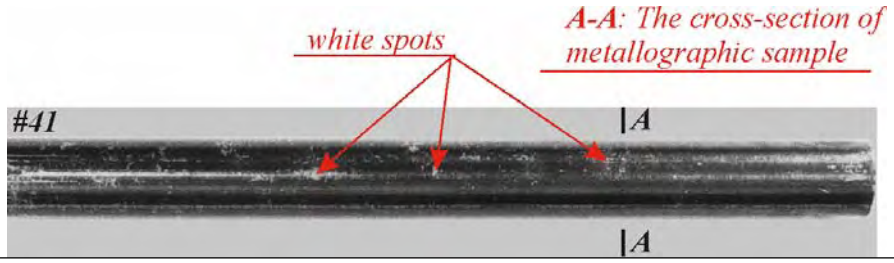
Microstructure of the oxidized cladding (etched)	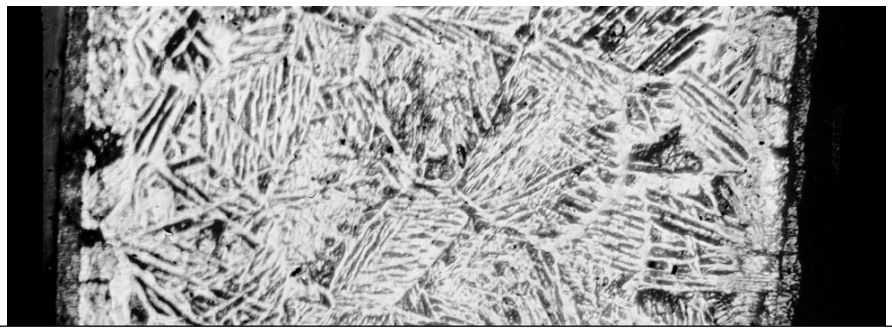
Microhardness across the cladding thickness	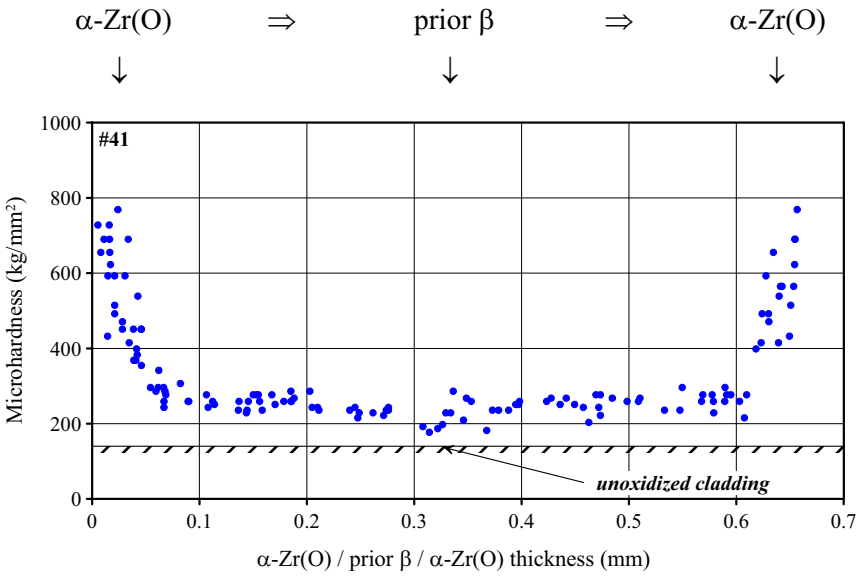
The oxygen distribution across the cladding determined by the Auger analysis	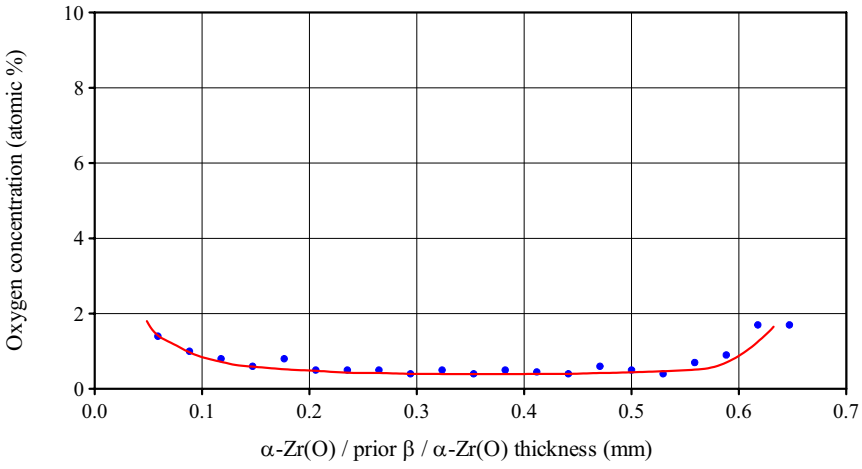

Fig. 3.42. The appearance of microstructure and characterization of oxygen distribution in the E110 cladding after the double-sided oxidation at 1100 C

Secondary electron image of the sample #41-4 with four tracks of oxygen concentration measurements	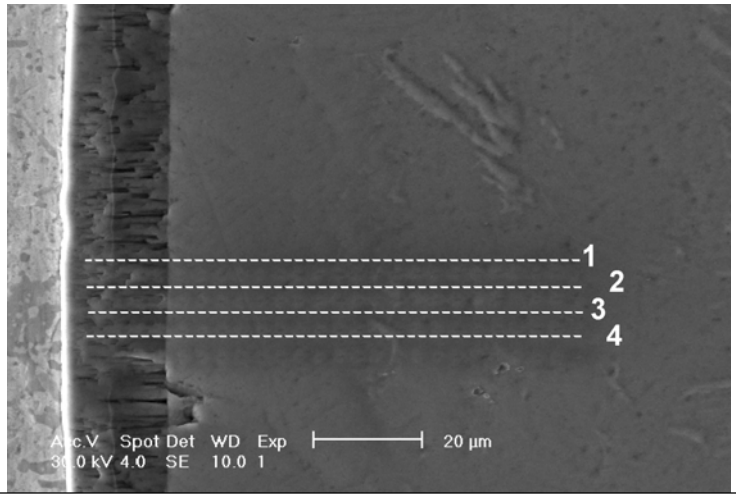
EPMA results (Electron probe x-ray analysis) characterizing the oxygen distribution Comments: 1. Averaged data on four tracks is presented 2. Measurements at the low oxygen concentration in the prior β-phase are more qualitative than quantitative. The systematic error in the measured data was caused by the parasitic oxidation of the sample surface	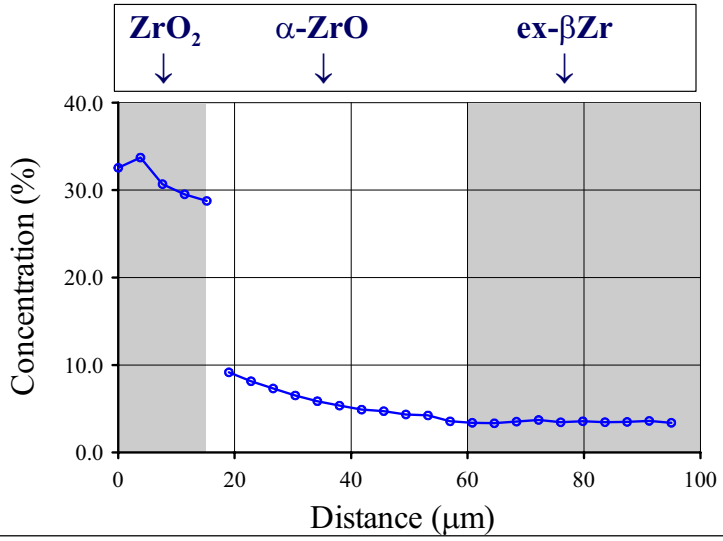
Oxygen EDX dot map	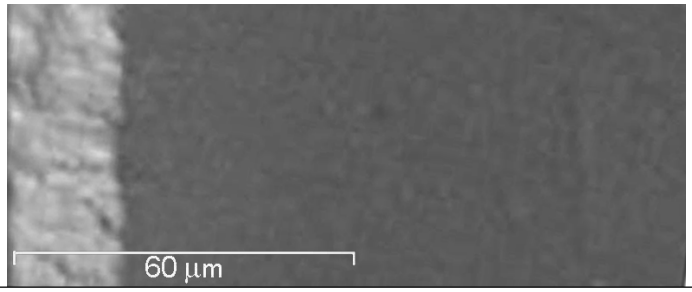

Fig. 3.43. The oxygen distribution in the E110 cladding (1100 C, 8.2% ECR) in accordance with results of SEM examinations

Obtained experimental data prompt to the formulation of the conclusion that general differences in the Zry-4 and the E110 ductility margin as a function of the ECR may be explained by the differences in the oxygen absorption and distribution. However, a more careful analysis shows that this explanation developed on the basis of previous described data contradicts the results presented in Fig. 3.44.

So, two E110 claddings one of which is brittle and another one is ductile have practically the same microhardness (oxygen) distributions across the cladding material. In this connection the question arises: is the oxygen concentration in prior β-phase the only criterion determining the ductility margin of the oxidized cladding?

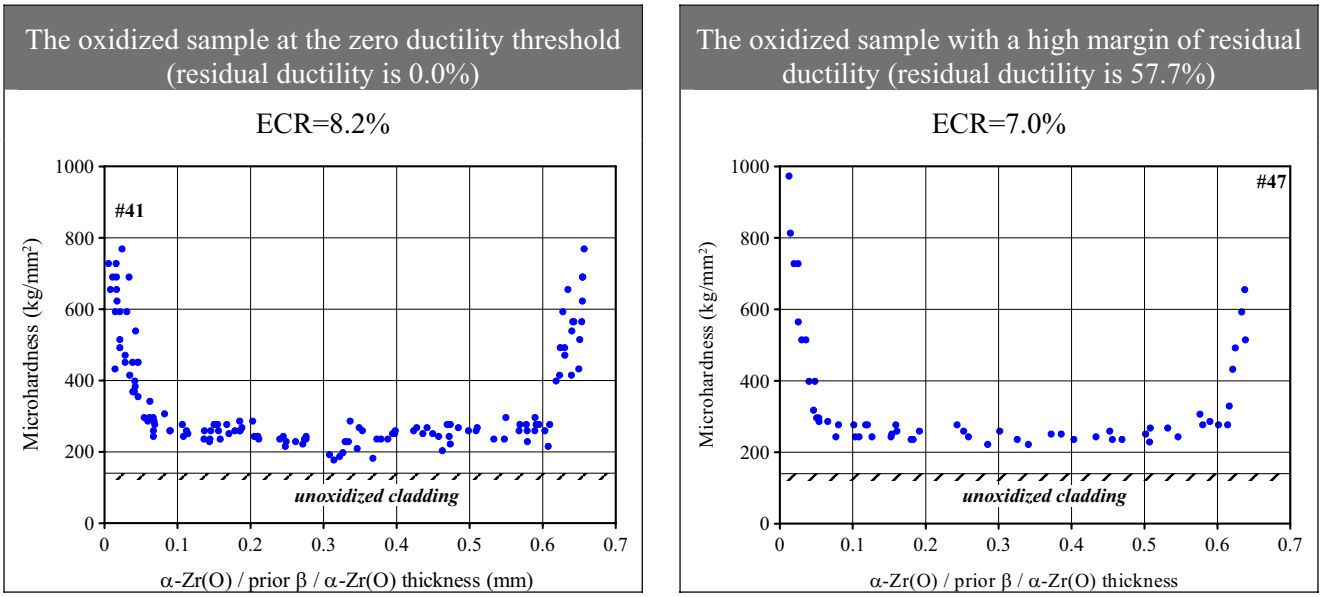

Fig. 3.44. The comparison of microhardness distributions for the brittle and ductile E110 oxidized cladding

The previous classical investigations performed with the Zry-4 claddings have shown that if the breakaway oxidation takes place then two competing processes determine the reduction of ductility margin of the oxidized cladding [13, 32, 33]:

- oxygen absorption by the prior β-phase;
- hydrogen uptake by the prior β-phase.

The significance of the hydrogen effect was later confirmed by the studies performed with the E110 cladding [17, 18, 24, 25, 26, 27]. In accordance with current conception, the effect manifests itself in those cases when the hydrogen concentration in the prior β-phase becomes higher than the hydrogen solubility limit in the zirconium. Taking into account that this limit is a strong function of the temperature, the following physical phenomena occur during the cooling phase with the oxidized cladding absorbing a significant hydrogen portion at the oxidation:

- the formation of solid hydrides at low temperatures;
- the decrease of residual ductility margin caused by hydriding of the prior β-phase.

Obviously, the process of solid hydrides formation is the function of cooling rates (the size of hydrides and, possibly, the orientation of hydrides). These physical phenomena allow to understand the sensitivity of the E110 residual ductility to the cooling rates considered earlier, in spite of the specific response of the E110 cladding on the slow cooling (the improvement of mechanical behavior) which requires the additional analysis.

The quantitative analysis of hydrogen absorption by the E110 claddings will be presented in the next section of the report. But the qualitative consideration of the physical phenomena corresponding to this process is performed in the completion of comparative studies of Zry-4 and E110 claddings.

As it was noted in the comments to Fig. 3.42, the brittle E110 cladding has two different layers of zirconium dioxide:

- white porous monoclinic oxide;
- black protective tetragonal oxide.

The characterization of these two layers of oxide may be also added with the data obtained due to the fracto-graphy observations (the SEM studies of fracture surfaces in the reference cladding sample) presented in Fig. 3.45.

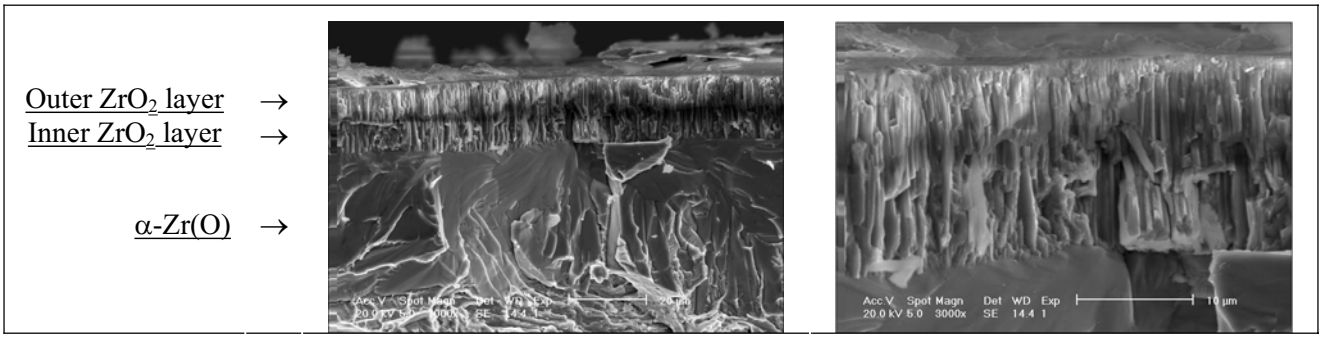

Fig. 3.45. Demonstration of the morphology of ZrO_2 layers in the E110 oxidized cladding (sample #41-4, 1100 C, 8.2% ECR)

To understand a general succession of phenomena that may be responsible for the E110 specific behavior, the following should be preliminary pointed out:

- stabilization of the tetragonal protective oxide layer on the cladding surface is explained, as a rule, by compressive stresses available which are the consequence of the fact that the oxide volume is significantly larger than the initial zirconium volume (in accordance with Pilling-Bedworth ratio) and then the modification of the surface energy balance in the separate ZrO_2 grains;
- besides, the stabilization of the tetragonal phase (slowing-down of the transition of this phase into monoclinic phase) or the improvement of its protective properties is determined also by the behavior of the alloying elements and secondary precipitates in the Zr matrix.

Thus, it is known that the improvement of the corrosion resistance of Zr-Sn alloys was obtained due to the addition of such transition metals as Fe, Cr, Ni at very low concentrations (<0.5%) [31]. A general explanation of this effect is the following: the presence of liquid unoxidized Sn and unoxidized Fe, Cr, Ni precipitates in the zirconium dioxide prevents the hydrogen diffusion and stabilizes the ZrO_2 tetragonal phase. It is also important to point out that tin oxides exist in the tetragonal form only that also leads to the stabilization of tetragonal ZrO_2. As for the niobium-bearing alloys, general considerations on this issue may be formulated in the following way:

- in accordance with results of the diffusion of niobium in the cladding surface layers and its oxidation into Nb_2O_5 may result in destabilization of ZrO_2 layer [29];
- the reason for this destabilization may be associated with the following circumstances:

– if niobium is distributed in ZrO_2 non-uniformly (that is, zirconium dioxide represents a heterogeneous structure containing niobium enriched areas) then, during oxidation of this heterogeneous structure, high volume stresses will occur due to the difference in densities of ZrO_2 and Nb_2O_5, as well as due to stresses caused by the phase transition;

– as it is known, the phase transition takes place practically instantly, therefore, it may be assumed that at that moment when the thickness of the oxide film achieves a definite value the phase transition occurs and the oxide film goes away from the oxide metal interface;

– thus, it becomes evident that all precipitates in the ZrO_2 that are oxidized slowly (such as Sn, Fe) will retain the understoichiometric state of oxide and will correspondingly hinder the sharp phase transition by the stabilization of the tetragonal phase and vice versa.

To clarify the niobium behavior in the E110 alloy at the oxidation, several types of SEM examinations were performed. The results of these examinations are presented in Fig. 3.46.

Secondary electron image of the sample #41-4 with four tracks of niobium concentration measurements	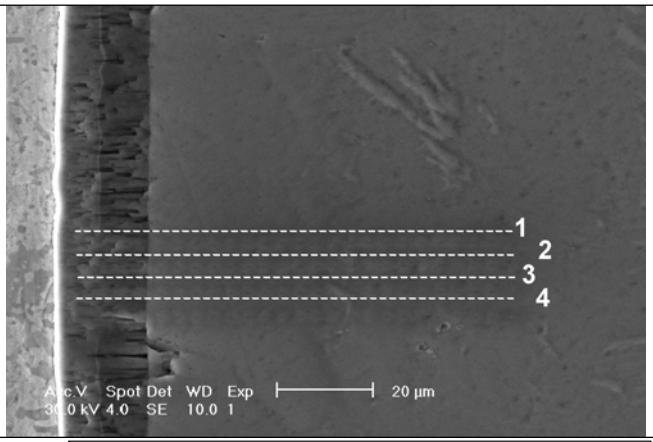
Niobium WDX (wave length dispersive x-ray analysis) dot map	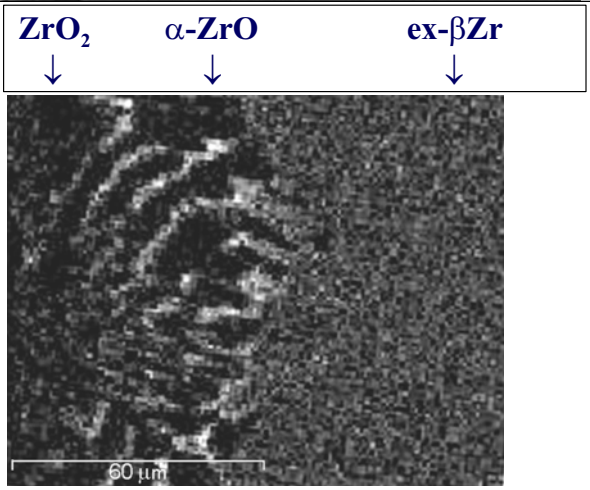

EPMA results characterizing the niobium distribution in accordance with four tracks

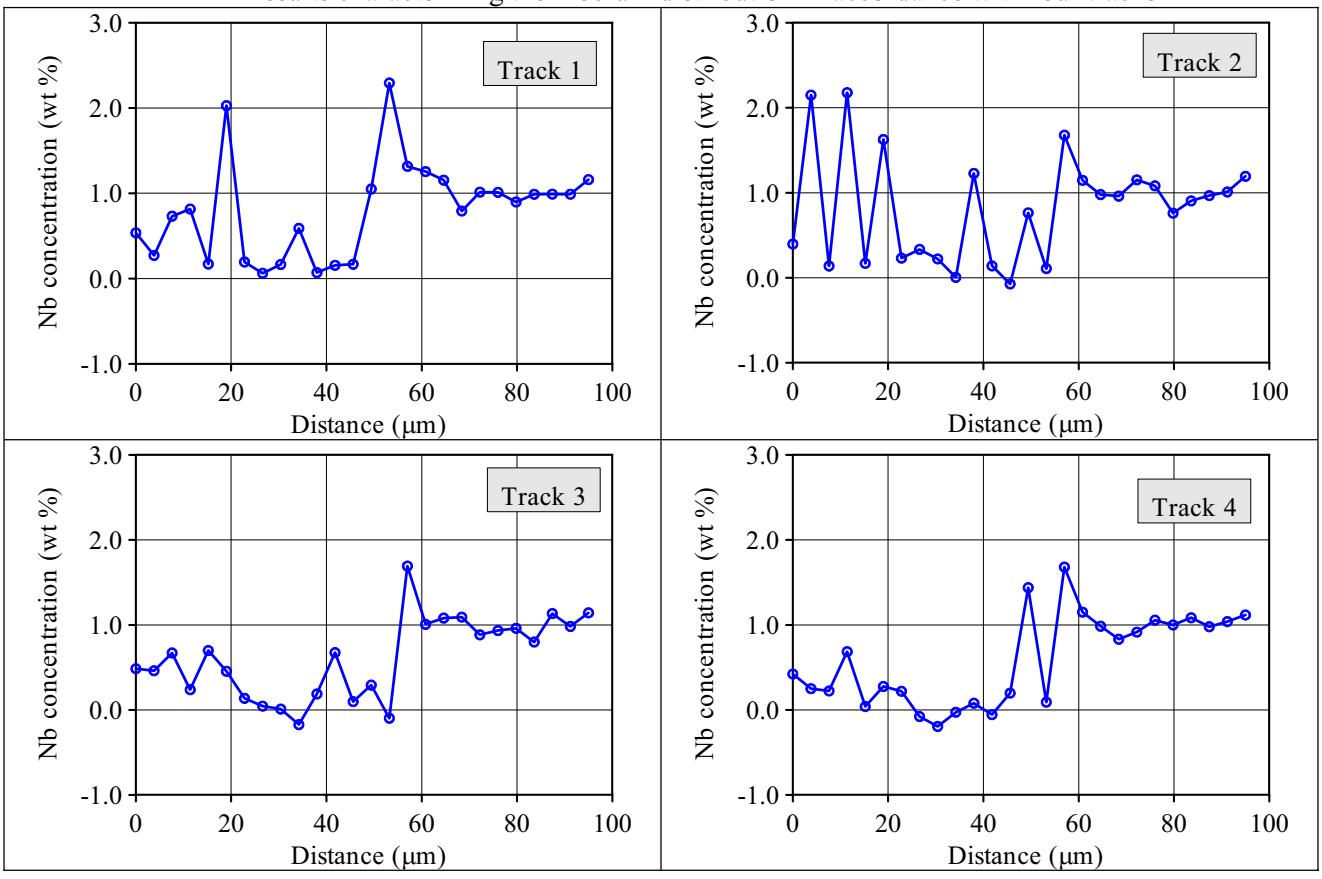

Fig. 3.46. The niobium distribution in the E110 cladding (1100 C, 8.2% ECR) in accordance with results of SEM examinations

The analysis of obtained data has shown that:

- in accordance with the niobium WDX dot map, prolonged niobium enriched areas (white areas) alternate with niobium depleted areas (dark areas) in the α-Zr(O) phase of the E110 cladding;
- the oxidation of α-Zr(O) into ZrO_2 results in the fact that these niobium enriched areas decay into separate niobium enriched points in which niobium concentration is still higher; thus, studied oxide represents heterogeneous ZrO_2 with disseminations of niobium enriched local areas;
- niobium distributions into four tracks obtained due to the EPMA confirm these observations; the irregular niobium distribution in ZrO_2 and α-Zr(O) reflects the niobium concentrations in the niobium enriched areas (up to 2.3%) and in the niobium depleted areas (0%);
- the dot map image and EPMA measurements show that the prior β-phase is characterized by quite a uniform distributions of niobium precipitates (white point on the dot map) in the α'-Zr matrix with the basic concentration in the alloy (1%).

Thus, the experimental data allow to understand the nature of the irregular boundary between α-Zr(O) and prior β-phases in the zirconium niobium alloys. The segregation of niobium with the formation of sequenced in the radial direction areas with different Nb concentration leads to the fact that niobium enriched areas transform into the α-Zr(O) phase at a higher oxygen concentration than the neighboring areas with lower niobium concentration. This effect determines the irregular boundary front between α-Zr(O) and prior β-phases in these alloys.

The performed cycle of studies allowed to return to the consideration of the postponed earlier issue concerning hydrogen absorption by the prior β-phase of the E110 cladding. One of the potential causes that may lead to hydrogen penetration through the oxide-metal boundary has already been named. This cause is the cracking and spallation of oxide due to the tetragonal-monoclinic phase transition in the heterogeneous oxide.

The following specific features of the niobium-bearing cladding discussed above determine other possible causes of hydrogen penetration:

- viens of Nb-rich β-phase in the α-Zr(O) phase represent some sort of channels providing hydrogen diffusion in the prior β-phase matrix;
- hydrogen concentration diffusion is also stimulated by the fact that hydrogen solubility is negligibly low in the α-Zr(O) phase and the surface through which hydrogen diffuses is very large (due to the fact that α-Zr(O) and β-phases have s complicated irregular boundary);
- the preferred radial direction of the α-Zr(O) grain revealed by metallographic examinations also facilitates hydrogen diffusion along grain boundaries into the cladding depth.

Numerical investigations, which were performed earlier with different zirconium alloys, allowed to establish the following principles of hydrogen embrittlement:

- during a high temperature oxidation, hydrogen absorbed by the β-phase is in the solid solution as H_2 solubility in the β-phase is very high under these temperatures;
- during the cooling phase, the precipitation of solid hydrides occurs because hydrogen solubility is a strong function of the temperature, a sharp decrease in hydrogen solubility takes place at the temperature less than 550 C; the solubility limit becomes very low at temperatures less than 100–150 C;
- investigations performed with Zry-4 claddings have shown that the number of hydrides in the prior β-phase is increased up to the hydrogen concentration of 300–400 ppm, at a higher level of hydrogen concentration, the number of hydrides is not increased but the size of these precipitates is enlarged; this effect leads to the initiation of internal stresses and deformation of the cladding matrix;
- the oxidized cladding embrittlement is not a function of hydrogen content only, the embrittlement is a function of hydrogen content, hydrides morphology and hydrides orientation;

- the most negative effect takes place in that case when hydrides form long chains along which a crack may extend.

To find out to what extent the hydrogen embrittlement problem is important for E110 samples tested in this program, two types of investigations were performed:

1. The SEM examinations provided the visualization of hydrides.
2. The hydrogen content was measured in the oxidized cladding samples.

The results of the first of these investigations are presented in Fig. 3.47.

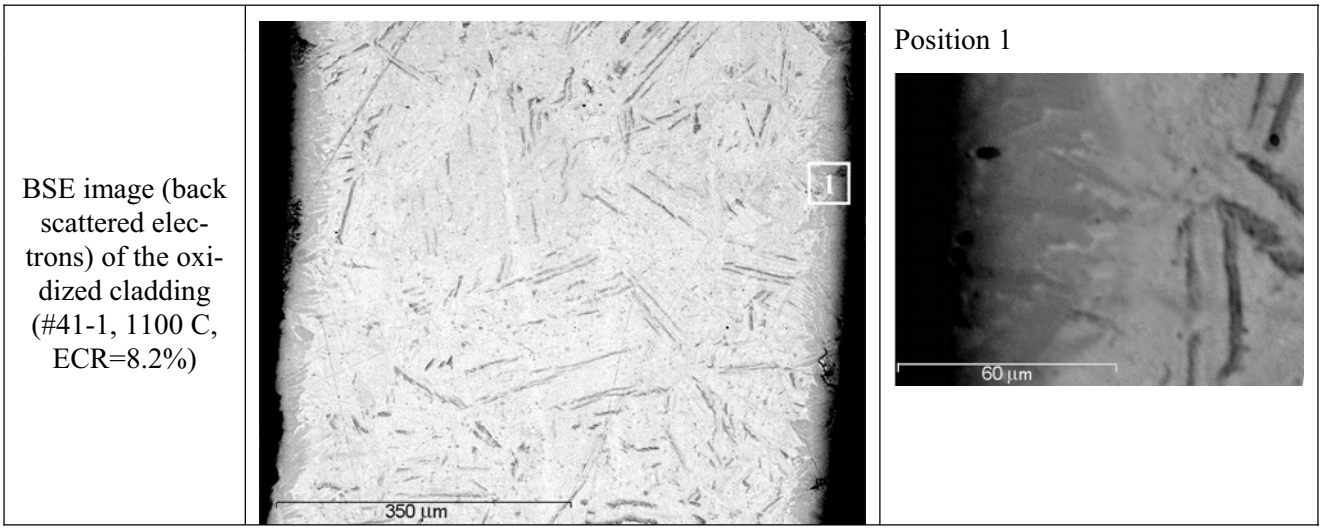

Fig. 3.47. The SEM micrograph of the E110 oxidized cladding

The backscattered electron (BSE) image of the oxidized cladding may be generally interpreted taking into account the following peculiar features of this method:

- the less is the atomic number of a chemical element in the scanning point the darker is the point on the BSE image;
- thus, the areas with high density look as the white ones at the micrograph (white areas), the areas with low density (such as hydrides) look as the black ones.

In accordance with this pattern of the BSE image interpretation, it may be assumed that dark lines scattered about the white field of the Zr prior β-phase represent hydrides (though one cannot also exclude that a part of these lines may indicate the α-Zr(O) phase located along the boundaries of β-Zr grains as this phase density is lower than that of Zr).

To extend the data base necessary for the analysis, the micrographs of one and the same sample obtained due to the optical microscopy are presented in Fig. 3.48:

- the etched structure if the sample allow to see the distribution of α-Zr(O) phase inside the prior β-phase;
- the polished structure of the sample shows the set of solid precipitates in Zr matrix, which could be interpreted as hydides.

Comparison of the BSE image and optical image of polished cladding allow to assume that the prior β-phase of this cladding contains the plate type hydrides. Much of these hydrides are oriented in radial direction and therefore are more critical from viewpoint of the crack propagation during the mechanical loading.

The measurement of the hydrogen contents in the E110 and Zry-4 cladding samples shows that:

- hydrogen content in the E110 sample oxidized at 8.2% ECR was 1130 ppm;
- the hydrogen content in the Zry-4 samples tested at 11.3–11.5% ECR and S/S and F/F combinations of heating and cooling rates was 34–37 ppm.

These measurements confirmed that the embrittlement of Zry-4 cladding is caused by the oxygen absorption in the prior β-phase. The embrittlement of the E110 cladding is provided by the oxygen absorption and hydrogen absorption in the prior β-phase.

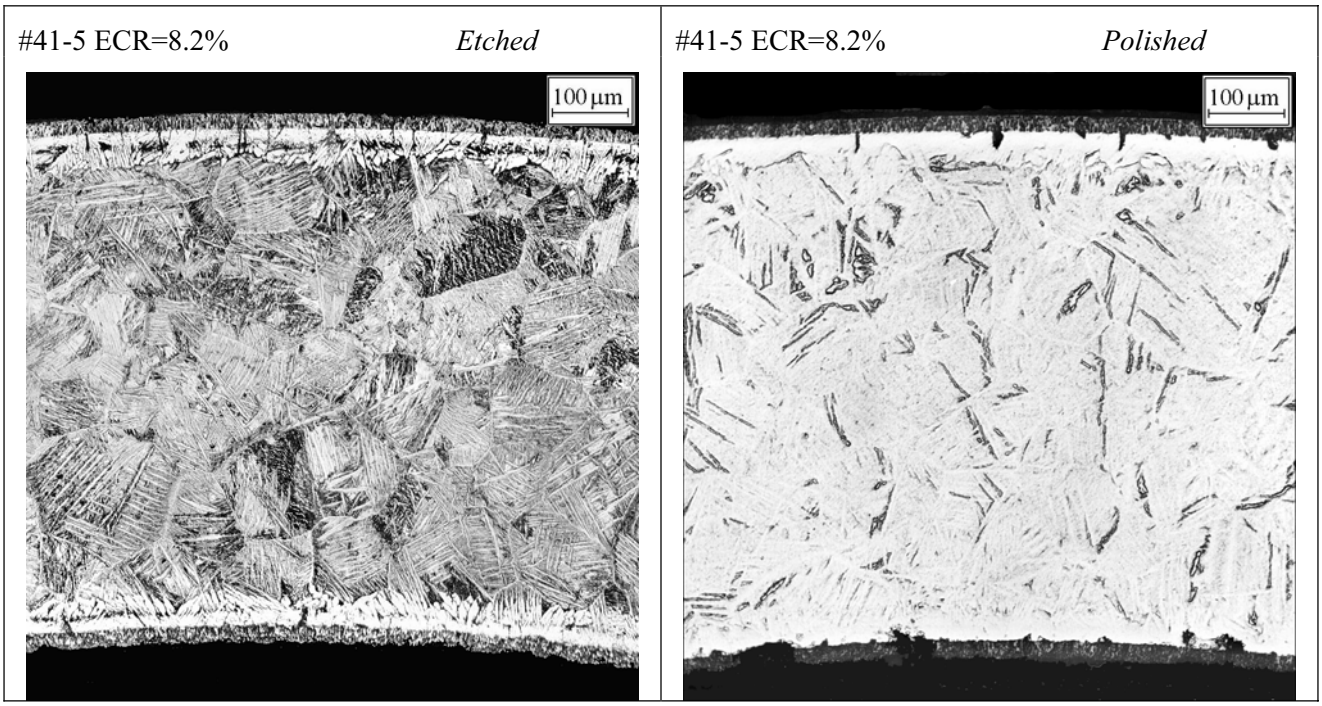

Fig. 3.48. The optical microstructure of the E110 oxidized sample with hydrides in the prior β-phase

3.3.3. Determination of sensitivity of the E110 cladding embrittlement to the oxidation type and the characterization of comparative behavior of E110 and M5 claddings

The previous stages of this research program revealed that the E110 cladding has the inclination to the early breakaway oxidation, and to the increased hydrogen pickup, which facts lead to the zero ductility threshold of the E110 cladding of 8.3% ECR at 1100 C with double-sided oxidation. In this connection, the following natural question was formulated after the analysis of obtained data: do these results characterize the whole family of niobium-bearing claddings or does this effect take place in the E110 cladding only? It is evident, that the comparison of the E110 cladding behavior with the behavior of any other cladding with a close chemical composition might become the best method to find the answer to the formulated question. The appropriate analysis has shown that the M5 cladding [34] is an ideal partner to perform this comparison as both claddings (E110 and M5) are fabricated from the alloys practically similar in the chemical composition: Zr-1%Nb (though it should be noted that they differ in oxygen concentration in the alloy).

However, the consideration of published data characterizing the mechanical behavior of the M5 oxidized cladding showed that the appropriate studies were performed employing a single-sided oxidation [23, 35, 36]. This circumstance became the major incentive to perform sensitivity studies and to develop the comparative data on the E110 cladding behavior as a function of the oxidation type. The results of E110 single-sided tests are presented Appendixes B and E.

The obtained data have shown that (see Fig. 3.49): the pronounced indications of the breakaway oxidation appear in the case of a single-sided oxidation at lower ECR than that on the double-sided oxidation. This fact confirms again the formulated earlier thesis that the tetragonal oxide transition to the monoclinic oxide takes place on some critical oxide thickness. Taking into account that the oxide thickness at the single-sided oxidation is higher than that at double-sided oxidation (with the same ECR), the breakaway oxidation occurs at lower ECR.

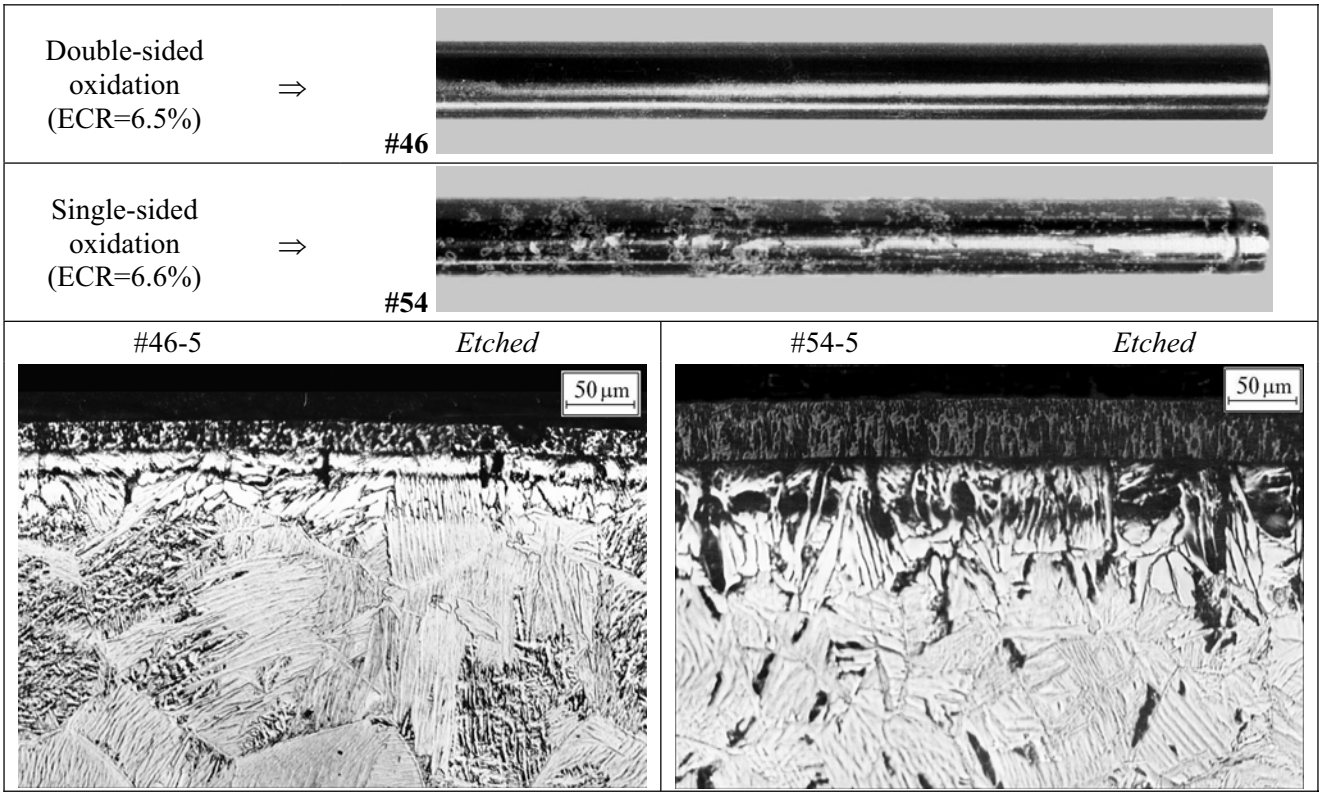

Fig. 3.49. The comparison of the E110 appearance and microstructure after single-sided and double-sided oxidation at 1100 C

The comparison of the E110 oxidized cladding mechanical behavior presented in Fig. 3.50 allows to conclude that the E110 cladding demonstrates the tendency to the increase of the residual ductility margin at the single-sided oxidation (in comparison with the double-sided oxidation) but this difference is not so great.

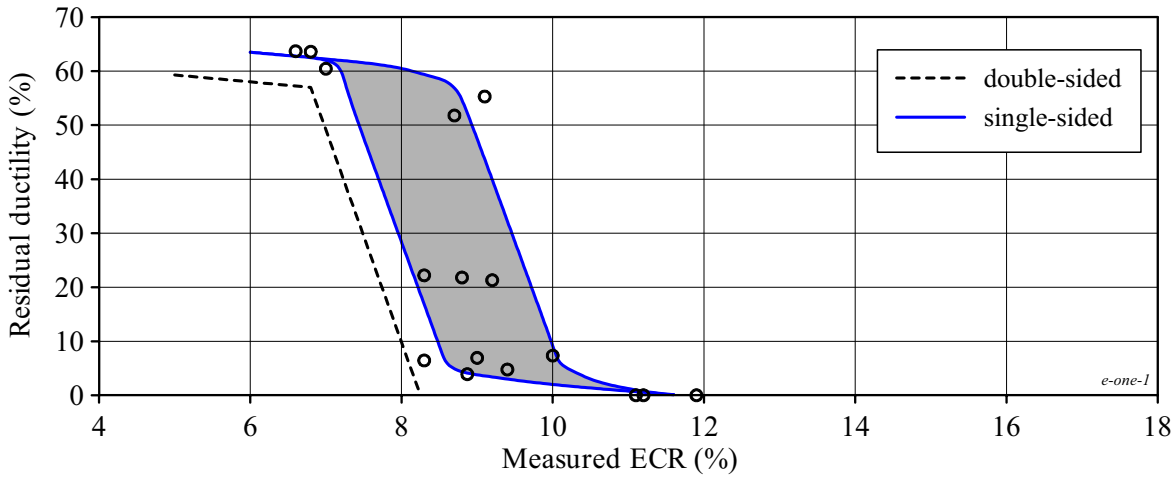

Fig. 3.50. Comparative data characterizing the E110 residual ductility as a function of the oxidation type

The E110 data base obtained due to the tests under the single-sided oxidation conditions allowed to perform a direct comparison of the mechanical behavior of the E110 and M5 claddings on the basis of ring compression tests and three-point bending tests at 20 C. To develop the comparative data, the M5 test results published in Reference 23 were used. Three-point bending test results are compared in this section and the section 3.3.7 of the report. The first set of comparative data organized in Fig. 3.51 allows to formulate several interesting observations listed in Fig. 3.51.

Ring compression tests with the E110 cladding General observations: 1. All tested E110 claddings had approximately the same effective elastic modulus 2. The fracture load at the zero ductility threshold (18.5 mg/cm^2) is corresponds to the "yield" point of load–displacement diagrams of partially ductile E110 samples (9.8–12.3 mg/cm^2)	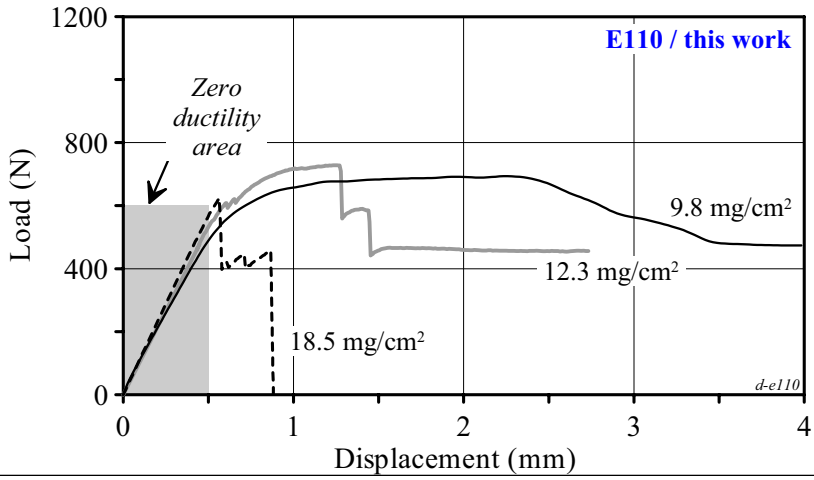
Ring compression tests with the M5 cladding General observations: 1. The claddings oxidized at 8.1–13.6 mg/cm^2) had the same effective elastic modulus 2. The elastic modulus of the sample oxidized at 22.9 mg/cm^2 is lower than that of other samples 3. The maximum load of 22.9 mg/cm^2 sample is lower significantly than the "yield" point	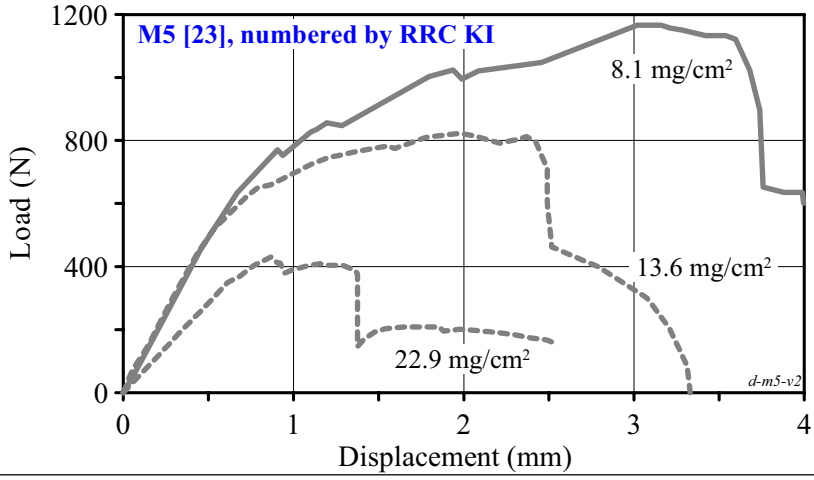
Three-point bending tests with the M5 cladding General observations: 1. All tested samples had approximately the same elastic modulus 2. Taking into account that the fracture load of 22.9 mg/cm^2 sample is significantly lower than the "yield" points of other samples the zero ductility threshold of M5 cladding is located in the range of 13.6–22.9 mg/cm^2	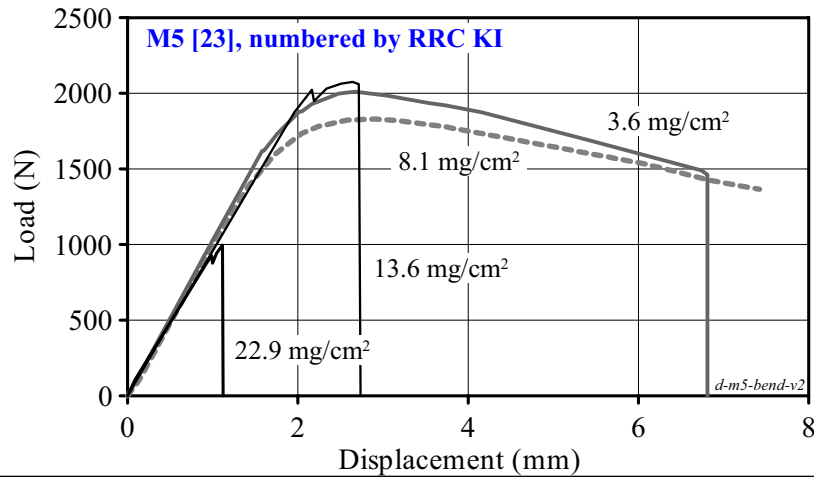

Fig. 3.51. The data base characterizing the mechanical behavior of the E110 and M5 claddings after a single-sided oxidation at 1100 C

The second set of E110 and M5 comparative data presented in Fig. 3.52 allows to make the following conclusions:

- at the low oxidation (8.1–9.8 mg/cm^2) the E110 cladding demonstrates a higher level of residual ductility and lower strength properties than the M5 cladding. Apparently, this may be explained by the effect of different initial oxygen concentration in this two claddings;

- at the middle oxidation (12.3–13.6 mg/cm^2) both claddings demonstrate a very similar behavior at the initial phase of the mechanical loading (the same elastic modulus and the similar level of the maximum load (800 and 720 N for the M5 and E110 claddings respectively) but the M5 cladding has a noticeably higher margin of residual ductility;
- at the high oxidation (18.5–22.9 mg/cm^2) the E110 cladding demonstrates the transition from partially ductile state (14.8 mg/cm^2) to fully brittle state (18.5 mg/cm^2); in this case, taking into account that the maximum load for this sample corresponds to the "yield" point, it may be considered that this sample was tested at the zero ductility threshold; as for the M5 cladding, the load–displacement diagram of the appropriate sample (22.9 mg/cm^2) shows that on the one hand, this sample has the margin of residual ductility (because the yield area is observed) but on the other hand, this sample had the maximum load that was significantly lower than the yield point, the effective elastic modulus of this sample was significantly lower than that of other samples, and, besides three-point bending test showed that this sample was fully brittle; that is why our opinion is that the zero ductility threshold of the M5 cladding is lower than 22.9 mg/cm^2.

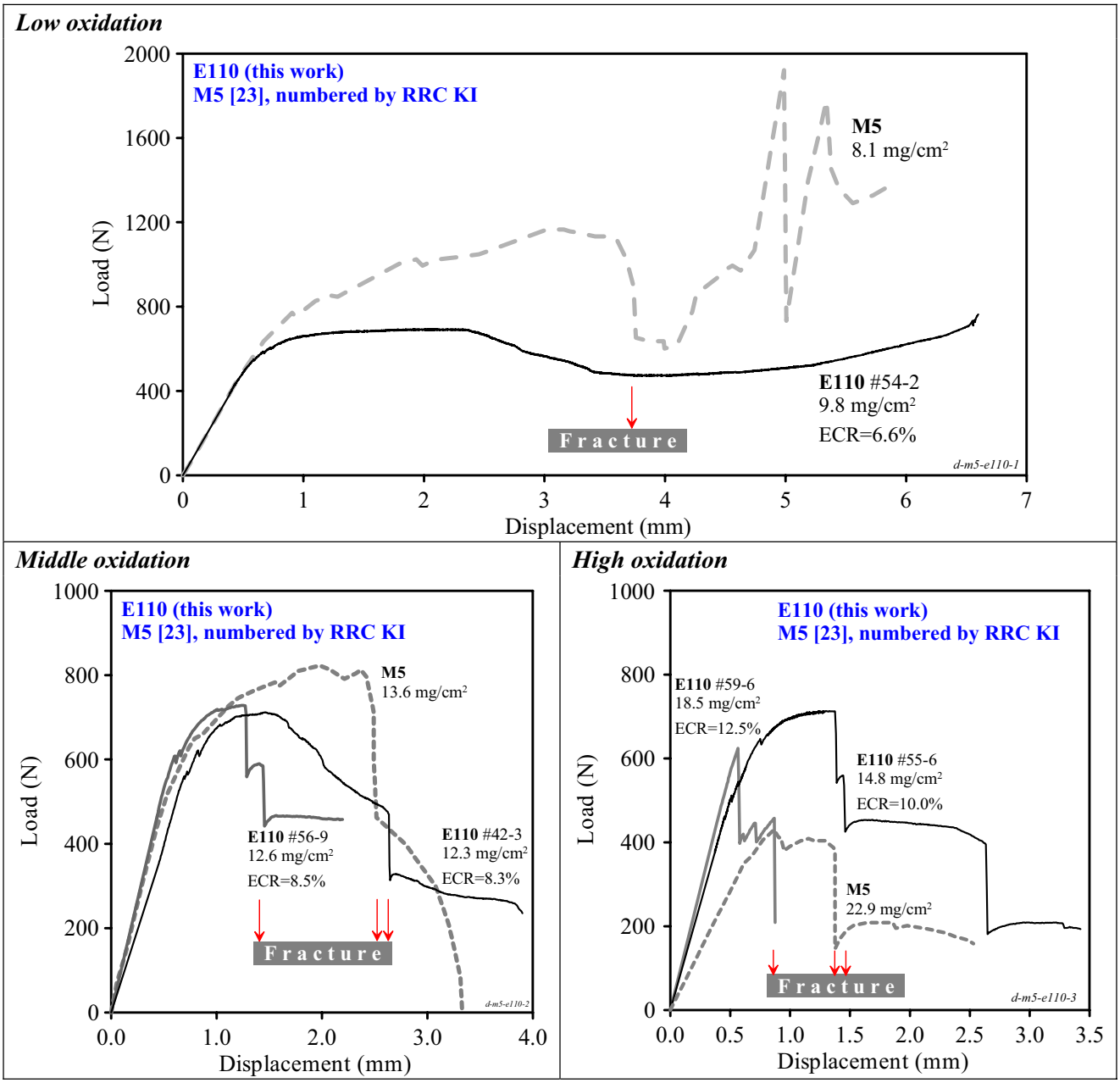

Fig. 3.52. The comparison of the E110 and M5 cladding mechanical behavior after the single-sided oxidation at 1100 C in accordance with the ring compression test results at 20 C

Nevertheless, the comparison of the E110 and M5 cladding mechanical behavior has shown that the M5 cladding has a higher margin of residual ductility at the oxidation level in the weight gain range of 13–20 mg/cm^2. Besides, the following should be pointed out:

- the E110 cladding is embrittled in accordance with the mechanism of the breakaway oxidation;
- the M5 cladding oxidation takes place without any indication of the breakaway oxidation (in accordance with the test data presented in [23], the hydrogen concentration in the oxidized samples was very low and the oxide was lustrous and black).

Thus, the results of this stage of research have shown that there is some cause that determines a specific behavior of the E110 cladding. To determine more accurately the temperature range of this E110 specific behavior, a special subprogram for the oxidation and mechanical tests was developed. The results of this subprogram are analyzed in the next section of the report.

3.3.4. The evaluation of the E110 oxidation and mechanical behavior as a function of oxidation temperature

The results of investigations performed with the E110 cladding on the oxidation at 1100 C have shown that this cladding has the tendency to the breakaway oxidation and the embrittlement caused by the oxygen and hydrogen absorption in the high temperature β-phase. Moreover, tests with the E110 cladding performed at slow heating have demonstrated that the breakaway oxidation effects become still more pronounced. This may be explained by the fact that the initial phase of oxidation took place under the temperatures that were significantly lower than 1100 C. These facts are also confirmed by the results of studies performed by V.Vrtilkova. She has shown that if the E110 cladding is heated up to 1100 C in the inert gas (argon) atmosphere and then is oxidized in water steam, the effect of early breakaway oxidation vanishes [10].

The analysis of these results leads to the conclusion that the most unfavorable test mode for the E110 alloy is the oxidation in the area of the alloy α+β-phase. As for the temperature range at which the E110 cladding has the α-phase, then numerous tests as well as the operation experience demonstrate that the E110 claddings are not susceptible to the breakaway oxidation that is confirmed by the results presented in Fig. 3.53 [37, 38].

Typical appearance of the E110 commercial cladding after irradiation at 60 MW d/kg U and representative parameters of the appropriate claddings: • oxide thickness 10 μm • hydrogen content 50 ppm	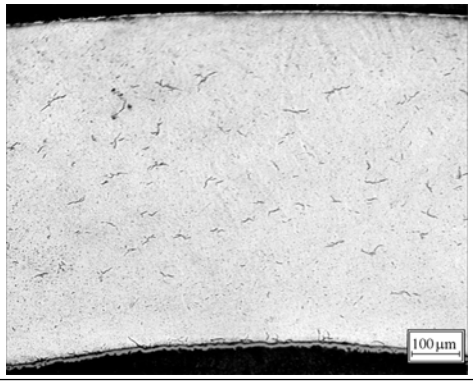
Mechanical properties of the E110 commercial irradiated cladding [19]	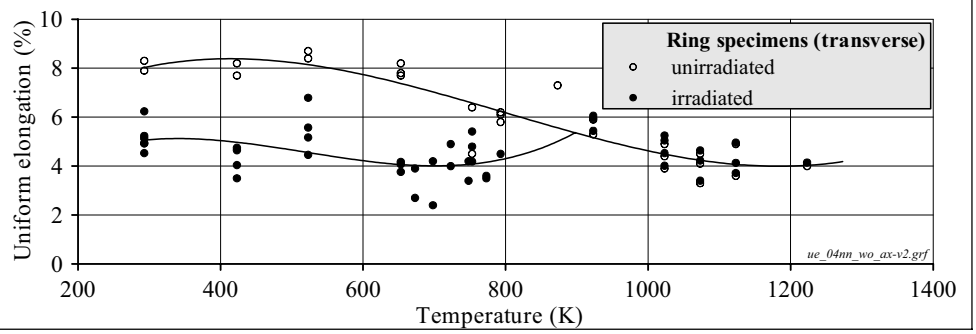

Fig. 3.53. The characterization of the E110 commercial cladding after irradiation and oxidation in the α-phase

To clarify the details for the oxidation and mechanical behavior of the E110 cladding as a function of temperature, special tests were performed in the range of 800–1000 C. Besides, to replenish the data base with the results characterizing the E110 behavior at the maximum temperature typical of the design basis accident area, several tests were performed at 1200 C. The results of these tests are presented in Appendixes B and D of the report.

But before analyzing the results of appropriate tests, it is useful to consider peculiar features of the α to β-phase transformation as applied to Zr-1%Nb alloys. The comparative data characterizing this phenomenon in the E110 and M5 alloys are presented in Fig. 3.54.

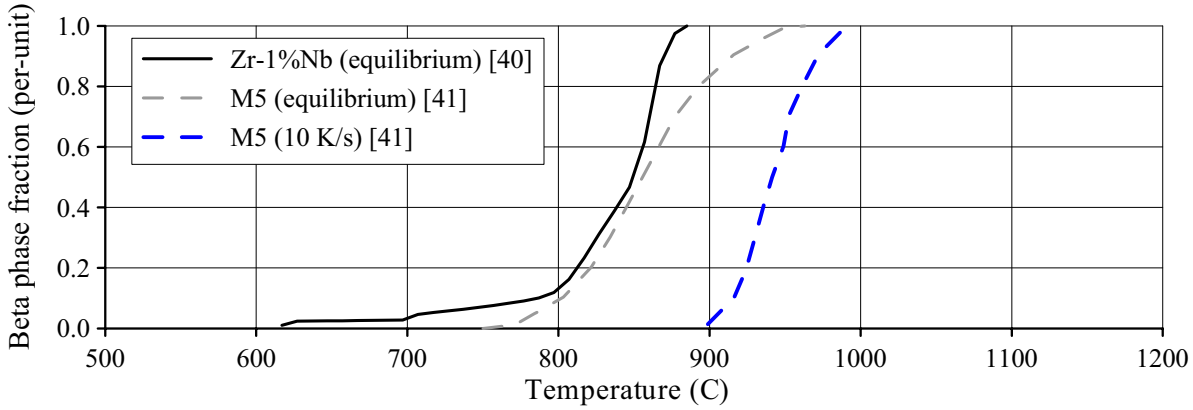

Fig. 3.54. The characterization of the allotropic phase transformation in the E110 and M5 alloys

The analysis of presented data on the M5 alloy shows that the increase of heating rate leads to the displacement of the zirconium α-β phase area towards higher temperatures; with heating rates typical of the fast mode (F) of these tests this effect will be still noticeable. The studies performed in the RIAR during the recent years to understand the behavior of VVER fuel rods with the E110 claddings under RIA conditions showed that in addition to the effects of heating rates as applied to the zirconium matrix the behavior of niobium should be also taken into account. So, the appropriate analysis shows that at the fast heating, the diffusion processes associated with the dissolution of β-Nb precipitates may take place not in full and, consequently, dissolved niobium atoms will localize close to those areas in which β-Nb precipitates are situated. In other words, the areas of niobium oversaturated solid solution may be generated in the zirconium matrix under these conditions. It has been already said before that such niobium-enriched areas may be responsible for the increased hydrogen absorption and other effects being of importance for understanding of the E110 alloy peculiar features.

The analysis of the E110 alloy real behavior in the temperature range 800–1100 C may be started from the consideration of data characterizing the appearance and microstructure of oxidized samples (see Fig. 3.55, Fig. 3.56). The results of this analysis may be formulated in the following way:

- the earliest appearance of the pronounced indications for the breakaway oxidation at the low level of ECRs is noted in the temperature range 900–1000 C;
- at the middle level of ECRs the breakaway oxidation is visually observed under all studied temperatures (800–1100 C), however, the strongest indication of appropriate effects was noted at 900–1000 C;
- at the high level of ECR the most striking demonstration of the breakaway oxidation was noted at the temperature of 950 C, in which connection the microstructure analysis showed that the effect of the oxide foliation was observed on samples tested at 800–950 C, but this effect manifested itself most obviously under the temperatures 900–950 C.

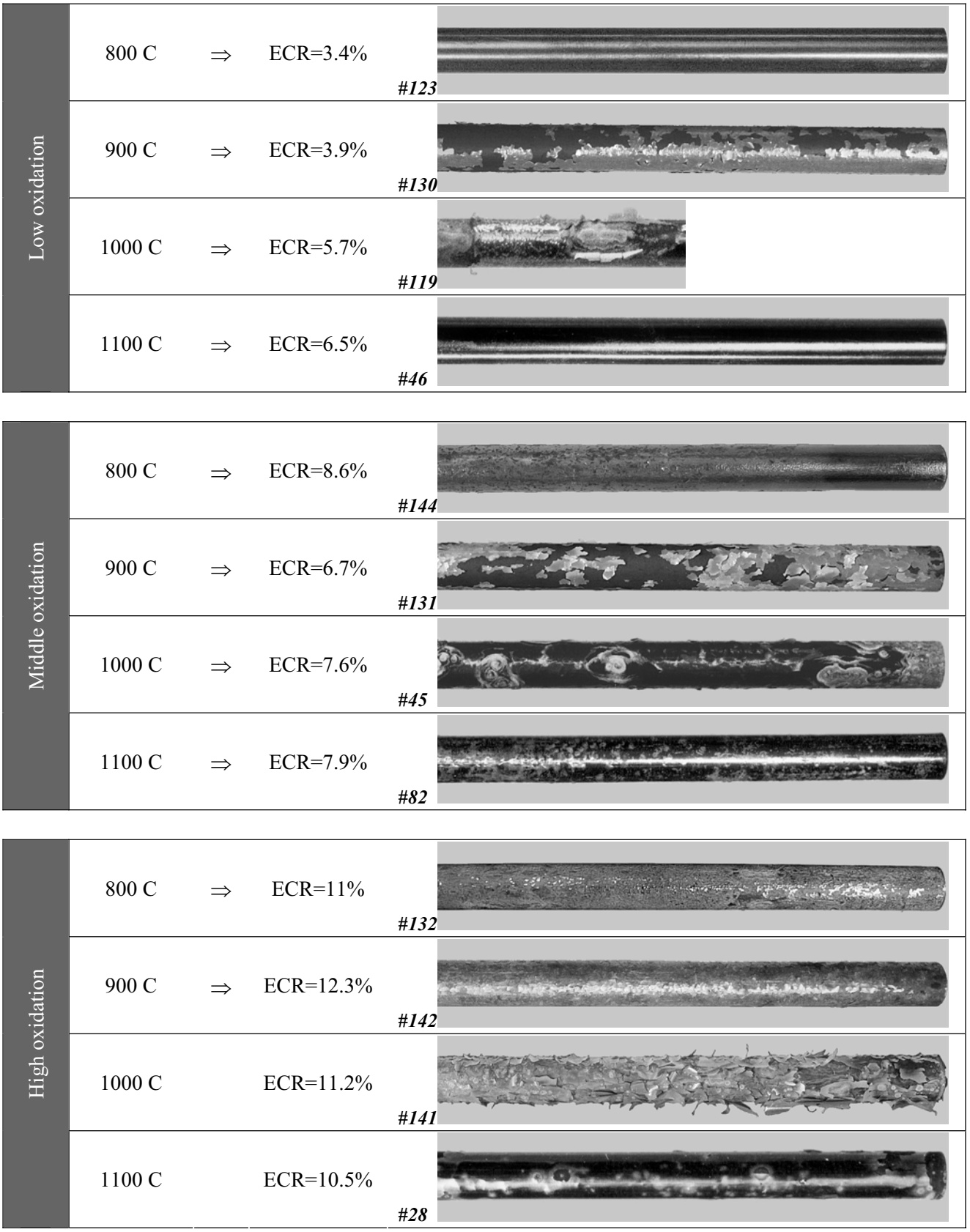

Fig. 3.55. Appearances of the E110 cladding after the double-sided oxidation at 800–1100 C and F/F combination of heating and cooling rates

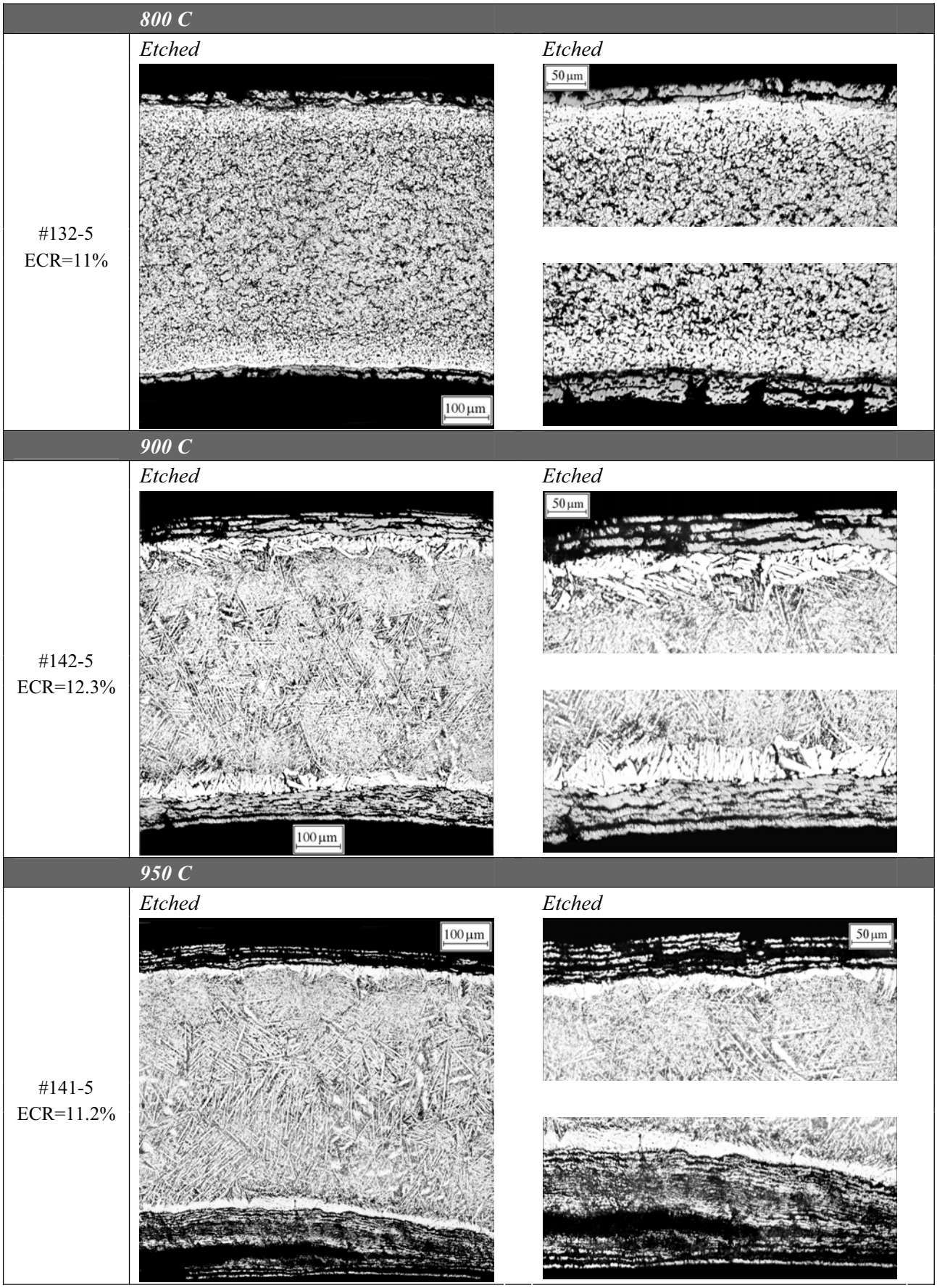

Fig. 3.56. The microstructure of the E110 cladding after a double-sided oxidation at 800–950 C and F/F combination of heating and cooling rates

To understand consequences associated with the availability of stated above effects of the E110 oxidation, the results of mechanical tests were specially organized (see Fig. 3.57).

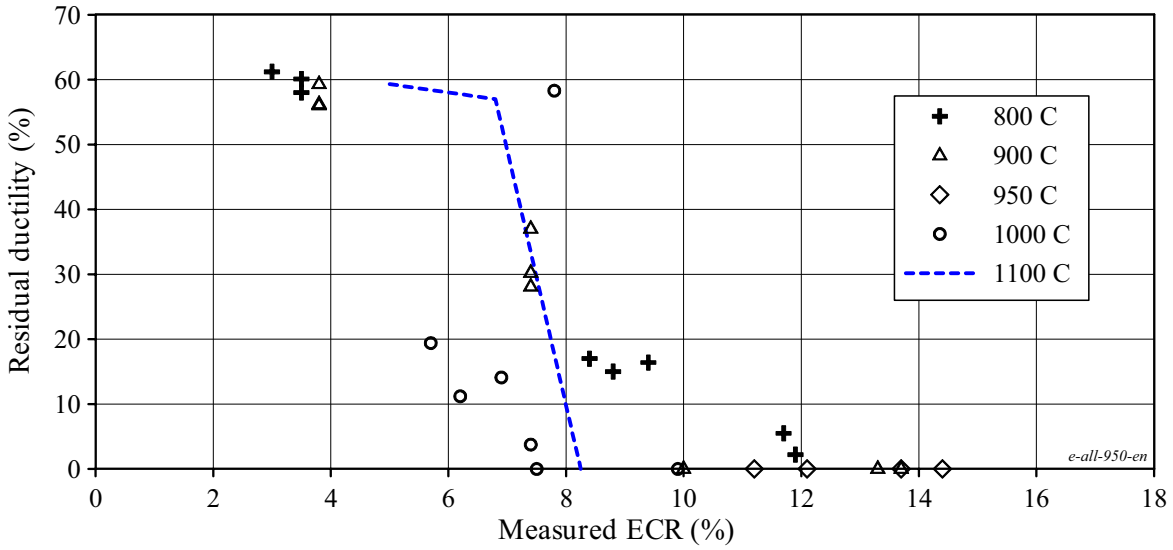

Fig. 3.57. The data base characterizing the residual ductility of the E110 cladding as a function of the ECR and oxidation temperature

In accordance with the data presented in Fig. 3.57, the following additional comments may be made:

- the zero ductility threshold of the E110 claddings oxidized at 800 C is noticeably higher than that in the reference oxidation mode (1100 C);
- the ECR of the E110 claddings oxidized at 900 C is approximately the same as the 1100-degree threshold, but the time threshold is much higher at 900 C than that at 1100 C; it is outside a practical LOCA;
- the zero ductility threshold at 1000 C is possibly a little lower than the 1100-degree threshold.

These observations are in some contradictions with the observations formulated according to the analysis of the cladding appearances and microstructures; but before we go on to the consideration of possible causes for these contradictions, it is useful to add the results of hydrogen concentration measurements in the oxidized claddings to the data base.

The systematic analysis of the data presented in Fig. 3.58 allows to reveal the following regularities in the E110 cladding behavior as a function of the ECR at 1100 C:

- the mechanical behavior of oxidized cladding is characterized with the very high margin of residual ductility in the ECR range approximately up to 7%;
- the cladding hydrogen content is very low in the same range of ECRs;
- the sharp decrease of residual ductility in the ECR range 7–8.3% corresponded with the sharp increase of hydrogen content in the E110 cladding;
- the zero ductility threshold of the E110 cladding is corresponded with the hydrogen concentration of 400 ppm approximately.

Thus, the data base characterizing the hydrogen content in the E110 cladding after the oxidation at 1100 C confirms formulated earlier assumptions concerning the fact that the embrittlement of the E110 cladding is a sum of the oxygen and hydrogen embrittlement. Besides, it should be noted that this critical value of the hydrogen content in the cladding (400 ppm) is in a good correlation with the above mentioned critical value of the hydrogen content, after which the increase of the hydrides volume and internal stresses in the cladding were observed.

Specific features for hydrogen absorption by the E110 cladding as a function of the oxidation temperature may be discussed using the data given in Fig. 3.59.

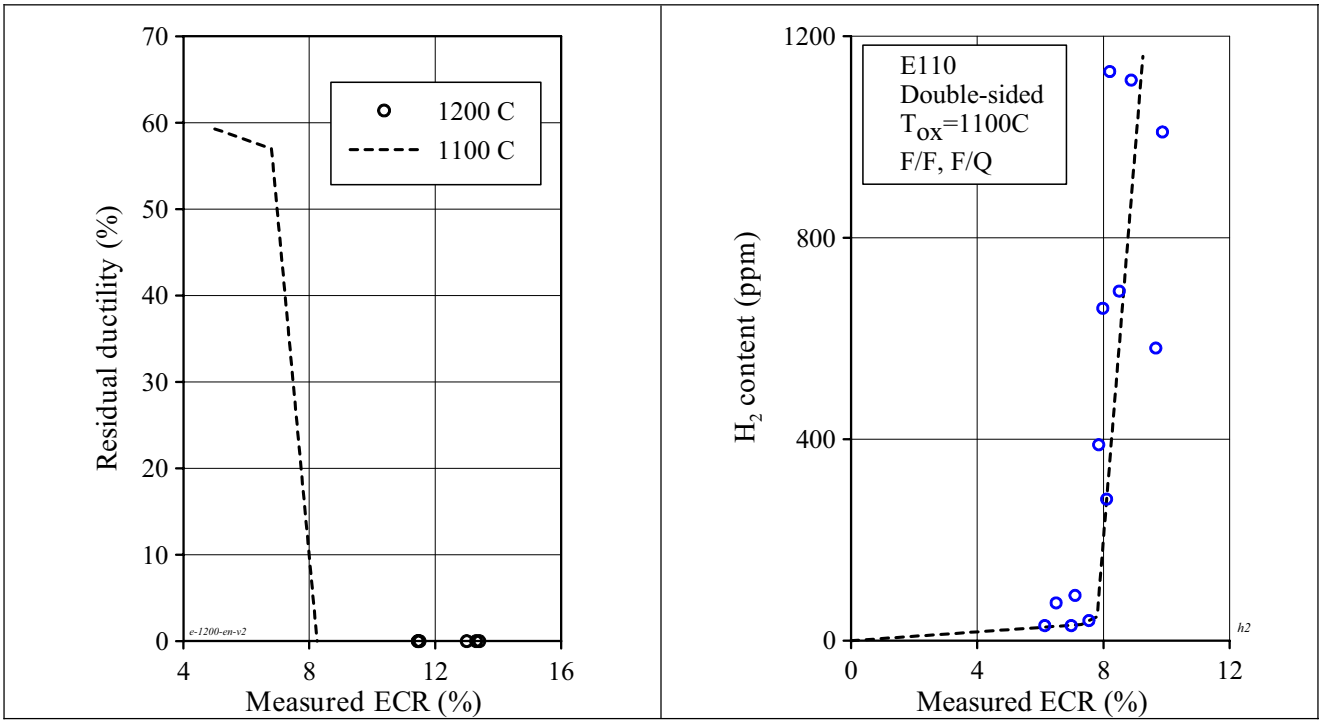

Fig. 3.58. The E110 residual ductility and hydrogen concentration as a function of the ECR after a double-sided oxidation at 1100 C and F/F, F/Q combinations of heating and cooling rates

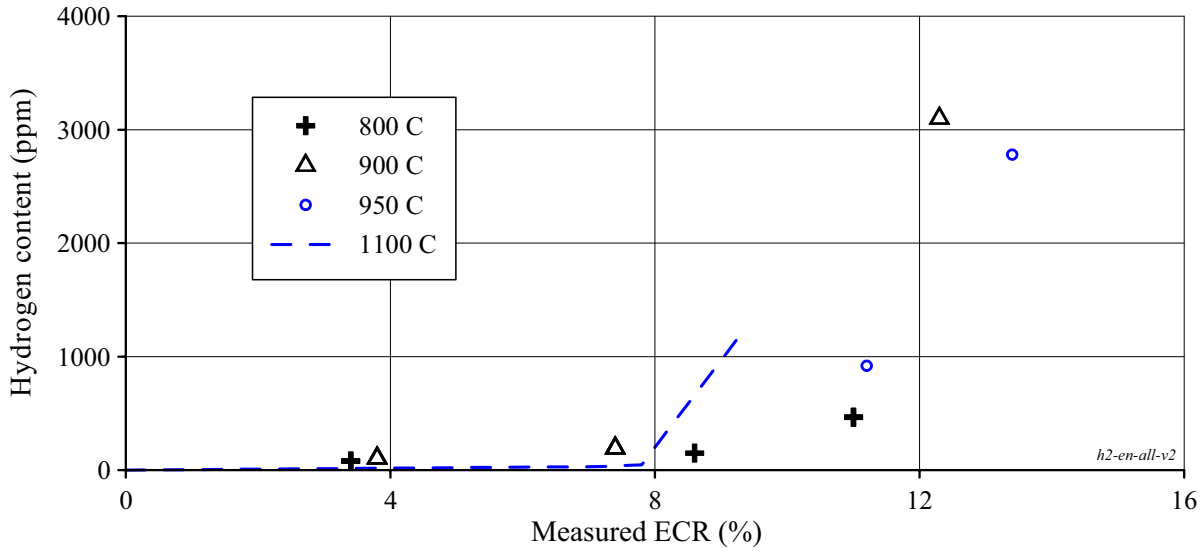

Fig. 3.59. The hydrogen content in the E110 cladding as a function of the ECR and temperature after a double-sided oxidation

A part of obtained data is in a good agreement with the results of mechanical tests presented in Fig. 3.57, so:

- the hydrogen absorption decrease at 800 C leads to the improvement of the E110 mechanical behavior and to the increase of the cladding zero ductility threshold up to the ECR higher than 12% (as-measured);
- the same (approximately) tendency of the hydrogen absorption at 900 C as at 1100 C leads to the same (approximately) mechanical properties of the oxidized cladding.

Unfortunately, it is impossible to continue the appropriate comparison for the second part of experimental data (950 C and 1000 C) in connection with the limited data on the hydrogen content but nevertheless, the

obtained results allow to assume that the transition to the accelerated hydrogen absorption will take place with approximately the same (or a little less) ECR as that for the temperature 1100 C.

As for revealed contradictions, then the following may be referred to those:

- according to the results of visual observations (see Fig. 3.55, Fig. 3.56) the claddings oxidized at 900–1000 C were to demonstrate the worst mechanical properties and, consequently, to show the maximum values for the hydrogen absorption. However, this is not so or not quite so as it can be seen from the above stated analysis;
- according to the data characterizing the allotropic phase transformation in the Zr-1%Nb alloys (see Fig. 3.54) the test results with the E110 cladding oxidized at 800 C may be logically explained by the fact that the β-phase fraction in the E110 cladding at this temperature is very small and, consequently, the general tendency of the cladding behavior corresponds to those of the low temperature oxidation of the E110 alloy in the area of the α-phase existence. All previous investigations have shown that the E110 alloy has the corrosion resistance in the α-phase temperature range;
- but in accordance with the same data (see Fig. 3.54), it is quite difficult to explain by what the oxidation conditions in the temperature range 900–1100 C differ (even if we take into account the effects associated with heating rates) as it is evident that the higher the temperature, the closer the Zr matrix composition approaches the β-phase that must provide the avoidance of the breakaway oxidation.

In connection with the list of revealed contradictions, it is appropriate to note the following:

1. The availability of such contradictions as a rule indicates that the number of key factors taken into account on analyzing is less than it is necessary.
2. The following factors may be referred to the unaccounted ones:

- the behavior of alloying elements (these aspects of the problem will be considered in the section 3.3.5 of the report;
- the behavior of oxygen and α-Zr(O) phase as a function of temperature and the size of Zr-matrix grains as a function of temperature.
- As for the behavior of oxygen α-Zr(O) phase and Zr-matrix as a function of oxidation temperature the appropriate data is organized in Fig. 3.60.

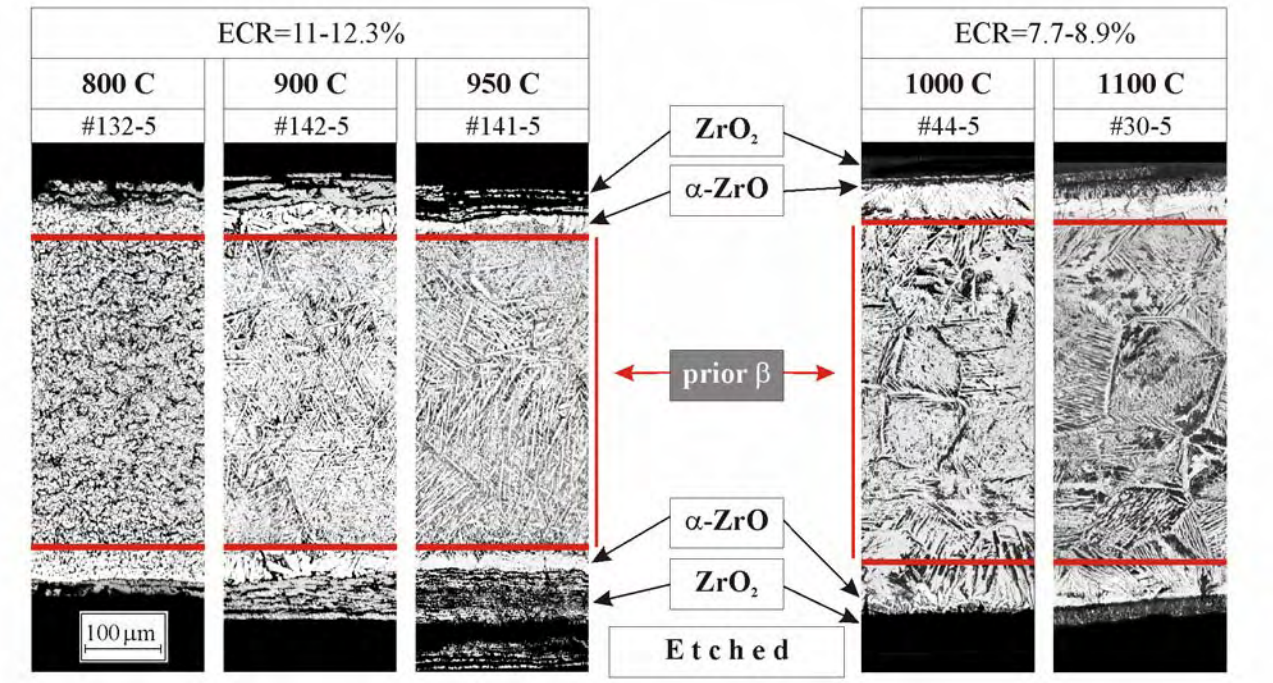

Fig. 3.60. The comparison of the E110 microstructure after a double-sided oxidation at different temperatures

The analysis of these data shown that:

- the thickness of α-Zr(O) phase at 800–950 C is significantly lower than that at 1000–1100 C in spite of difference in the oxidation level: 11–12.3% ECR at 800–950 C and 7.7–8.9% at 1000–1100 C; this effect leads to the fact that the thickness of the prior β-phase is approximately the same for both of the considered sets of data. But it is obvious that the prior β-phase thickness is one of most important factors that determine the residual ductility margin;
- besides, the size of Zr-matrix grain at the lower temperature is a little less than that at 1000–1100 C;
- moreover, the comparison of these two sets of experimental data shows that the tendency to the formation of α-Zr(O) needles that penetrate into the prior β-phase and the tendency to the formation of α-Zr(O) layers along large grains of the prior β-phase are typical only for the temperature range 1000–1100 C.

The revealed features of the E110 behavior at different temperatures allow to understand that multiparametric effects determine the cladding oxidation behavior under these conditions. But the resulting component of the combined effects from many factors may be characterized in the following way:

- the oxidation at 800 C is the upper threshold for a good behavior of the E110 cladding providing the approximate accordance between the experimental zero ductility threshold and the safety criterion;
- the oxidation at 900–1100 C results in the fact that the experimental zero ductility threshold is lower than the safety criterion.

The last position in this cycle of works was concerned with the investigation of peculiar features of the E110 cladding oxidation and embrittlement at the temperature 1200 C. The comparative data base characterizing this item of research is presented in Fig. 3.61.

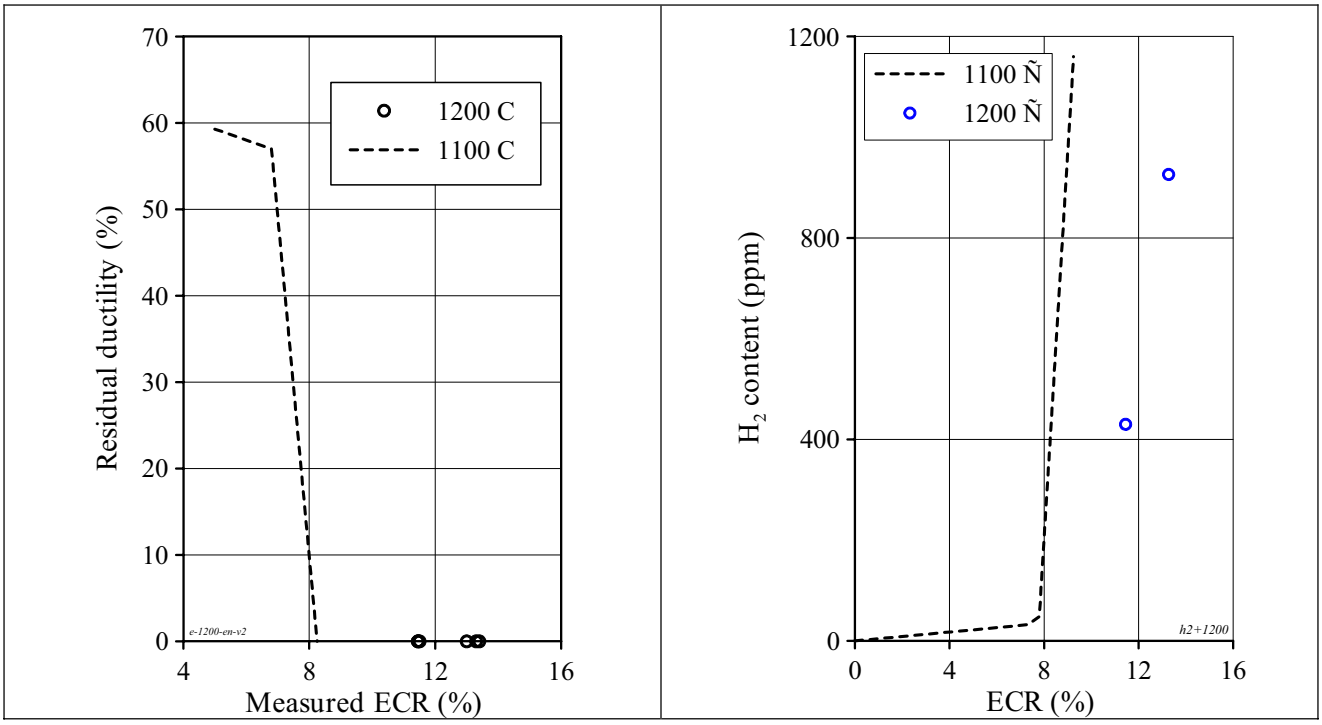

Fig. 3.61. The characterization of the E110 cladding behavior after a double-sided oxidation at 1200 C

The analysis of obtained data leads to the following conclusions:

- the zero ductility threshold of the E110 cladding oxidized at 1200 C is most likely not better than that at 1100 C;
- the tendency to the decrease of hydrogen absorption was observed in accordance with the results of this test. But it is known that the tendency to the increase of the oxygen content in the β-phase characterizes the cladding behavior at this temperature in the comparison with 1100 C.

- the E110 claddings continue to demonstrate the tendency towards the breakaway oxidation under this temperature.

3.3.5. The sensitivity of the behavior of Russian niobium-bearing alloys to the alloying composition

In the previous section of the report it was noted that:

- the oxidation behavior of the Russian Zr-1%Nb cladding (E110) and French Zr-1%Nb cladding (M5) is different;
- the analysis of appropriate effects has shown that the first difference that draws the attention is the following:
  - the initial oxygen concentration in the E110 cladding is 400 ppm (for claddings used in these tests);
  - the nominal oxygen concentration in the M5 cladding is 1350 ppm [35];
- the oxidation behavior of zirconium based claddings is sensitive to the concentration of such elements as Sn and Fe in the alloy.

To verify the sensitivity of the niobium-bearing cladding behavior to these factors, several tests were performed with two following cladding types:

- the E110K cladding: this is the E110 cladding with the increased oxygen concentration (up to 1100 ppm);
- the E635 cladding: this is the niobium-bearing cladding with the following alloying composition: (Zr-1%Nb-1.2%Sn-0.35%Fe [41].

The summary of test results with the E110K cladding is presented in Fig. 3.62.

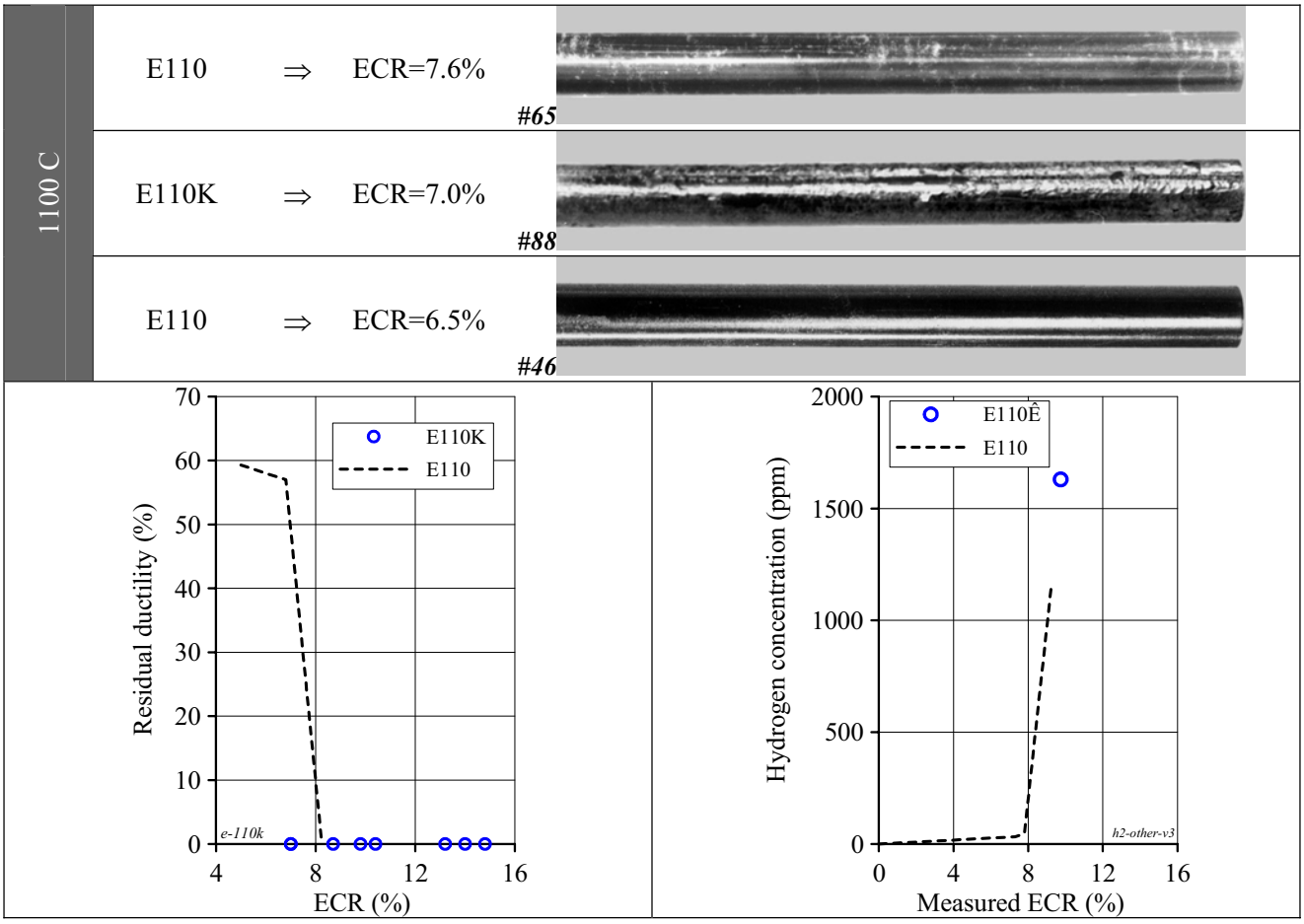

Fig. 3.62. The summary of results characterizing the E110K behavior under oxidation and ring compression test conditions

The analysis of obtained results allows to establish with confidence the following:

- the oxygen concentration increase in the E110 alloy does not lead to the elimination of the effect of of the early breakaway oxidation;
- the zero ductility threshold for the E110K oxidized cladding is not higher than that for the E110 cladding with the standard oxygen concentration. The E110K cladding has the same tendency of the hydrogen absorption by the prior β-phase.

Thus, these results bring to the conclusion that the general difference in the E110 and M5 cladding behavior is not connected with the initial oxygen concentration in the cladding material. The cladding response on the variation of Sn and Fe composition in the cladding material was studied in the experiments with the E635 cladding. The data base characterizing this test direction is presented in Appendixes B and F of the report. The organized results of these tests are shown in Fig. 3.63.

The consideration of test results has led to the following conclusions:

- the oxidation at 1000 C leads to more unfavorable consequences than those occurring at 1100 C, clear indications of the breakaway oxidation are observed on the appearance and microstructure of the cladding oxidized at 1000 C;
- the appearance and microstructure of the E635 cladding oxidized at 1100 C are noticeably better than those of the E110 cladding at 9.3% ECR;
- the hydrogen measurements confirm these observations:

– the hydrogen content in the E635 cladding oxidized up to the 9.3% ECR at 1100 C is significantly less than that in the E110 cladding;

- the hydrogen content in the E635 cladding oxidized at 1000 C even higher than that in the E110 cladding at the 5.3% ECR;
- the results of ring compression tests performed with the E635 cladding oxidized at 1000 C are in a good agreement with the above listed observations. In accordance with these results, all general characteristics for the E635 cladding oxidized at 1000 C are not better than those for the E110 cladding;
- the results of mechanical tests with the E635 cladding oxidized at 1100 C are rather contradictory as some rings have demonstrated the improvement of the mechanical behavior and the increase of residual ductility margin, but many rings have demonstrated the same results as those obtained for the E110 cladding or even worse ones.

The results of this analysis show that apparently, the chemical composition of niobium-bearing alloys is the important factor for the behavior of these alloys under high temperature oxidation conditions. However, tests of the E635 cladding for just another time bring us to the conclusion that there are some other factors unaccounted in the present analysis that influence the oxidation mechanism. The analysis of these will be continued in 4 chapter of the report.

3.3.6. Interrelation between the zero ductility threshold and the temperature of mechanical tests

All test results presented in the previous report sections were obtained in mechanical tests at the temperature 20 C (room temperature). However, it is evident that for safety practical analysis, it is of importance to understand to what extent the zero ductility threshold is sensitive to the temperature at the stage of proceeding from quenching during reflood to post-LOCA cooling. It is known that this stage is characterized by the achievement of the saturation temperature during reflood. This temperature may slightly differ for different reactors, however, by the existing tradition, the value of that is estimated as 135 C.

The preliminary analysis of results from the studies performed earlier allowed to establish the following:

- there are very limited data characterizing the oxygen induced embrittlement in this temperature range (20–135 C);
- quite a number of investigations were performed to study the effect of the hydrogen induced embrittlement.

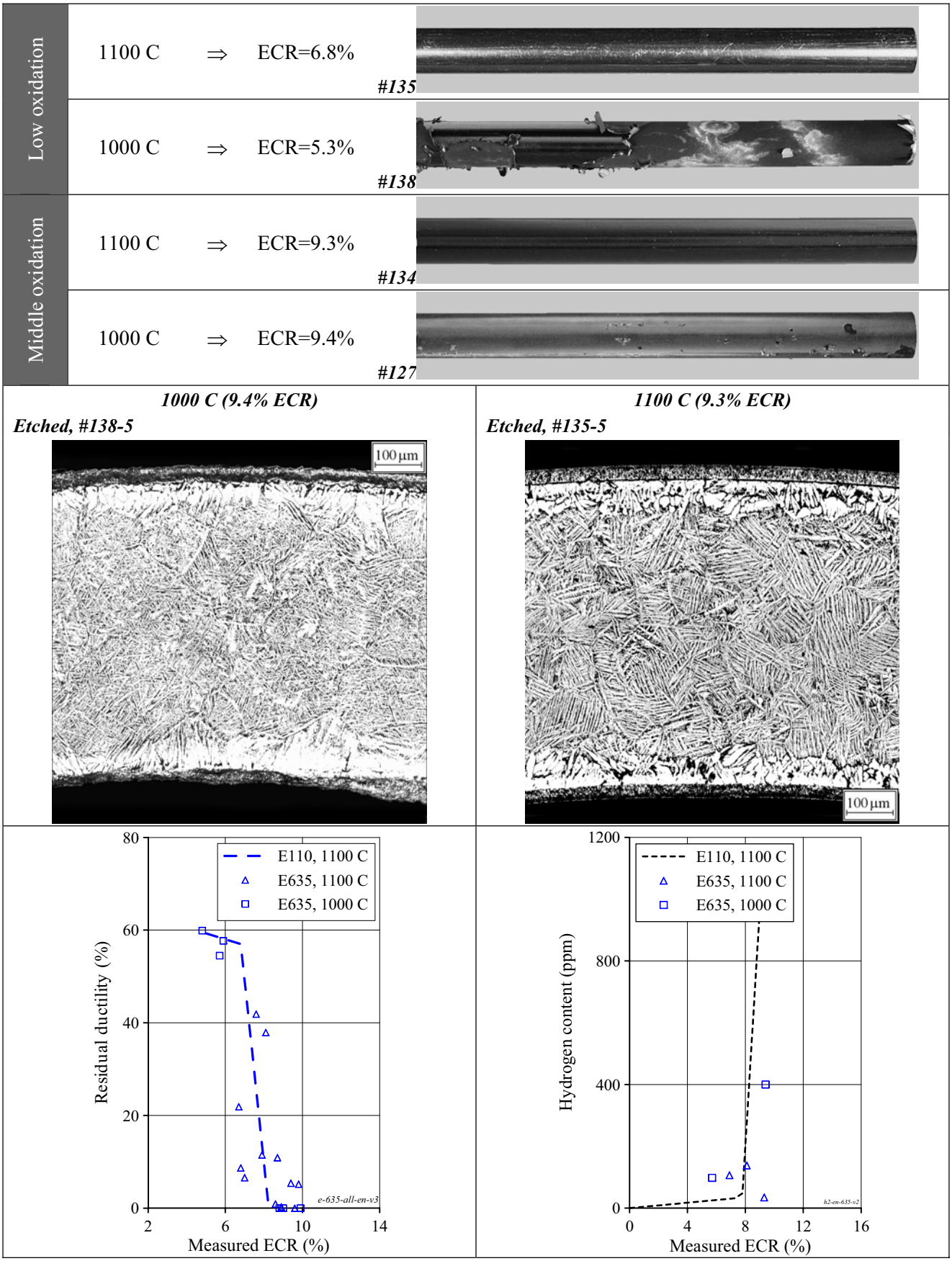

Fig. 3.63. The characterization of the E635 cladding behavior under oxidation and mechanical test conditions

So, as for the oxygen embrittlement, the most part of published data was devoted to the studies of the zirconium cladding mechanical behavior as a function of the initial oxygen concentration in the cladding material. In accordance with Russian data (for Zr-1%Nb) and other data for alloys of the zircaloy type, the elongation of the claddings with oxygen concentration 0.05–0.16% (by weight) in the α-phase is not sensitive to the temperature within the range 20–200 C. The previous Russian investigations performed in the Bochvar Institute (VNIINM, V.Tonkov) have shown that the ductility of the E110 oxidized claddings as a function of temperature of mechanical tests in the range 20–200 C is subjected to the following regularities:

- ZrO_2 and α-Zr(O) ductility is not increased in this temperature range;
- α-phase (prior β-phase) ductility is the function of the temperature especially in the range 100–200 C; however, the researcher associated this effect with the hydrogen behavior in the cladding material.

Unfortunately, this issue (the oxygen induced embrittlement) did not meet with due elucidation even in such a complete monograph which is the monograph of D.L. Douglass [42]. Though, the review made by D.L. Douglass contains the illustration that demonstrates that the samples manufactured from Zr-2.5%Cu alloy and oxidized up to 0.6% of the oxygen content in the zirconium matrix elongate from 2 up to 31% on the temperature increase from 20 up to 200 C.

The previous investigations performed by the authors of this report with unirradiated and irradiated Zr-1%Nb claddings have shown that the cladding elongation is not sensitive to the temperature of mechanical tests (20–200 C) in the presence of irradiation damage effects (50 MWd/kg U), low oxidation (oxide thickness 5 μm) and low hydrogen concentration (30 ppm) [19].

As for the hydrogen embrittlement, the appropriate effects revealed in a number of studies may be characterized in the following way:

- the oxidized cladding fracture resistance is a strong function of precipitated hydrides;
- the cladding ductility margin is a function of hydride concentration, size, orientation and morphology;
- the ductility of hydrides is a function of the temperature in the range from approximately 100 C and higher;
- it was experimentally demonstrated that brittle cracks initiated in the brittle α-Zr(O) layer slow down and are not developed in the prior β-phase while the hydride ductility is increased. In its turn, this effect results in the fact that the cladding elongation is increased also.

Besides, some additional observation of importance should be noted:

- the hydride-related embrittlement of such alloy as the irradiated Zry-4 is a function of a transformed beta microstructure [43];
- the temperature of ductile-brittle transition (DBT) is slowly increased with the hydrogen concentration increase [42];
- for the low hydrogen concentration in the prior β-phase, the transition from the brittle to ductile fracture is very sensitive to the temperature [42];
- the cladding ductility is not sensitive to the hydrogen concentration up to 70 ppm [44];
- the unirradiated cladding ductility at the room temperature is decreased very sharply down to low values with the hydrogen content of about 700 ppm [45];
- the worst ductile behavior was demonstrated at the room temperature in the cladding material with uniformly distributed hydrides [46].

The obvious illustration for some of the listed effects is demonstrated in Fig. 3.64 [47]. In accordance with these data, the cladding samples with lower hydrogen concentration (180 ppm) have demonstrated significantly higher sensitivity to the temperature of mechanical tests in the range 50–150 C than that of the cladding samples with hydrogen concentration of about 700 ppm. At 200 C, the mechanical behavior of both types of samples was quite ductile.

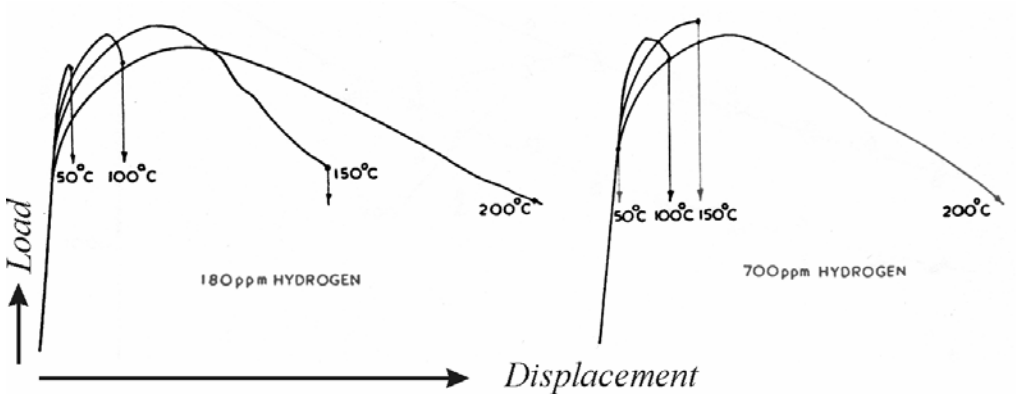

Fig. 3.64. Load-displacement diagrams for two Zry-2 samples hydrided (specially) up to 180 ppm and 700 ppm, respectively, as a function of the temperature mechanical tests of the bending type (reprinted from [47])

To reveal the temperature effects in the E110 oxidized and hydrided cladding after the oxidation tests performed in the frame of this work, the following approach was applied:

- the representative scope of mechanical tests (ring compression tests) was performed at 135 C with the E110 cladding samples oxidized at 800–1200 C and F/F, F/Q combinations of heating and cooling rates;
- several reference ring compression and ring tensile tests were performed with the E110 oxidized cladding samples in the temperature range 20–300 C.

The results of ring tensile reference tests are presented in Fig. 3.65.

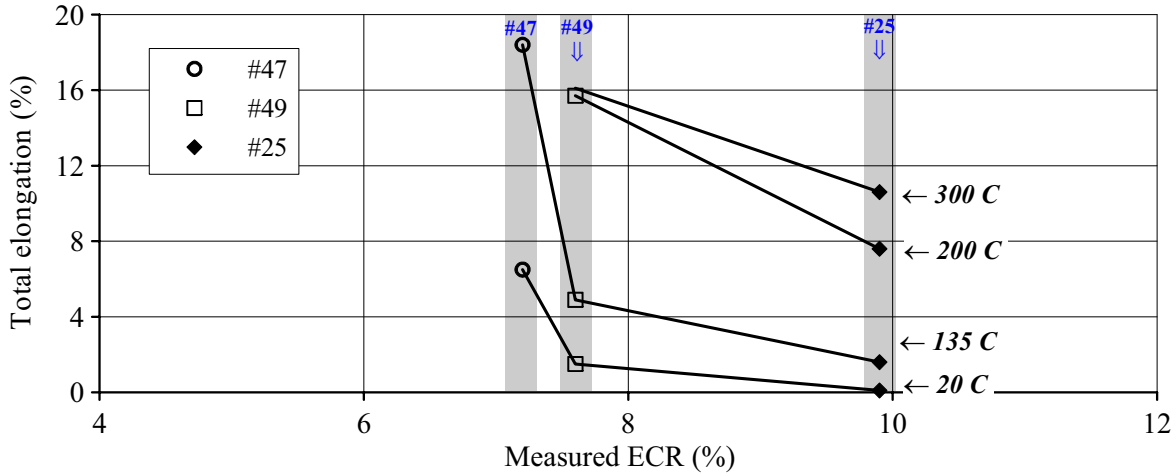

Fig. 3.65. Dependence of the E110 cladding ductility on the ECR (oxidation at 1100 C) and temperature of ring tensile tests

In accordance with these results the following comments can be made:

- the ductile cladding sample (#47, 7% ECR, the residual ductility 55–65% according to ring compression tests, low hydrogen content 30 ppm) demonstrated maximum sensitivity to the temperature of ring tensile tests in the range 20–135 C. The total elongation of this sample increased from 7% at room temperature to 17.5% at 135 C;
- the almost brittle sample (#49, 7.5 % ECR, the residual ductility 1.3–3.6 % according to ring compression tests, critical hydrogen content ~ 500 ppm) demonstrated:

– pronounced sensitivity to the temperature of ring tensile tests in the range 20–135 C. The total elongation increased from 1.5 to 5% respectively;

– very high sensitivity to the tensile test temperature in the range 135–200 C. Total elongation of this quite brittle sample increased from 5 to 16%;

– further increase of tensile test temperature to 300 C did not lead to the increase of ductility;

- the brittle sample with very high hydrogen content in the prior β-phase (#25, 9.9% ECR, hydrogen content 1000 ppm) shown a low sensitivity to the tensile test temperature between 20 and 135 C and high sensitivity in the range 135–300 C, where the total elongation increased from 1.7 to 10.6%.

Before we analyze the above stated comments, it will be useful to supplement this data base with results of the ring compression test performed at 20–300 C. The results are presented in Fig. 3.66.

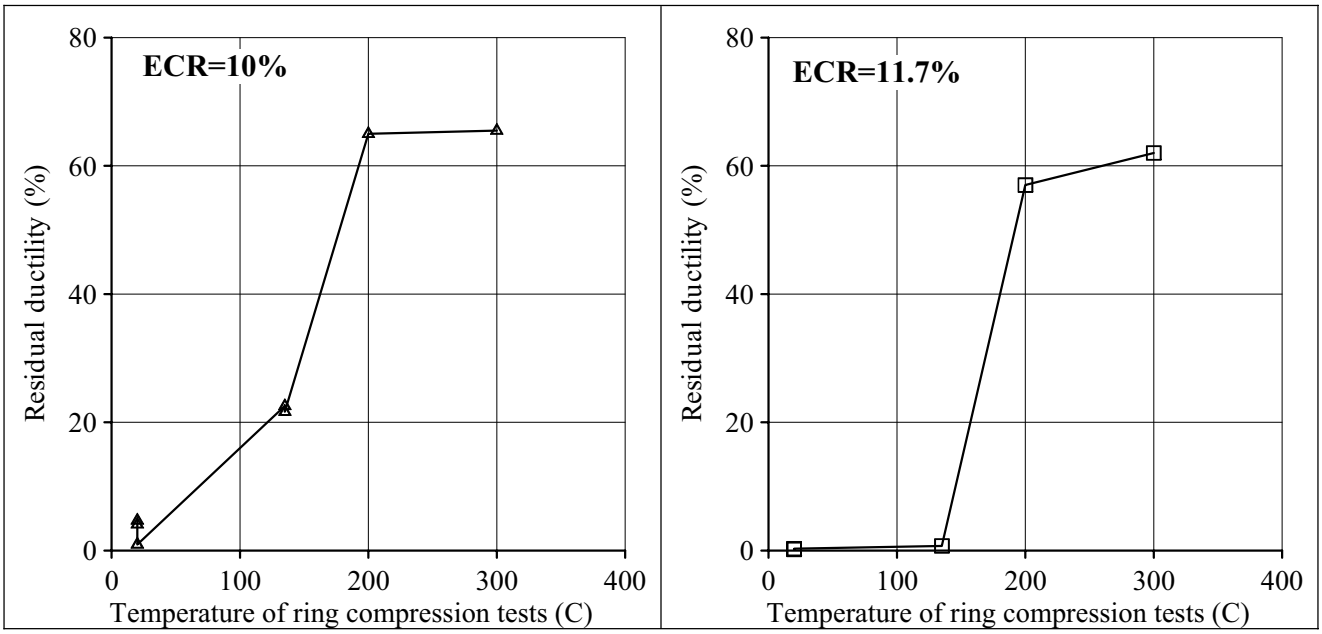

Fig. 3.66. Residual ductility of two E110 samples oxidized at 10 and 11.7% ECR (1100 C) as a function of temperature ring compression tests

The obtained data lead to the following observations:

- the sample (#68), which was oxidized somewhat higher than the zero ductility threshold (10% ECR) up to the hydrogen concentration of about 1000 ppm, has demonstrated definite sensitivity to the temperature of mechanical tests ranging from 20 up to 135 C; the residual ductility of this sample significantly increase in the range 135–200 C. However, we did not manage to reveal the influence of the temperature range 200–300 C over this sample ductility due to the fact that the maximal grip displacement (in these tests corresponded to the residual ductility of about 65%) was already achieved at the 200 C;
- the brittle sample (#36, ECR=11.7%) with a very high concentration of hydrogen (1500 ppm) was insensitive to the temperature of mechanical tests in the range 20–135 C, this sample ductility sharply increased in the temperature range 135–200 C, after that, the additional ductility increase was observed in the temperature range 200–300 C.

If we summarize the results of the preliminary analysis then the following tendencies may be noted:

- the less is the hydrogen concentration, the higher sensitivity to the temperature increase is demonstrated by E110 oxidized samples in the temperature range 20–135 C;
- the influence of the temperature of mechanical tests within the range 20–135 C over ductility of the E110 oxidized samples manifests itself still at the hydrogen concentration 1000 ppm, however, on the further hydrogen concentration increase (up to 1500 ppm), the cladding ductility is insensitive to the temperature within this range;
- the temperature increase up to 200 C leads to the significant increase of the cladding ductility in the whole studied range of the hydrogen concentrations;
- the temperature increase up to 300 C will influence the cladding ductility the more noticeably, the higher it was hydrided at 20 C.

The peculiar features revealed for the mechanical behavior of the E110 oxidized cladding may be clarified still more with the help of the representative data base obtained on the basis of ring compression tests performed at 20 C and 135 C. The first organized data characterize the relationship between the residual ductility of the E110 oxidized cladding and the hydrogen concentration at two temperature levels (see Fig. 3.67).

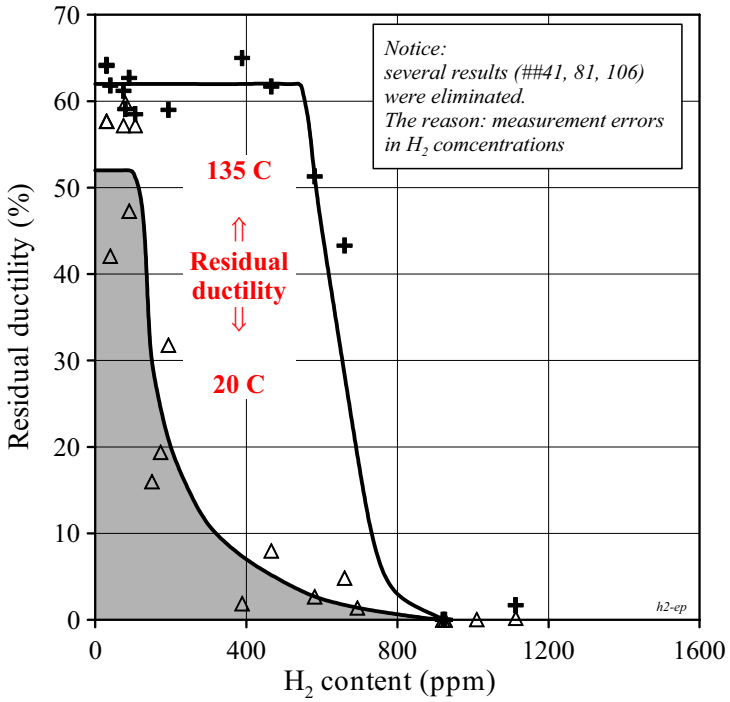

Fig. 3.67. The sensitivity of the E110 residual ductility (800–1200 C, F/f and F/Q) to the hydrogen concentration at 20 and 135 C

These data allow to make the following general conclusions:

- the residual ductility of the E110 oxidized cladding is a function of the hydrogen concentration;
- the E110 cladding has a very high level of residual ductility (higher than 50%) at 20 C within the interval of hydrogen solubility at 20 C (0–100 ppm);
- the residual ductility at 20 C decreases vary sharply in the narrow range of the hydrogen concentration: 100–200 ppm;
- the zero ductility threshold at 20 C is situated between 400–800 ppm of the hydrogen concentration;
- taking into account that the hydrogen solubility limit and ductility of hydrides are increased at 135 C, the E110 cladding samples demonstrate a very high level of residual ductility in the range of the hydrogen concentration 0–500 ppm;
- at 135 C, the decrease of residual ductility takes place very sharply with the hydrogen concentration 500–700 ppm and the zero ductility threshold corresponds to 900 ppm of the hydrogen concentration at this temperature.

The relationship between revealed effects and the oxidation level may be characterized using the second organized data presented in Fig. 3.68. In this case, the increment of residual ductility at 135 C (residual ductility at 135 C minus residual ductility at 20 C) was determined as a function of the ECR.

As it was already mentioned above, the results of ring compression tests do not allow to observe the effect of ductility increase with the temperature increase in mechanical tests for samples with high residual ductility at 20 C because the grip displacement of test machine was specially limited. In this connection, the increment of residual ductility at 135 C was not revealed in the range 0–6.5% (0–100 ppm of the hydrogen concentration). The ECR range of 6.5–8.3% characterizes a sharp decrease of residual ductility at 20 C, the sharp increase of the hydrogen content up to 700 ppm and a fast increase of increment of residual ductility at

135 C up to the maximum value that corresponds to the zero ductility threshold at 20 C (the critical ECR is 8.3%). After that, the increment of residual ductility at 135 C decreases fast down to zero that is associated with the increase of oxygen and hydrogen concentration in the prior β-phase.

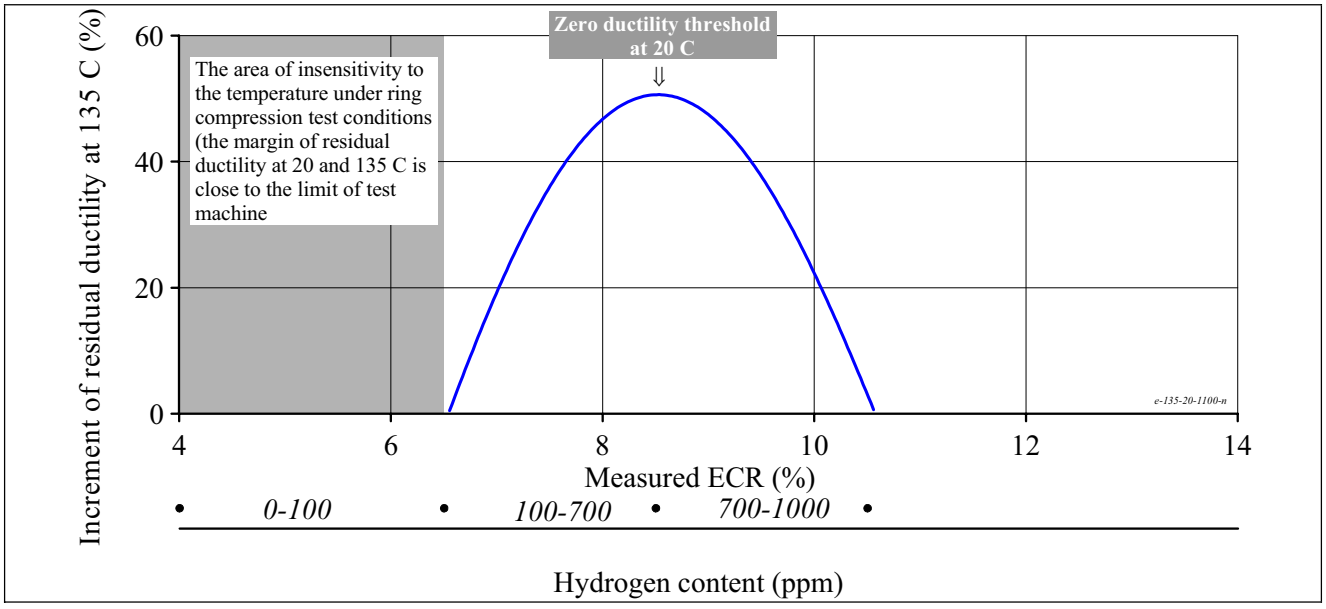

Fig. 3.68. The data characterizing the sensitivity of the E110 residual ductility at 135 C to the ECR (900–1100 C, F/F and F/Q)

Thus, this cycle of investigations allowed:

- to reveal the major effects associated with the hydrides behavior as a function of temperature;
- to reveal the sensitivity of the E110 residual ductility to the temperature.

But the analysis shows that one aspect of this issue remained not quite clear, namely, the consideration of temperature effects, associated not so much with the hydrogen embrittlement as with the oxygen embrittlement. Therefore, the analysis will be continued in chapter 4 of the report.

3.3.7. The analysis of representativity of the zero ductility threshold determined due to ring compression tests

It is obvious that the oxidized claddings of fuel rods will experience complicated multi-dimensional loadings during the real LOCA. Therefore, the problem of representativity of the zero ductility threshold determined using relatively simple ring compression tests is discussed simultaneously with performing studies of this type and during the time of this performance. The cycle of appropriate investigations performed in the frame of this work is the immediate contribution into the solution of this problem.

The approach, developed to obtain the comparative data for this issue analysis included the following items:

- the performance of several tests with other types of mechanical loading for the cladding samples and the comparison of the whole set of obtained results;
- the extension of the test data base involved into the determination of the zero ductility threshold due to the processing of data characterizing the maximum loads at the fracture;
- the comparison of macroscopic and microscopic data to confirm brittle or ductile fracture of oxidized claddings.

The test performed in accordance with the first item of this list included the ring tensile tests and three-point bending tests. The procedures for these tests are described in sections 3.2.2.2, 3.2.2.3 of the report. The comparative data characterizing results of ring tensile and ring compression tests are presented in Fig. 3.69.

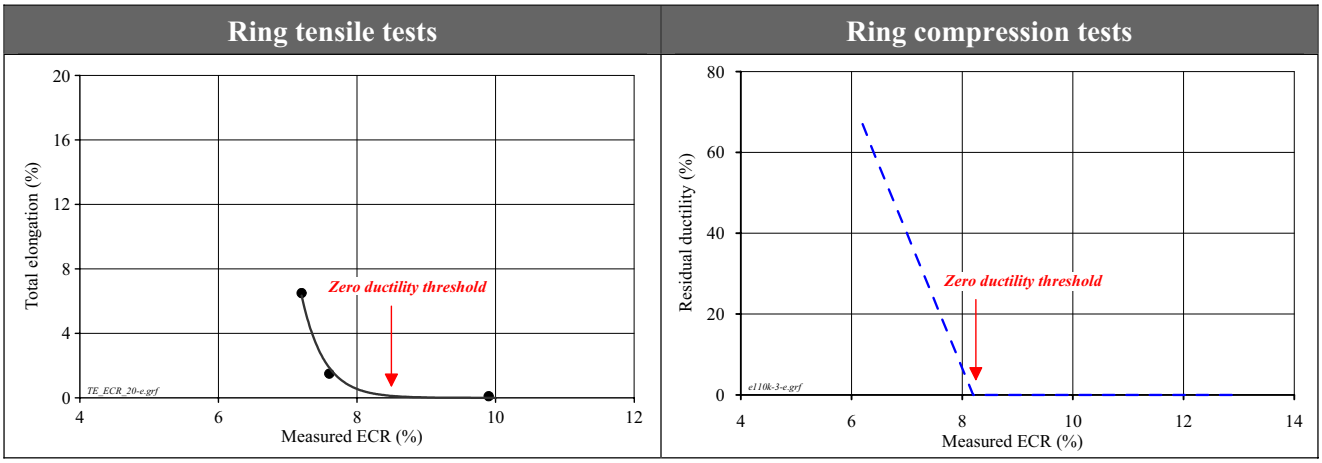

Fig. 3.69. The comparison of zero ductility thresholds determined from the results of ring tensile and ring compression tests (E110, 1100 C)

The obtained data indicate clearly that there is no difference in the zero ductility threshold determined using the ring tensile tests or ring compression tests. The results of three-point bending tests presented in Fig. 3.70 allow to conclude that the zero ductility threshold determined due to this type of tests is higher than that determined using the ring compression tests (11.8% and 8.3% ECR, respectively).

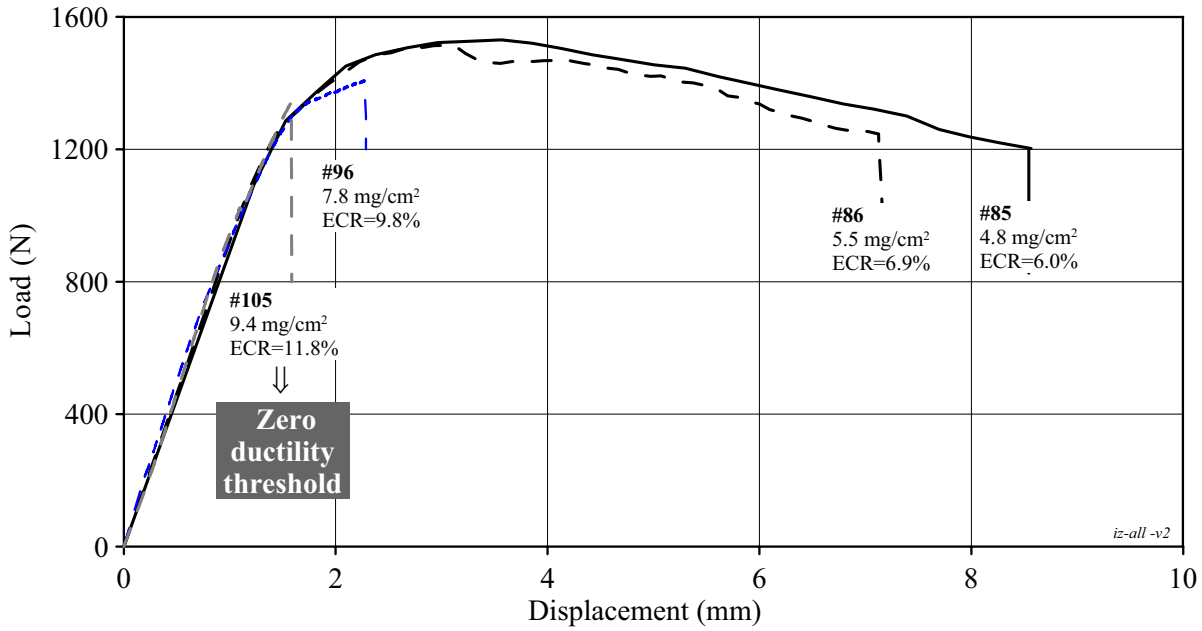

Fig. 3.70. The zero ductility threshold of the E110 cladding determined due to three-point bending tests (1100 C, F/F)

Thus, the comparative data base obtained due to different types of mechanical tests shows that ring compression tests allow to obtain the conservative estimation of the zero ductility threshold. This conclusion made on the basis of macroscopic tests is confirmed by the results of microscopic observations obtained using the fractography examinations. The fragments of two rings were selected for the fractography examinations after the fracture under the ring compression test conditions:

- a brittle ring: 1100 C, 8.2% ECR, double-sided oxidation;
- a ductile ring: 1100 C, 6% ECR, single-sided oxidation.

Two fracture surfaces of the brittle ring fragments were studied in detail (see Fig. 3.71):

- fracture surface characterizing the behavior of sample segment, which experienced the compression stresses on the outer surface and tensile stresses on the inner surface (the first fracture surface);

- fracture surface characterizing the behavior of other part of cladding, which experienced the tensile stresses on outer surface and compression stresses on the inner surface (the second fracture surface).

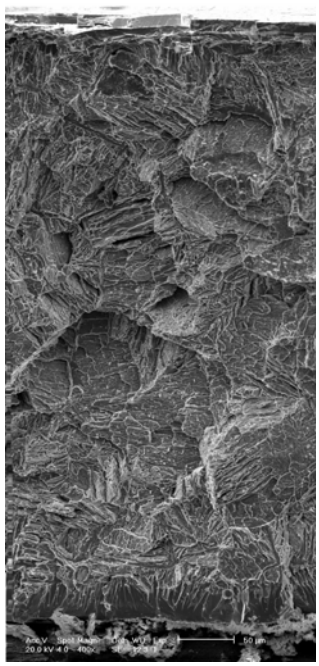

The first fracture surface

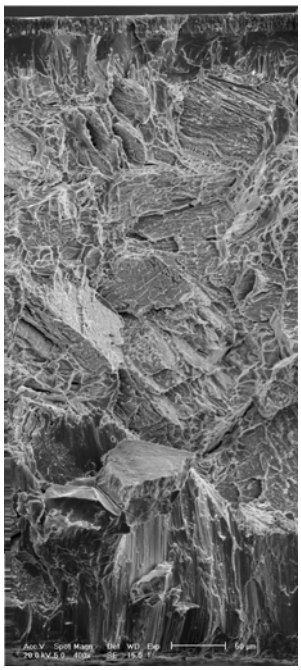

The second fracture surface

Fig. 3.71. SEM micrographs for fracture surfaces of the E110 brittle cladding

The examinations of the first fracture surface performed using the SEM micrographs with a high magnification (see Fig. 3.72) have shown that:

- the oxide layers on the outer and inner cladding surface are of the columnar structure and the oxide thickness is 15 μm (Fig. 3.72a,b);
- a typical pattern for α-Zr(O) surface is of the cleavage type (see Fig. 3.72b);
- the fracture pattern of the prior β-phase layer is quasi-cleavage (Fig. 3.72c), the fracture surface may be characterized as the "terrace" type (Fig. 3.72d), separate small regions of a dimple rupture are observed on the boundary between the α-Zr(O) and prior β-phase layers (Fig. 3.72e); besides, the transition from the quasi-cleavage fracture to the cleavage fracture is revealed in this region.

The structure of the second fracture surface as a whole does not differ from the first fracture surface though, a somewhat higher number of ductile fracture regions was fixed in this sample. Moreover, the fracture surface of the prior β-phase in this sample is characterized by the mixed type of the fracture pattern: the combination of quasi-cleavage facets and the dimples of the ductile fracture (Fig. 3.72f).

The analysis of the fracture surface in the ductile cladding sample confirms that the surface pattern of the prior β-phase is typical for the ductile fracture (see Fig. 3.73). Only separate small regions of the quasi-cleavage fracture type were observed in this sample. Thus, the fractography data have shown that small areas with the residual ductility are present in the material of even brittle samples but on the whole, the reasonable agreement between the microscopic and macroscopic assessments of the zero ductility threshold is observed in the fractography examinations.

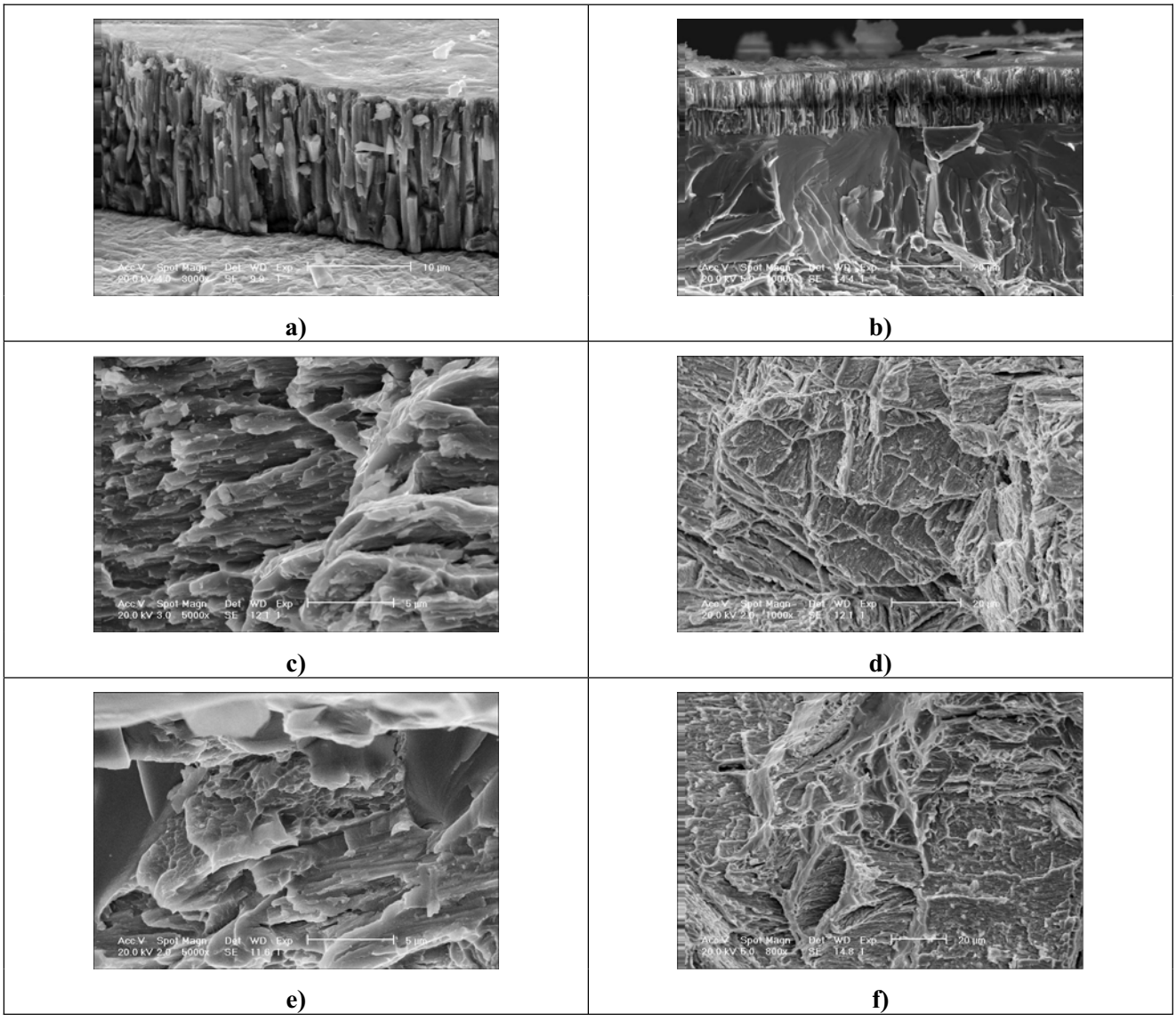

Fig. 3.72. High magnification SEM micrographs of fracture surface regions of the E110 brittle cladding

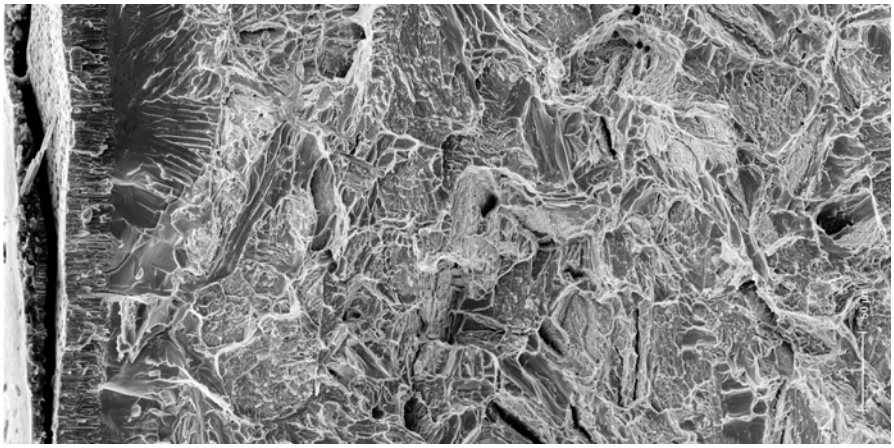

Fig. 3.73. The SEM micrograph for the fracture surface of the E110 ductile sample

It should be noted that the performed cycle of investigations employing ring compression tests for the determination of the zero ductility threshold in the E110 oxidized cladding allowed to reveal some more

issues connected with the representativity of these tests. The following two of those are considered in this report:

- the analysis of correlation between the fracture load and fracture displacement;
- the additional analysis of the sensitivity of the ring compression test results to the test procedures.

The first issue essence my be characterized in the following way: from the practical point of view, the significance of what strain the oxidized cladding has undergone during post-quench actions is not so important as that of what maximum load the cladding can stand before its fragmentation. It may be assumed that this was the reason for the authors of one of the recent papers dedicated to the M5 cladding behavior under the LOCA relevant conditions to present the characterization of the M5 fracture on the basis of the analysis of maximum loads at ring compression tests [46]. The approach of this type was the subject of the analysis performed in the frame of this work also. The organized data to clarify the appropriate issue are presented in Fig. 3.74.

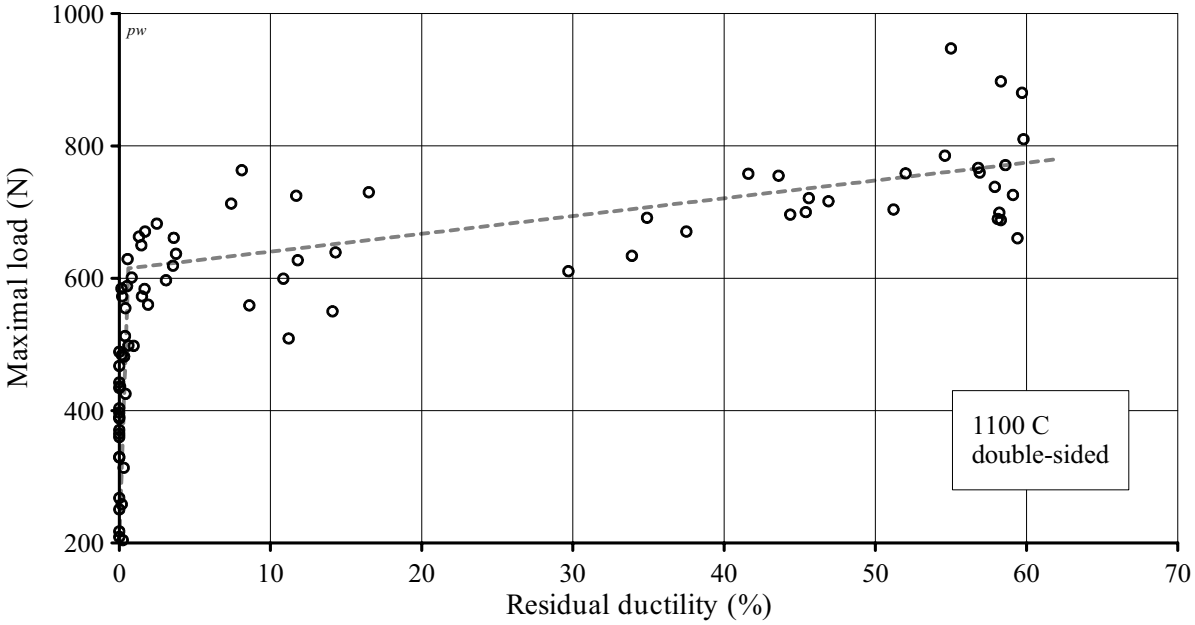

Fig. 3.74. The maximum load on the E110 oxidized sample as a function of residual ductility

The obtained data show the following:

- the decrease in the cladding residual ductility down to several percent affects its capability to withstand the load and indicates low strain hardening of the E110 oxidized cladding;
- there is a clear correlation between the zero ductility threshold and the sharp reduction in the strength properties of the E110 oxidized cladding (thus, the maximum load is decreased 3-fold as the ECR is increased from 8% up to 12%).

In other words, these data confirm that the zero ductility threshold determined as the zero residual ductility margin strongly corresponds to the appropriate critical load. But it should be noted that the employment of the critical load for the evaluation of the zero ductility threshold is not convenient as the critical load is not only the function of the ECR but it is also the function of the cladding sample length. Taking into account that there is no standard sample length for the ring compression tests and that different laboratories use samples with different lengths, in this case, it is impossible to compare the results.

The second issue that will be touched upon in this section of the report concerns just the comparison of the E110 zero ductility thresholds obtained in the ring compression tests performed in different laboratories. The analysis of comparative data base presented in Fig. 3.75 is devoted to the consideration of possible reasons for differences in evaluations of the E110 zero ductility threshold obtained by different laboratories.

The first observations concerning this comparative data base may be formulated in the following way:

- the relative order of the E110 regression correlations for test data obtained at VNIINM [15], KFKI [18, 25], NC Rossendorf [17, 24] and Scoda-UJP [10, 26] corresponds exactly to the order of the Zry-4 regression for these laboratories (see Fig. 3.28); this fact leads to the conclusion that this order is the function of experimental procedures used in each laboratory;
- in contrast to the data characterizing the Zry-4 mechanical behavior, the systematic difference is observed between the RRC KI/RIAR data and all other results;
- the zero ductility threshold of the E110 oxidized cladding is about 4.5–6% ECR in accordance with the VNIINM, KFKI, NC Rossendorf, Scoda-UJP results, while that is about 8.3% ECR in accordance with RRC KI/RIAR results.

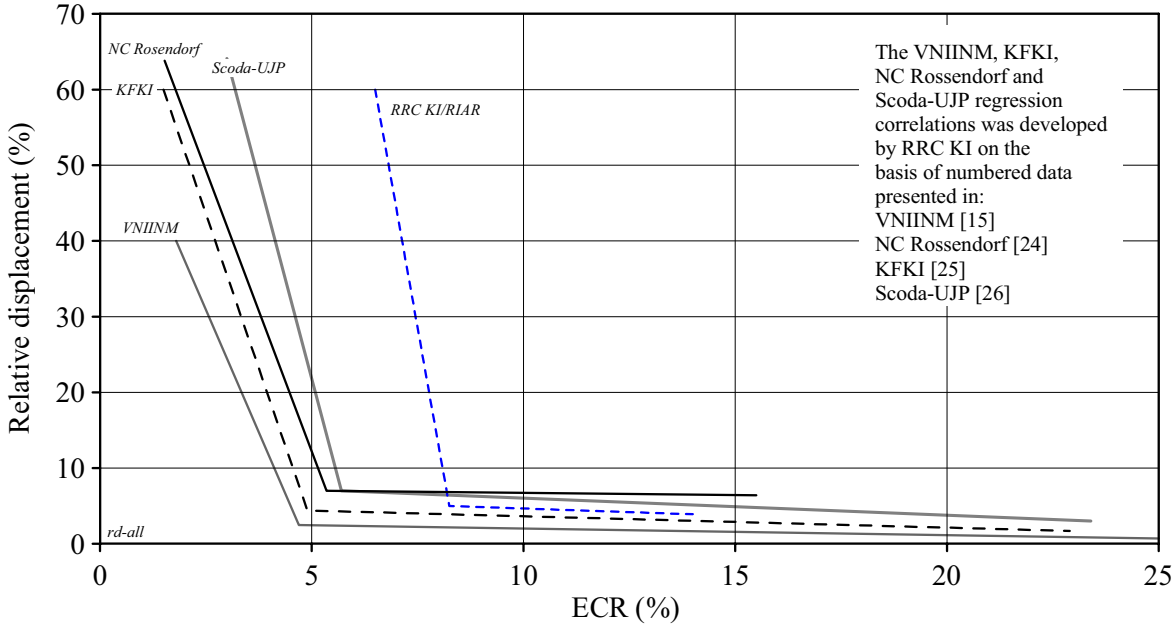

Fig. 3.75. The comparative data characterizing the E110 residual ductility as a function of the ECR obtained on the processing of test data of different laboratories

The special analysis results show that the following effects may be responsible for this difference:

- systematic errors in the procedure of the weight gain determination;
- differences in the E110 cladding material used for the oxidation tests;
- differences in the procedures of the oxidation tests (coolant type (water steam, water steam/argon mixture), heating and cooling rates) and differences in the procedures for the processing of load-displacement diagrams.

As for the procedure of the weight gain determination, the data base presented in Fig. 3.29 may be employed to assess the scale of this effect. These data show that the KFKI data really somewhat underestimate the weight gain in the Zry 4 cladding in comparison to the RRC KI/RIAR and NC Rossendorf data, but this effect is very small; the data presented in Fig. 3.28 allow to assume that the weight gain was very underestimated in the VNIINM tests. Besides, it is known that the Scoda-UJP tests were performed with the E110 claddings manufactured using the previous method of the E110 alloy fabrication, namely, the E110 claddings were fabricated from the iodide zirconium in contrast to iodide/electrolytic Zr used to manufacture the E110 cladding employed in the RRC KI/RIAR tests. The nature of the E110 cladding material used in the VNIINM, NC Rossendorf and KFKI tests is unknown. Besides the steam/argon mixture was used in the some of these tests. The sensitivity of test results to this parameter is not quite understood also.

And, finally, one more important potential cause for revealed differences must be considered. This cause is associated with the procedure for the preparation of the cladding samples for the mechanical tests. So, in section 3.2.2 it was demonstrated that results of the ring compression tests are not the function of the sample length. But this conclusion is referred to the procedure adopted in this study according to which the end parts

of the oxidized cladding were cut off and the mechanical tests with these parts of the cladding were not performed in contrast to the KFKI and VNIINM tests. Besides, the VNIINM tests were performed with very long oxidized samples (30 mm). The end parts of 20 mm samples were apparently removed in the NC Rossendorf tests because in accordance with the description of tests, two ring samples 8 mm and 5 mm long, respectively, were prepared from each of 20 mm oxidized claddings for compression tests and metallography investigations. But in our opinion, the lengths of cut off ends may appear to be not enough to compensate the effects described below. As for the Scoda-UJP tests the 7 mm rings were prepared from 30 mm oxidized samples.

The effects of the end parts of the E110 oxidized cladding may be characterized in the following way:

- the cladding oxidation takes place not only on the sample side surfaces but also on end surfaces of that. This results in the fact that the prior β-phase small cladding sample (for illustration, the sample 6 mm long was used in the KFKI tests) absorbs the oxygen from four sides. It is evident that the residual ductility of such sample will be lower than that of the sample oxidized from two sides only. In this case, this effect will be especially expressed at relatively low ECRs;
- the fact that the similar process taking place at the hydrogen absorption is still of more importance as the E110 alloy embrittlement occurs not so much according to the mechanism of the oxygen embrittlement as to that of the hydrogen embrittlement.

The effect of the hydrogen absorption by the end surface may be qualitatively illustrated by the results presented in Fig. 3.76 (Reprinted from Reference 48, Fig 5b).

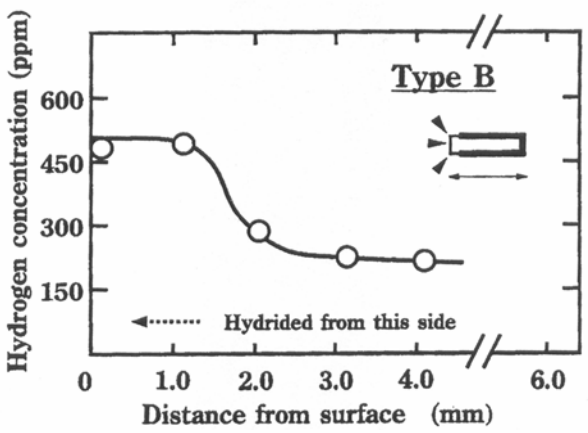

Fig. 3.76. Hydrogen distribution along the width of a special Zry-4 sample

Special investigations performed in JAERI [48] allowed to see that the end effect is strongly expressed on the length of 3 mm under these test conditions. The hydrogen concentration is 2.5 times reduced along the whole length.

Besides, it is necessary to point out once more that the hydrogen absorption by the E110 cladding is the consequence of the breakaway effect. In this case, as it was repeatedly noted earlier, the precise connection is between stresses in the oxide layer and the initiation of this effect. A special analysis performed during this research allowed to establish that the initiation of the breakaway effect takes place at the end parts of the cladding sample as, apparently, this part of the cladding sample represents a special concentrator of stresses occurring on the boundary between the end and side cladding surfaces. This statement is obviously demonstrated by the data presented in Fig. 3.77.

The obtained data obviously indicate that the initiation of the breakaway oxidation and, consequently, the initiation of the cladding hydriding, and then, the cladding embrittlement takes place in the end part of the oxidized cladding noticeably earlier than in the sample basic part.

Taking into account this analysis results, it may be assumed that the difference between the RRC KI/RIAR assessment of the E110 zero ductility threshold and assessments of this threshold performed in other laboratories is explained in the first turn by the fact that the RRC KI/RIAR test data are independent of the end

effects while the results of other investigators are overburdened with the end effect. Though, it is evident that other factors listed in the discussion of this issue additionally contributed into revealed differences.

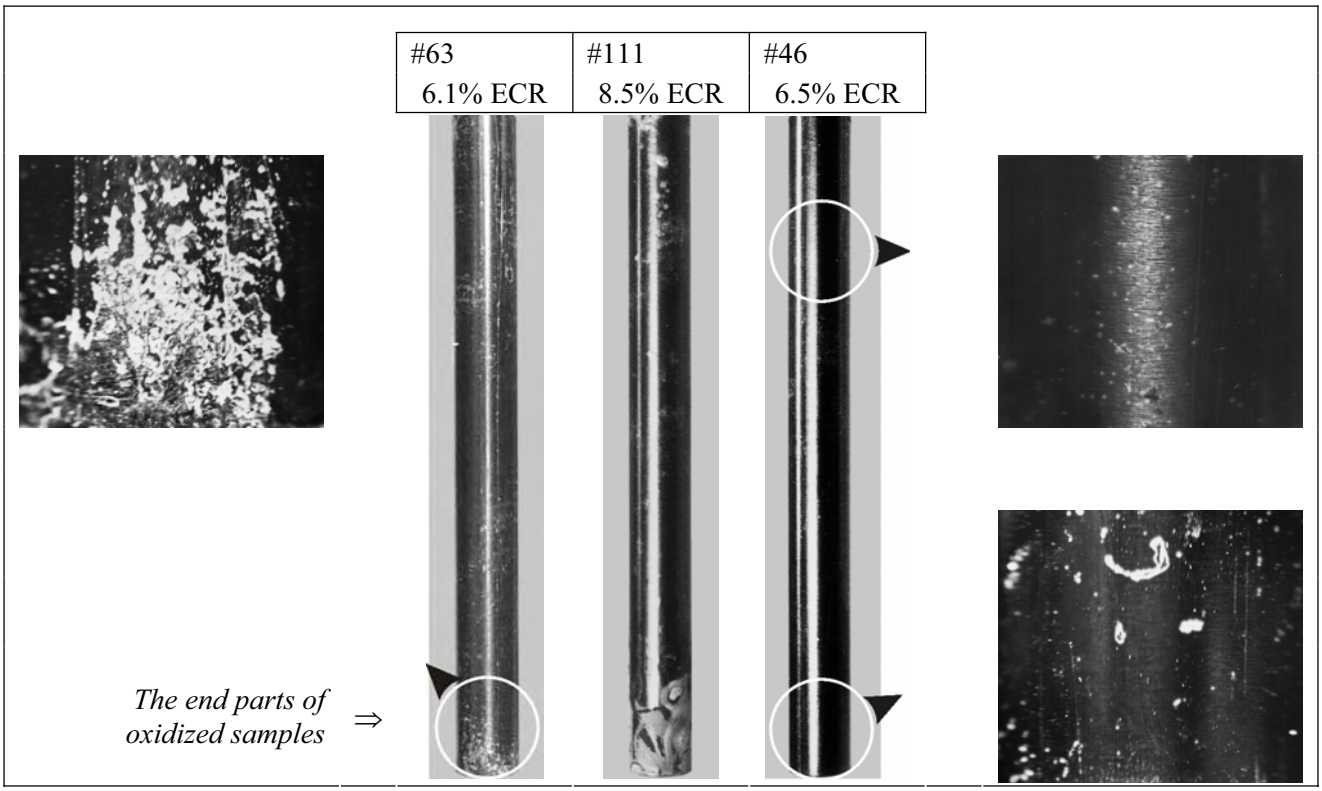

Fig. 3.77. Demonstration of the end effects on the E110 oxidized cladding samples

3.3.8. Consideration of the zero ductility threshold of the E110 cladding as a function of the irradiation effect

It is important to note that this stage of research does not pretend to be completed. The goal of this stage was to obtain the first experimental data characterizing the scale of the irradiation effect as applied to the E110 cladding. To study the appropriate phenomena, eleven irradiated claddings refabricated from the VVER high burnup fuel rods (50 MWd/kg U) were tested. The initial characteristics of irradiated claddings are presented in Appendix A–3. The oxidation and hydrogenation of the E110 irradiated cladding were characterized by the following values before the oxidation tests:

- the outer oxide thickness is 5 μm;
- the inner oxide thickness is 0 μm;
- hydrogen content is 47 ppm.

The results of the irradiated cladding tests are presented in Appendixes B and I of the report. These tests consisted of two stages:

1. Scoping oxidation tests performed at the test modes with S/S (slow/slow) and S/F (slow/fast) combinations of heating/cooling rates.
2. Basic oxidation tests performed at the F/F combination of heating and cooling rates with the variation of temperature in the range 1000–1200 C.

The analysis of the cladding appearance and microstructure after the basic oxidation tests at 1100 C allows to note the following (see Fig. 3.78):

- any indications of the breakaway oxidation are not observed on the outer cladding surface up to 7.0% ECR;
- insignificant indications of the breakaway oxidation occur at the higher ECR, however, these indications are expressed significantly weaker than those for the unirradiated cladding;
- the oxidation behavior of the irradiated cladding differs considerably by the following processes:

– the obviously expressed tendency towards the increase of the oxide thickness on the inner cladding surface in comparison with the outer oxide thickness;

– the obviously expressed tendency towards the formation of the oxide lamination and the tendency towards the oxide spallation starting from 7.7% ECR on the inner cladding surface;

– the more expressed tendency towards the generation of the α-Zr(O) phase along the grain boundaries of the prior β-phase.

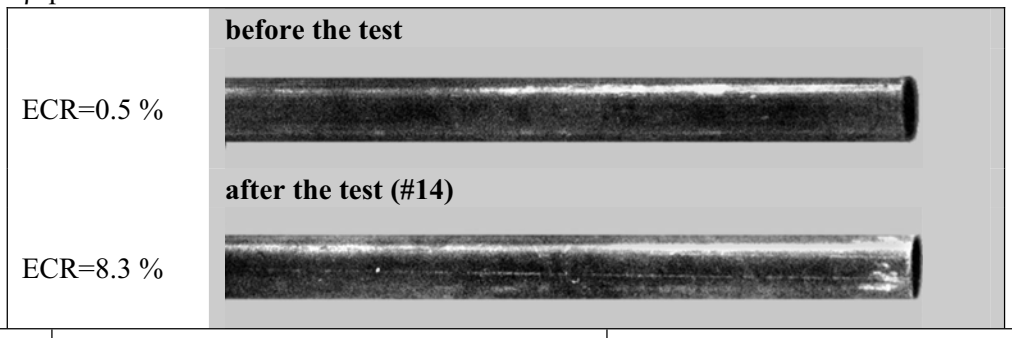

Sample	Outer surface	Inner surface
Before oxidation tests (Polished)	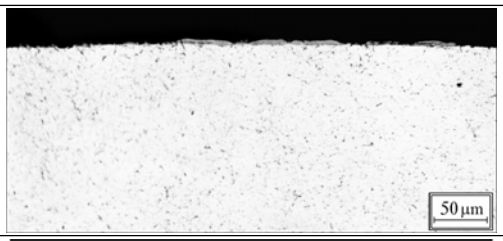	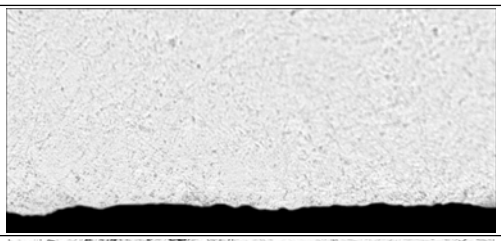
#20-4 ECR=6.3 % (Etched)	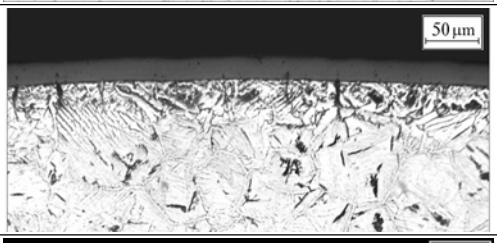	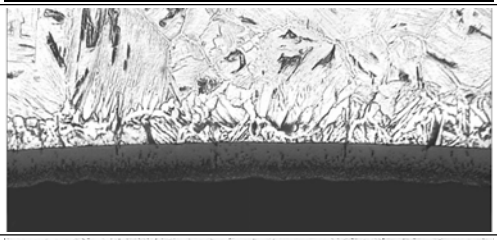
#10-4 ECR=7.7 % (Polished)	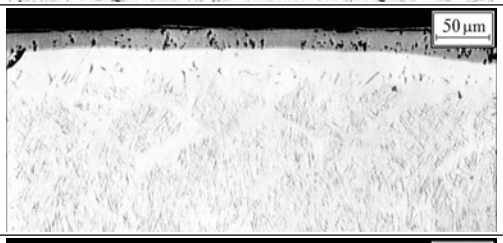	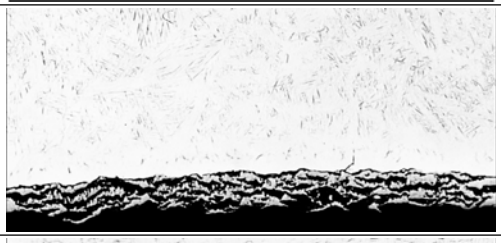
#14-4 ECR=8.3 % (Polished)		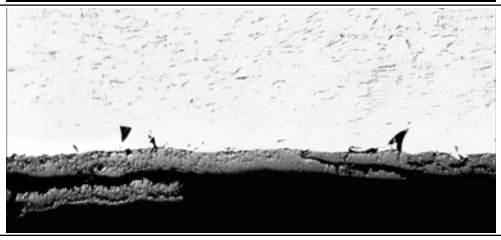

Fig. 3.78. The appearance and microstructure of the E110 irradiated cladding before the tests and after the oxidation tests at 1100 C and F/F combination of heating and cooling rates

It may be assumed that the revealed peculiar features are associated, first, with the presence of fission products on the inner cladding surface and with the participation of some of those in the oxidation reaction and, second, with the change of the cladding microstructure during the base irradiation.

As for the dependence of the oxidation behavior on the test conditions, then the performed studies have shown that:

- the irradiated cladding oxidation under slow transient conditions (S/S combination of heating and cooling rates) leads to the macroscopic effects of the oxide spallation at 10.5% ECR (see Fig. 3.79);
- the oxidation at 1200 C leads to the significant decrease or disappearance of the breakaway effect from the microscopic point of view, nevertheless the microstructure demonstrates the "hydrogen-modified" type (see Fig. 3.79).

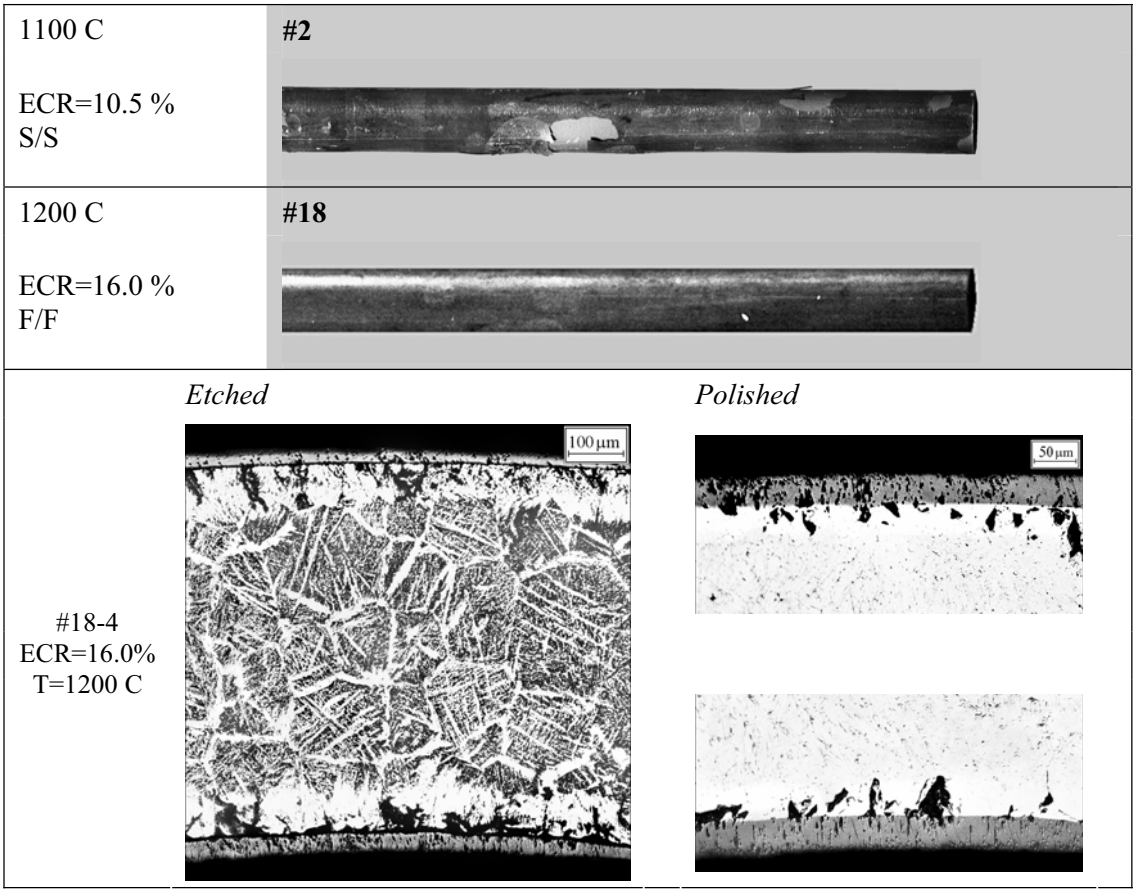

Fig. 3.79. The appearance and microstructure of the E110 oxidized cladding after the slow transient oxidation at 1100 C and standard oxidation at 1200 C

The ring compression tests performed with the E110 oxidized irradiated claddings allows to obtain the results presented in Fig. 3.80. The preliminary analysis of these results shows that a general tendency towards the decrease in the zero ductility threshold (ZDT) is observed in the irradiated claddings. To extend the data base for the more accurate analysis of specific physical processes in these claddings, the following additional investigations were performed:

- the microhardness measurement;
- the hydrogen content measurement.

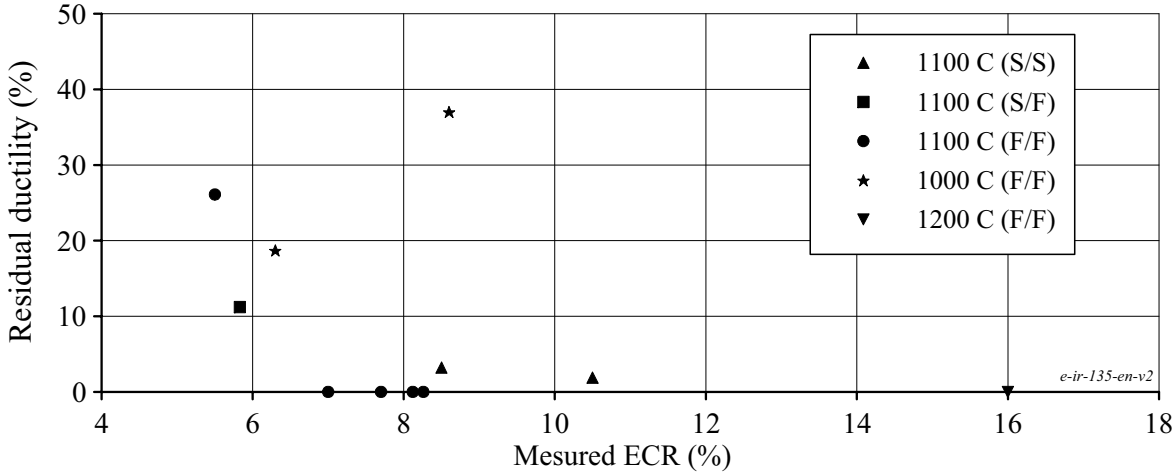

Fig. 3.80. The residual ductility of the E110 irradiated cladding as a function of the ECR

The comparative data presented in Fig. 3.81 to characterize the microhardness of different types of the E110 cladding (unirradiated, irradiated, oxidized and unoxidized) allow to make the following important observations:

- the initial microhardness of the E110 irradiated cladding (before the oxidation) is higher than that of the E110 unirradiated cladding by 60 kg/mm^2;
- the microhardness of the E110 unirradiated oxidized cladding (7.0% ECR) with a high margin of residual ductility (sample #47) is about 250 kg/mm^2 and (as it was demonstrated earlier, see Fig. 3.44) the microhardness of the E110 unirradiated oxidized cladding (ECR=8.2%) at the zero ductility threshold (sample #41) is the same;
- the microhardness of the E110 irradiated oxidized cladding (6.5% ECR) with a significant margin of residual ductility (sample #17) is practically the same as that in the E110 irradiated oxidized cladding (7.7% ECR) close to the ZDT (sample #10); this microhardness is about 300 kg/mm^2;
- the microhardness of the E110 irradiated oxidized cladding increases significantly in the ECR range 7.7–8.3% ECR and after that the microhardness is not practically changed up to 16% ECR.

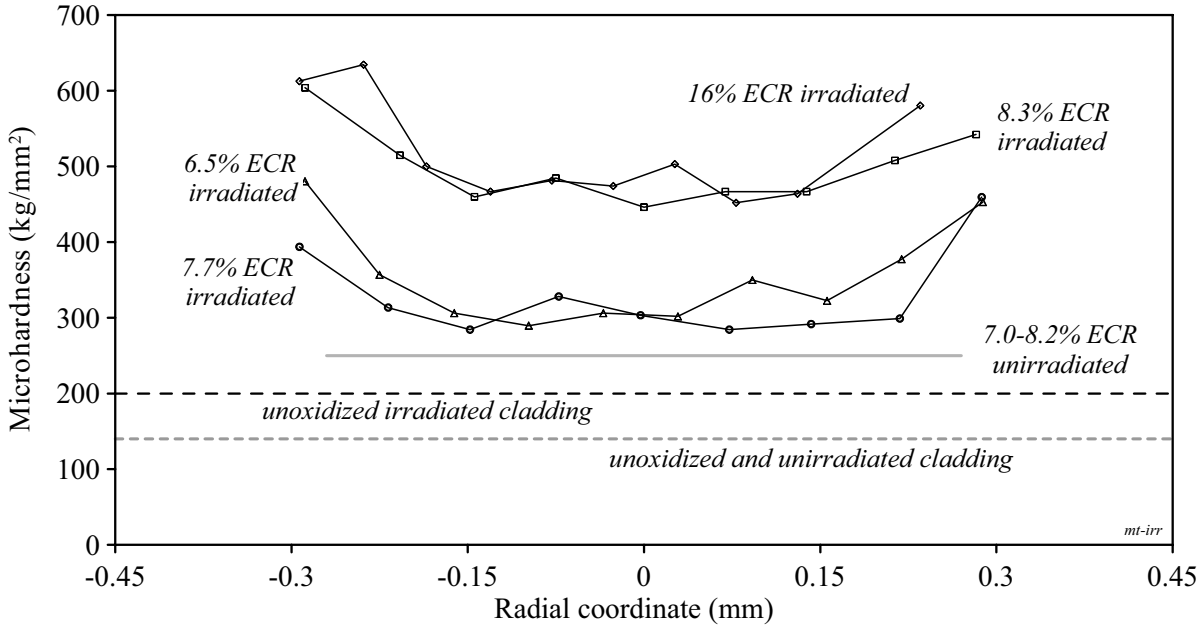

Fig. 3.81. Comparative data characterizing the microhardness of the E110 oxidized irradiated claddings

The analysis of these observations leads to the following conclusions:

- some initial embrittlement effect is observed even in such a “good” irradiated cladding as the E110 cladding;
- the oxygen concentration exceeding the oxygen embrittlement threshold (0.6–0.9% by weight) of the prior β-phase is apparently achieved in the E110 irradiated cladding at the ECR≥8.3%;
- the zero ductility embrittlement threshold of the E110 irradiated oxidized cladding is apparently determined by the same combination of factors that was determined for the E110 unirradiated cladding, namely: by the combined effect of the oxygen and hydrogen embrittlement of the oxidized cladding prior β-phase.

The continuation of this analysis performed using the results of the hydrogen concentration measurements allowed to reveal the following additional peculiar features for the behavior of the E110 irradiated cladding:

- in spite of the fact that the oxide spallation was obviously demonstrated in the oxidation mode under slow transient conditions (S/S combination of heating and cooling rates), all three cladding samples tested at slow heating had a relatively low hydrogen concentration in comparison with the samples tested at fast heating;
- the cladding samples tested under slow heating conditions demonstrated the tendency towards the increase of the zero ductility threshold in comparison with the samples oxidized at fast heating.

Taking into account all above mentioned considerations, two correlations were developed to characterize residual ductility of the E110 irradiated oxidized cladding as a function of the ECR and oxidation modes (see Fig. 3.82).

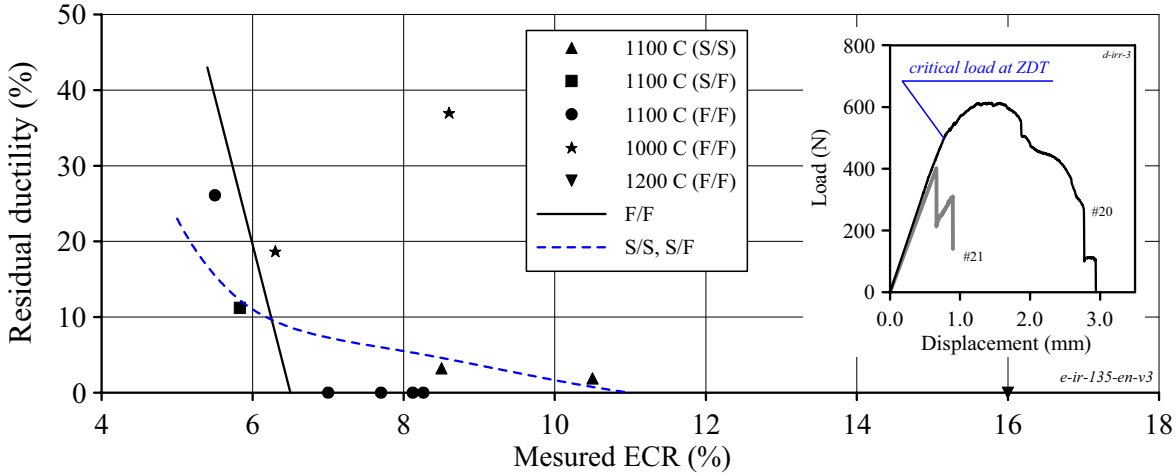

Fig. 3.82. The zero ductility threshold of the E110 irradiated cladding after different oxidation modes

It should be also noted that to minimize a possible error in the assessment of the zero ductility threshold at the F/F oxidation mode, the load-displacement diagrams were additionally analyzed. As it can be observed in the data presented in Fig. 3.82, the cladding sample #21 was tested at the ECR that was somewhat higher than the zero ductility threshold. The quantitative analysis of this discrepancy performed using the analysis of other load-displacement diagrams has shown that the zero ductility threshold for this oxidation mode F/F may be evaluated with a good accuracy as 6.5% ECR.

The organization of the data base characterizing the hydrogen content in the E110 irradiated oxidized cladding as a function of the ECR was performed in accordance with the similar approach (see Fig. 3.83).

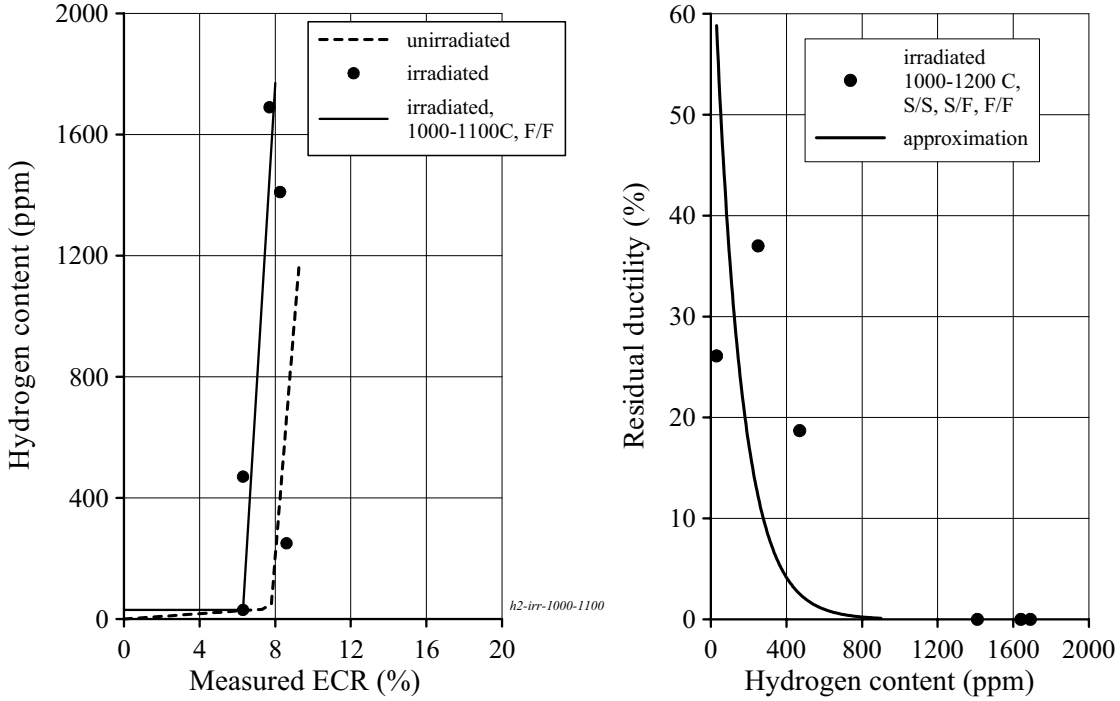

Fig. 3.83. The E110 hydrogen concentration as a function of irradiation and ECR, residual ductility of the E110 irradiated cladding as a function of hydrogen concentration

The regression dependence presented in Fig. 3.83 characterizing the hydrogen content in the E110 irradiated cladding was developed for the F/F oxidation mode in the temperature range 1000–1100 C. The appropriate dependence at the temperature 1200 C will apparently demonstrate a smoother increase of the hydrogen content as a function of the ECR. The comparison of obtained data with results obtained for the E110 unirradiated cladding shows that the hydrogen absorption takes place in the irradiated cladding still more intensively. However, coming back to the results of the analysis performed using the metallographic views, it may be assumed that special processes occurring on the inner cladding surface are responsible for revealed differences.

Additional data presented in Fig. 3.83 to describe the relationship between residual ductility of the E110 irradiated cladding and hydrogen content (developed with regard to all test modes and all temperatures) are in a good agreement with the similar data obtained for unirradiated claddings. Nevertheless, it is impossible to exclude the fact that a definite peculiarity in the behavior of the irradiated cladding during the oxidation may be caused by the changes in its microstructure that took place during the base irradiation. Thus, the SEM investigations performed with the E110 irradiated cladding allowed to reveal the following tendencies:

- the cladding material structure is characterized by the α-Zr phase containing the global β-Nb precipitates;
- the niobium concentration in the matrix is practically equal to zero.

Taking into account the considered earlier oxidation effects associated with niobium, it may be assumed that in this case, the change of the Zr-1%Nb material structure results in some change of its oxidation behavior.

3.3.9. The analysis of the E110 oxidation kinetics

To develop the E110 oxidation kinetics, the parabolic law was used:

$\Delta W^2 = Kt$,

where ΔW – the weight gain (mg/cm^2);

t – time (s);

K – rate constant (mg^2/cm^4 s).

Besides, it was assumed that the rate constant may be described by Arrhenius relation:

$$K = A \exp\left(-\frac{Q}{R\,T}\right),$$

where A – empirical coefficient (mg^2/cm^4 s);

Q – activation energy (J/mol);

R – gas constant (J/mol K);

T – temperature (K).

The processing of test data started from the determination of K using each measured combination of ΔW and t. The averaged value of ΔW obtained in the several ring samples cut off from one 100 mm cladding sample was employed for this goal. These data were used to develop the regression dependence presented in Fig. 3.84. It should be noted that the data obtained at the F/F and F/Q combinations of heating and cooling rates only were used for this procedure.

The obtained correlation is valided for the following oxidation duration as a function of the oxidation temperature:

- 1073 K → 29000 s;
- 1173 K → 4800 s;
- 1223 K → 5000 s;
- 1273 K → 1800 s;
- 1373 K → 1800 s;
- 1473 K → 400 s.

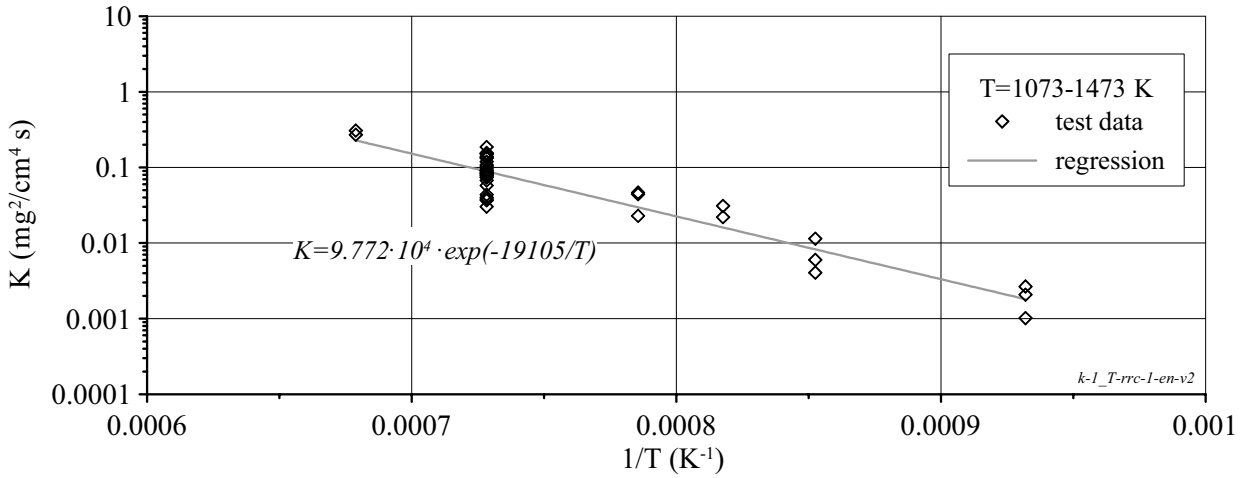

Fig. 3.84. Determination of the rate constant at the oxidation of the E110 unirradiated cladding in the temperature range of 1073–1473 K

The sensitivity of the E110 oxidation kinetics to the irradiation effect may be preliminary estimated using the data presented in Fig. 3.85.

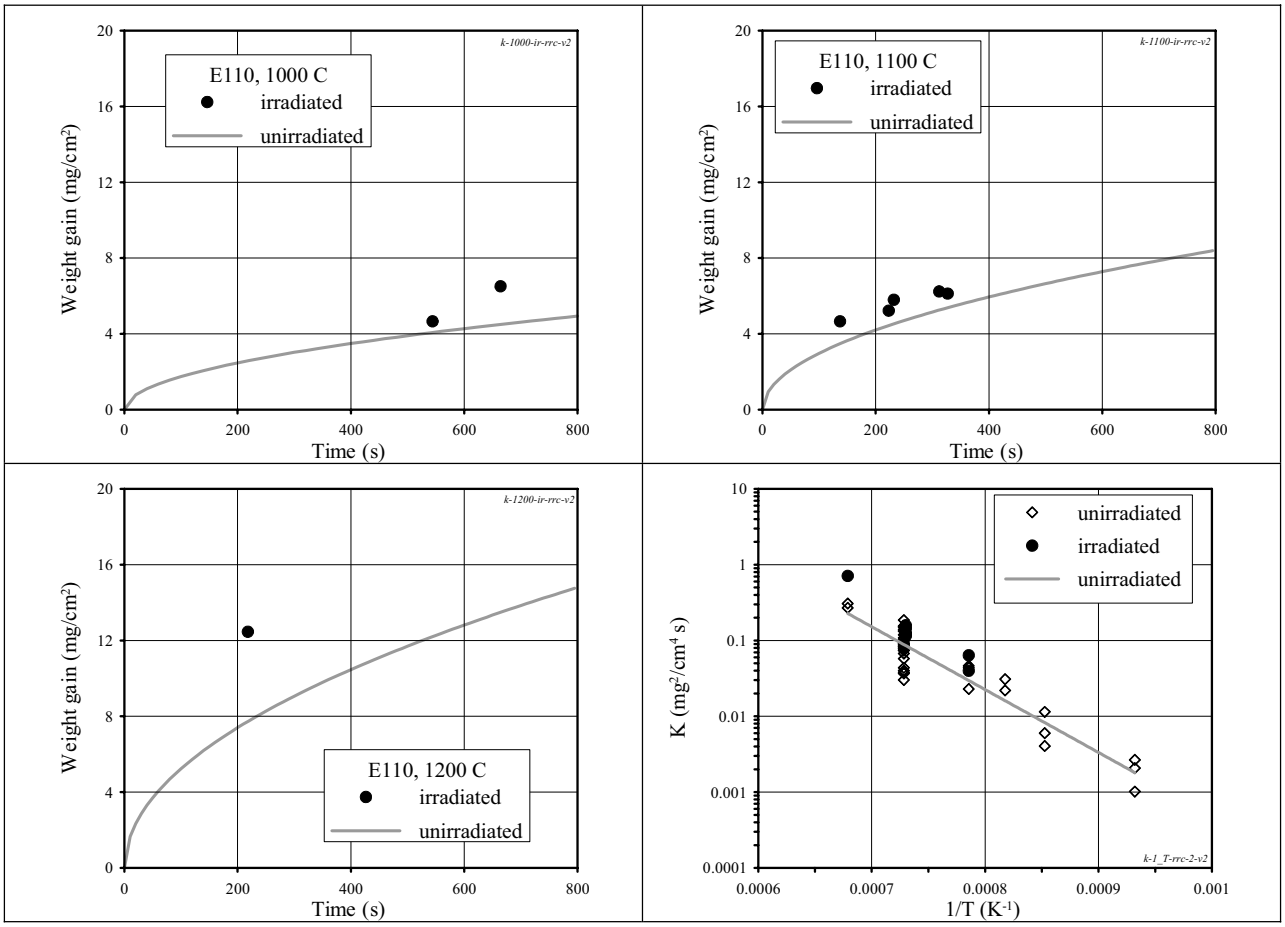

Fig. 3.85. Comparison of the oxidation kinetics for the E110 unirradiated and irradiated claddings

These data show that the oxygen weight gain in the irradiated cladding is somewhat higher than that in the unirradiated cladding, however, taking into account the sparsity of test data available for the E110 irradiated cladding, it seems to be impossible to estimate this effect quantitavely.

The E110 oxidation kinetics was additionally analyzed to clarify the following important issues:

- the assessment of the applicability of the E110 oxidation kinetics (developed basing on the test data with fast heating and fast cooling modes) for the transient oxidation modes such as slow heating and slow cooling (S/S), slow heating and fast cooling (S/F), fast heating and slow cooling (F/S);
- the comparison of the E635, Zry-4, and E110 oxidation kinetics;
- the comparison of the E110 oxidation kinetics developed in different laboratories.

The temperature–time histories of several tests performed at F/S, S/F, S/S combinations of heating and cooling rates were processed using the same procedure of the effective time determination, which was employed for this goal on the processing of F/F and F/Q appropriate data. The major provisions for the procedure are described in Appendix A-6 of the report. The comparative data characterizing the oxidation kinetics at different oxidation modes are presented in Fig. 3.86. In accordance with the obtained data, reasonable correlations are observed between all types of experimental results.

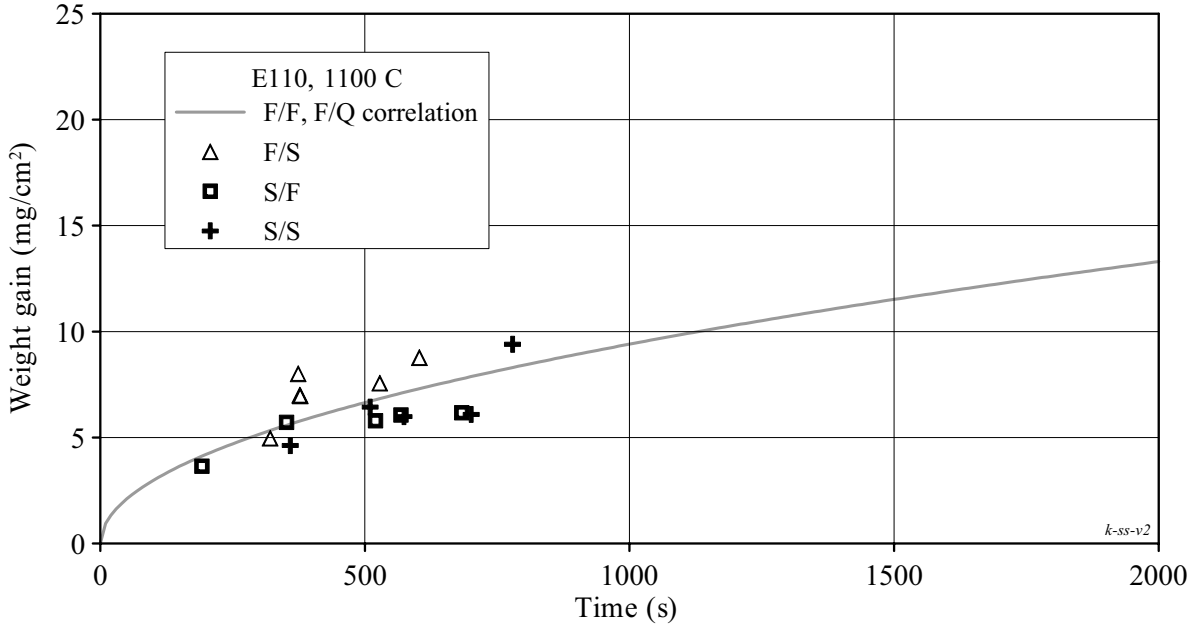

Fig. 3.86. The comparison of data characterizing the transient test modes with the E110 oxidation kinetics

The oxidation kinetics sensitivity of zirconium niobium alloys to the alloying composition was verified using the data presented in Fig. 3.87. The comparison of the E110 and E635 test data shows that the oxidation kinetics of these two alloys are either the similar or very close to each other.

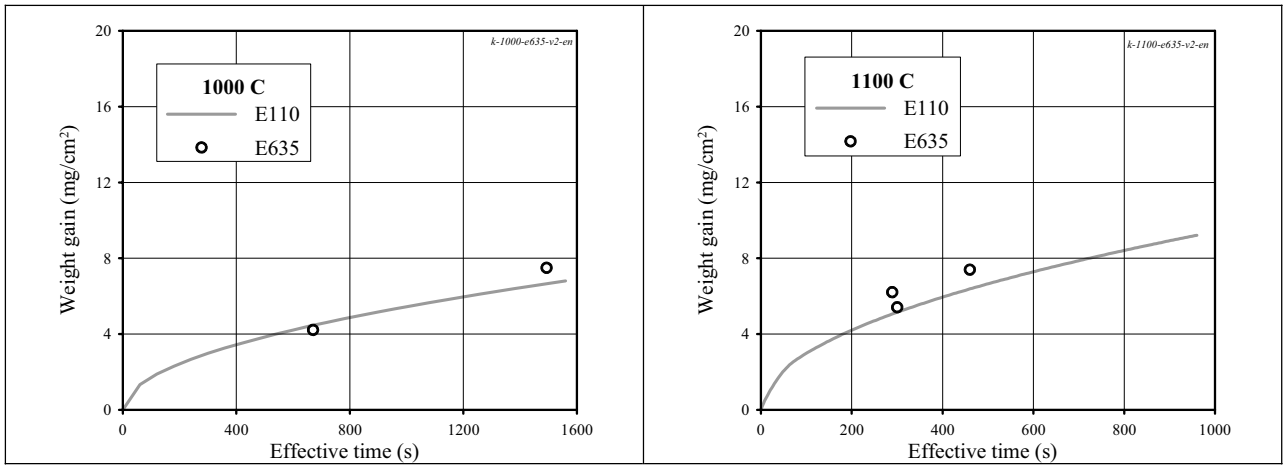

Fig. 3.87. The comparative data on the E110 and E635 oxidation kinetics

The comparison of the E110 and Zry-4 oxidation kinetics confirmed the results obtained by other researchers earlier. The E110 oxidation rate is somewhat less than that for the Zry-4 cladding (see Fig. 3.88).

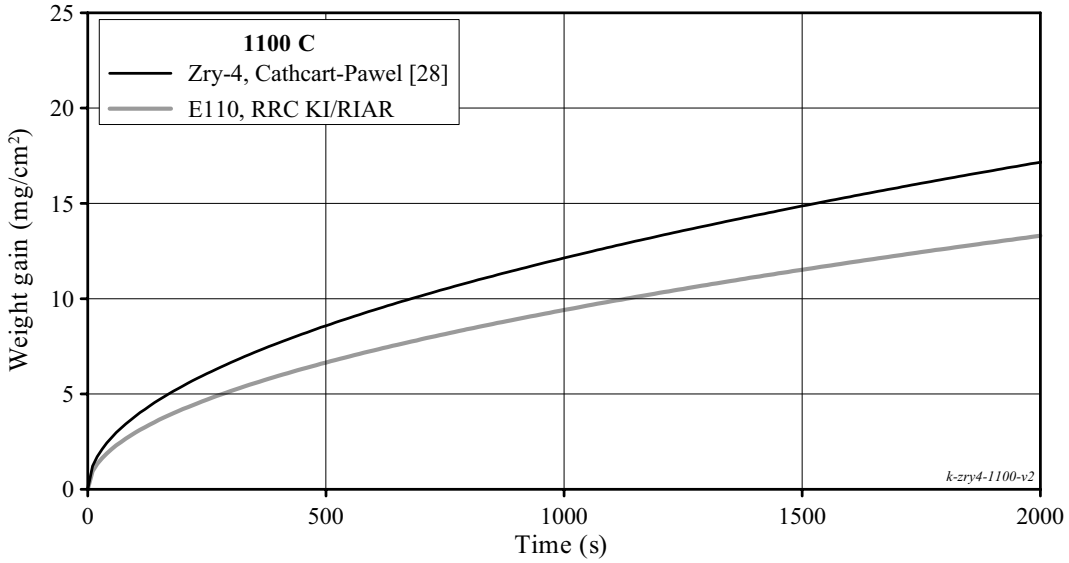

Fig. 3.88. The comparison of the E110 and Zry-4 oxidation kinetics

To estimate the agreement between the E110 oxidation kinetics stated basing on results of this work with the results of other researchers, the appropriate data were compared on the basis of published investigation data obtained in the following organizations:

- KFKI, Hungary [9];
- NFI, Czech republic [26];
- VNIINM, Russia [6];
- NC in Rossendorf, Germany [24].

The comparison of the appropriate results performed at 1100 C allows to conclude that a good agreement is observed between the data of the RRC KI/RIAR (this work), NFI, VNIINM, and NC in Rossendorf (Fig. 3.89). The KFKI data overestimate significantly the E110 oxidation kinetics (may be due to end effects, see section 3.3.7).

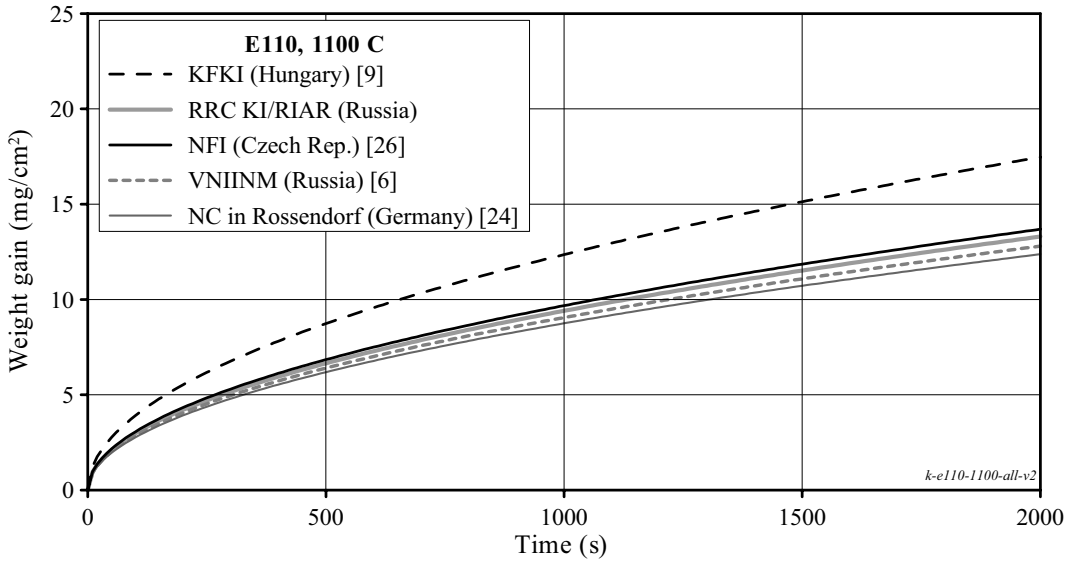

Fig. 3.89. The E110 oxidation kinetics at 1100 C in accordance with the data obtained in different laboratories

REFERENCES FOR SECTION 3

[1] Atomic Energy Commission Rule-Making Hearing, Opinion of the Commission, Docket RM-50-1, 28 December, 1973.

[2] Bibilashvili Yu.K., Sokolov N.B., Andreeva-Andrievskaya L.N., Tonkov V.Yu., Salatov A.V., Morozov A.M., Smirnov V.P. "Thermomechanical Properties of Zirconium-Based Alloys Oxidized Claddings in LOCA Simulationg Conditions", *Proc. of IAEA Technical Commettee Meet. on "Fuel Behavior under Transient and LOCA conditions"*, Halden, Norway, September 10-14, 2001.

[3] Baker L., Just L.C. "Studies of Metal Water Reactions at High Temperatures", Technical report of ANL-6548, 1962.

[4] Solyany V.I., Bibilashvili Yu.K., Dranenko V.V., Izrailevskiy L.B., Levin A.Ya., Morozov A.A. "Characteristics of Corrosion Behavior of Zr-1%Nb WWER Fuel Claddings Within 700-1000°C on Long Term Exposures", *Proc. of IAEA Technical Committee Meet. on "Water Reactor Fuel Behavior and Fission Products Release in Off-Normal and Accident Conditions"*, Vienna, 10-13 November, 1986.

[5] Solyany V.I., Bibilashvili Yu.K., Dranenko V.V., Izrailevskiy L.B., Levin A.Ya., Morozov A.A. "Studies of the corrosion behavior of Zr-1%Nb claddings in steam at high temperatures", VANT, series *" "Materials for Atomic Energy "*, Vol.2(27), 1988, (in Russian).

[6] Bibilashvili Yu.K., Sokolov N.B., Salatov A.V., Andreyeva-Andriyevskaya L.N., Nechayeva O.A., Vlasov F.Yu. "RAPTA-5 Code: Modelling of Behaviour of Fuel Elements of VVER Type in Design Accidents. Verification Calculations", *Proc. of IAEA Technical Committee Meeting on "Behaviour of LWR Core Materials under Accident Conditions", Dimitrovgrad, Russia, on 9-13 October 1995*. IAEA-TECDOC-921, Vienna, 1996.

[7] Bibilashvili Yu.K., Sokolov N.B., Andreyeva-Andriyevskaya L.N., Salatov A.V. "High Temperature Interaction of Fuel Rod Cladding Material (Zr-1%Nb Alloy with Oxygen-Containing Mediums", *Proc. of IAEA Technical Committee Meeting on "Behaviour of LWR Core Materials under Accident Conditions", Dimitrovgrad, Russia, on 9-13 October 1995.*

[8] Böhmert J. "Embrittlement of Zr-1%Nb at Room Temperature after High-Temperature Oxidation in Steam Atmosphere", Kerntechnik ,57 No1, 1992

[9] Gyori Cs. et.al. "Extension of Transuranus code applicability with niobium containing models (EXTRA)". *Proc. of FISA-2003 Conference EU Research in Reactor Safety,* EC Luxembourg, November 2003.

[10] Vrtilkova V., Valach M., Molin L. "Oxiding and Hydrating Properties of Zr-1%Nb Cladding Material in Comparison with Zircaloys", *Proc. of IAEA Technical Committee Meeting on "Influence of Water Chemistry on Fuel Cladding Behavior"*, Rez (Czech Republic), October 4-8, 1993.

[11] Yegorova L., Asmolov V., Abyshov G., Malofeev V., Avvakumov A., Kaplar E., Lioutov K., Shestopalov A., Bortash A., Maiorov L., Mikitiouk K., Polvanov V., Smirnov V., Goryachev A., Prokhorov V., and Vurim A. "Data Base on the Behavior of High Burnup Fuel Rods with Zr-1%Nb Cladding and UO_2 Fuel (VVER Type) under Reactivity Accident Conditions", RRC "Kurchatov Institute" report NSI RRC 2179, Vol.1-3, 1999 (also USNRC report NUREG/IA-0156 and IPSN report IPSN 99/08 - 2).

[12] Hobson D.O. and Rittenhouse P.L. "Embrittlement of Zircaloy Clad Fuel Rods by Steam During LOCA Transient", ORNL-4758, Oak Ridge National Laboratory, 1972.

[13] Chung H.M. and Kassner T.F. "Embrittlement Criteria for Zircaloy Fuel Cladding Applicable to Accident Situations in Light-Water-Reactors", NUREG/CR-1344, January 1980.

[14] Uetsuka H. et.al. "Failure-Bearing Capability of Oxidized Zircaloy-4 Cladding under Simulated Loss-of-Coolant Conditions", J. Nucl. Sci. Tech. 20 (1983).

[15] Bibilashvili Yu.K., Sokolov N.B., Dranenko V.V., Kulikova K.V., Izrailevskiy L.B., Levin A.Ya., Morozov A.M. "Influence of Accident Conditions due to Loss of Tightness by Primary Circuit on Fuel Claddings", *Proc. of the Ninth Int. Symp. on Zirconium in the Nuclear Industry*, Kobe, Japan, November 5-8, 1990.

[16] Bibilashvili Yu.K. et al.,"Influence of Accident Conditions due to Loss of Tightness by Primary Circuit on VVER-1000 Fuel Rod State", VANT, series *"Materials for Atomic Energy"*, Vol.2(42), 1991(rus).

[17] Böhmert J. "Embrittlement of Zr-1%Nb at Room Temperature after High-Temperature Oxidation in Steam Atmosphere", Journal, Kerntechnik 57 No1, 1992.

[18] Hozer Z., Griger A., Matius L., Vasaros L., Horvath M. "Effect of Hydrogen Content on the Embrittlement of ZR Alloys", *Proc. of IAEA Technical Committee Meeting on "Fuel Behavior under Transient and LOCA Conditions"*, Halden, Norway, September 10-14, 2001.

[19] Kaplar E., Yegorova L., Lioutov K., Konobeyev A., Jouravkova N., Smirnov V., Goryachev A., Prokhorov V., Yeremin S., Svyatkin A. "Mechanical Properties of Unirradiated and Irradiated Zr-1%Nb Cladding", RRC "Kurchatov Institute" report NSI RRC 2241, 2001 (also USNRC report NUREG/IA-0199 and IPSN report IPSN 01-16).

[20] Prokhorov V., Makarov O., Smirnov V., Goryachev A., Yegorova L., Kaplar E., and Lioutov K. "Improvement of method to measure tensile properties of Zr-1%Nb alloy cladding with simple ring specimens". *Proceedings of the 6th inter-branch conference on reactor material science*, Dimitrovgrad, Russia, September 11-15, Vol.2, pp. 209-212 (rus).

[21] Bernstein M.L., Zaimovsky V.A. "Mechanical Properties of Metals", Moscow, Metallurgy, 1979, (rus).

[22] Zaimovsky A., Nikulina A., Reshetnikov N. "Zirconium alloys in the Nuclear Industry", Moscow, Energoizdat, 1981 (rus).

[23] Brachet J., Pelchat J., Hamon D., Maury R., Jaques P., Mardon J. "Mechanical Behavior at Room Temperature and Metallurgical Study of Low-Tin Zry-4 and M5™ (Zr-NbO) Alloys after Oxidation at 1100°C and Quenching", *Proc. of IAEA Technical Committee Meeting on "Fuel Behavior under Transient and LOCA Conditions"*, Halden, Norway, September 10-14, 2001.

[24] Böhmert J., Dietrich M., Linek J. "Comparative Studies on High-Temperature Corrosion of Zr-1%Nb and Zircaloy-4", Nuclear Engineering and Design, 147 No1, 1993.

[25] Hozer Z. et. al. "Ring Compression Tests with Oxidised and Hydrided Zr-1%Nb and Zirkaloy –4 Cladding", Hungarian Academy of Sciences, CRIP, Budapest, Report KFKI-2002-01/G.

[26] Vrtilkova V. et. al. "An Approach to the Alternative LOCA Embrittlement Criterion", *Proc. of SEGFSM Topical Meeting on LOCA Fuel Issues,* Argonne National Laboratory, May 2004 (NEA/CSNI/R(2004)19).

[27] Billone M.C., Yan Y. and Burtseva T. "Post-Quench Ductility of Advanced Alloy Cladding", *Nuclear Safety Research Conference (NSRC-2004)*, Washington, DC, October 25-27, 2004.

[28] Cathcart J.V. and Pawel R.E. "Zirconium Metal-Water Oxidation Kinetics: IV. Reaction Rate Studies". ORNL/NUREG-17, 1977.

[29] Chung H.M. "The Effects of Aliovalent Elements on Nodular Oxidation of Zr-based Alloys", *Proceedings of the 2003 Nuclear Safety Research Conference*, Washington DC, October 20-22, 2003, NUREG/CP-0185, 2004.

[30] Yegorova L., Lioutov K., Smirnov V., Goryachev A., Chesanov V. "LOCA Behavior of E110 Alloy", *Proceedings of the 2003 Nuclear Safety Research Conference*, Washington DC, October 20-22, 2003, NUREG/CP-0185, 2004.

[31] Lemaignan C. "Physical Phenomena Concerning Corrosion Under Irradiation of Zr Alloys", *Zirconium in the Nuclear Industry: Thirteenth International Symposium*, ASTM STP 1423, 2002, pp.20-29.

[32] Uetsuka H. et al. "Zircaloy-4 Cladding Embrittlement due to Inner Surface Oxidation under Simulated Loss-of-Coolant Conditions", J. Nucl. Sci. Tech. 18 (1981).

[33] Uetsuka H. et al. "Embrittlement of Zircaloy-4 due to Oxidation in Environment of Stagnant Steam", J. Nucl. Sci. Tech. 19 (1982).

[34] Mardon J.P. et al. "Update on the Development of Advanced Zirconium Alloys for PWR Fuel Rod Claddings", *Proceedings of the International Topical Meeting on Light Water Reactor Fuel Performance,* Portland, Oregon, March 2-6, 1997.

[35] JC. Brachet, L. Portier, V. Maillot, T. Forgeron, JP. Mardon, P. Jacques, A. Lesbros, "Overview of the CEA data on the influence of hydrogen on the metallurgical and thermal-mechanical behavior of Zircaloy-4 and M5™alloys under LOCA conditions", *Nuclear Safety Research Conference (NSRC-2004)*, Washington, DC, October 25-27, 2004.

[36] Mardon J., Frichet A., Bourhis A. "Behavior of M5™ Alloy under Normal and Accident Conditions", *Proc. of Top Fuel-2001 Meet.*, Stockholm, May 27-30, 2001.

[37] Asmolov V., Yegorova L., Lioutov K., Smirnov V., Goryachev A., Chesanov V., Prokhorov V. "Understanding Loca-Related Ductility in E110 Cladding", Proceedings of the 2002 Nuclear Safety Research Conference, Held at Marriott Hotel at Metro Center Washington, DC, October 28-30, 2002, NUREG/CP-0180, pp.109-125.

[38] Yegorova L., Lioutov K., Smirnov V. "Major Findings of E110 Studies under LOCA Conditions", *Proc. of SEGFSM Topical Meeting on LOCA Fuel Issues,* Argonne National Laboratory, May 2004 (NEA/CSNI/R(2004)19).

[39] Pirogov Ye.N., Alimov M.I., Artiuchina L.L. "Creep of H-1 alloy in the range of phase transition" Journal of Soviet Atomic Energy, v.65 (3), p. 293, 1988 (rus).

[40] Forgeron T. et. al, "Experiment and Modeling of Advanced Fuel Rod Cladding Behavior Under LOCA Conditions: Alpha-Beta Phase Transformation Kinetics and EDGAR Methodology", *Zirconium in the Nuclear Industry: Twelfth International Symposium,*. ASTM STP 1354, 2000, pp. 256-278.

[41] Nikulina A. et.al. "Zirconium Alloy E635 as a Material for Fuel Rod Cladding and Other Components of VVER and RBMK Cores", *Zirconium in the Nuclear Industry: Eleventh International Symposium*, ASTM STP-1295, November 1996.

[42] Douglass D.L. "The Metallurgy of Zirconium", International Atomic Energy Agency, 1971.

[43] Garde A.M. "Influence of Cladding Microstructure on Low Enthalpy Failures in RIA Simulation Tests", *Zirconium in the Nuclear Industry: Twelfth International Symposium,* ASTM STP 1354, 2000.

[44] Hache G., Chung H. "The History of LOCA Embrittlement Criteria", Proc. of the 28th Water Reactor Safety Information Meeting, NUREG/CP-0172, 2000.

[45] Bai J., Prioul C., Pelchat J., Barcelo F. "Effects of Hydrides on the Ductile Brittle Transition in Stress–Relieved, Recrystallized and β-Treated Zircaloy", *Proc. of the International Topical Meeting on the LWR Fuel Performance,* Avignon, France, 1991.

[46] Waeckel N., Mardon J.P. "Recent data on M5™Alloy under LOCA Conditions", *Proceedings of the 2003 Nuclear Safety Research Conference*, Washington DC, October 20-22, 2003, NUREG/CP-0185, 2004.

[47] G. Fearnehough and A. Cowan "The effect of hydrogen and strain rate on the "ductile–brittle" behavior of Zircaloy", Journal of Nuclear Materials №22, 1967.

[48] F. Nagase, K. Ishijima, and T. Furuta, "Influence of Locally Concentrated Hydrides on Ductility of Zircaloy-4", *Proc. of the CSNI Specialist Meeting on Transient behaviour of High Burnup Fuel,* Cadarche, France, September 12-14, 1995.